Classical and Quantum Chaos

Part II: Semiclassical Chaos

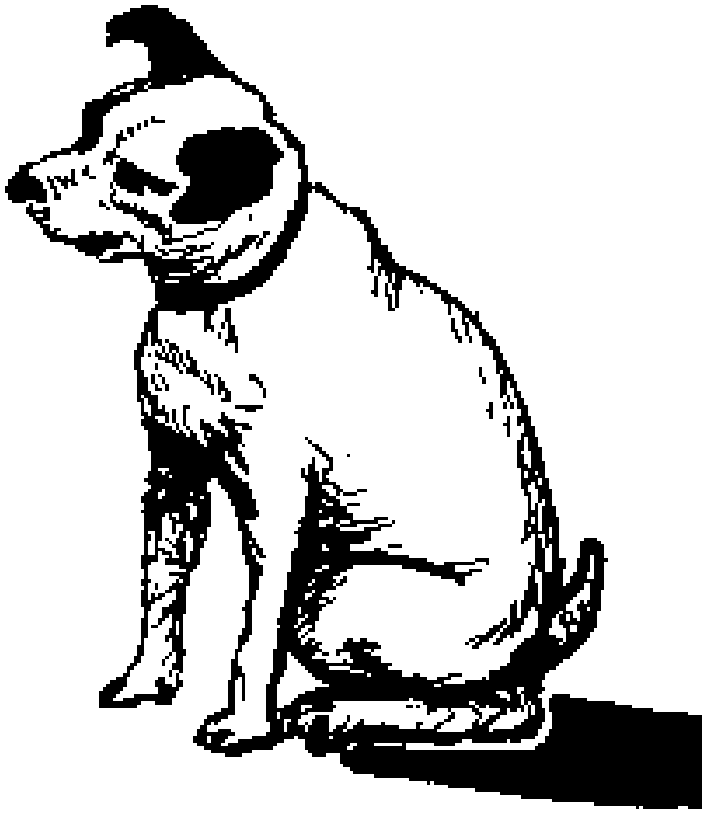

Predrag Cvitanović – Roberto Artuso – Per Dahlqvist – Ronnie Mainieri
– Gregor Tanner – Gábor Vattay – Niall Whelan – Andreas Wirzba

version 9.3.9 **Feb 15 2003** printed February 16, 2003
www.nbi.dk/ChaosBook comments to: predrag@nbi.dk

Chapter 23

Semiclassical evolution

> Anyone who uses words "quantum" and "chaos" in the same sentence should be hung by his thumbs on a tree in the park behind the Niels Bohr Institute
> Joseph Ford

(G. Vattay, G. Tanner and P. Cvitanović)

So far we have obtained information about the nonlinear dynamics by calculating spectra of linear operators such as the Perron-Frobenius operator of sect. 23.2.3 or the associated partial differential equations such as the Liouville equation (7.37) of sect. 7.4.1. The spectra of these operators could then again be described in terms of the periodic orbits of the deterministic dynamics by means of trace formulas and cycle expansions. We also noted that the type of the dynamics has a strong influence on the convergence of cycle expansions and thus also on the spectra; this made it necessary to develop very different approaches for different types of dynamical behavior such as, on one hand, the strongly hyperbolic and, on the other hand, the intermittent dynamics of chapters 15 and 18.

We now address the converse question: can we turn the problem round and study linear PDE's in terms of the underlying deterministic dynamics? And, is there a link between structures in the spectrum or the eigenfunctions of a PDE and the dynamical properties of the underlying classical flow? The answer is yes, but ... things are becoming somewhat more complicated when studying 2nd or higher order linear PDE's. We can find a classical dynamics associated with a linear PDE, just take geometric optics as a familiar example. Propagation of light follows a second order wave equation but may in certain limits be well described in terms of geometric rays. A theory in terms of properties of the classical dynamics alone, referred to here as the *semiclassical theory*, will, however not be exact, in contrast to the classical periodic orbit formulas obtained so far. Waves exhibit

new phenomena, such as interference, diffraction, and the higher $\hbar$ corrections which still need to be incorporated in the periodic orbit theory.

We will restrict the discussion in what follows to a wave equation of great import for physics, the non-relativistic Schrödinger equation. Our approach will be very much in the spirit of the early days of quantum mechanics, before its wave character has been fully uncovered by Schrödinger in the mid 1920's. Indeed, were physicists of the period as familiar with classical chaos as we are today, this theory could have been developed 80 years ago. It was the discrete nature of the hydrogen spectrum which inspired the Bohr - de Broglie picture of the old quantum theory: one places a wave instead of a particle on a Keplerian orbit around the hydrogen nucleus. The quantization condition is that only those orbits contribute for which this wave is stationary; from this followed the Balmer spectrum and the Bohr-Sommerfeld quantization which eventually led to the more sophisticated theory of Schrödinger and others. Today we are very aware of the fact that elliptic orbits are an idiosyncracy of the Kepler problem, and that chaos is the rule; so can the Bohr quantization be generalized to chaotic systems? The answer was provided by Gutzwiller as late as 1971: a chaotic system can indeed be quantized by placing a wave on each of the *infinity* of unstable periodic orbits. Due to the instability of the orbits, the wave, however, does not stay localized but leaks into neighborhoods of other periodic orbits. Contributions of different periodic orbits interfere and the quantization condition can no longer be attributed to a single periodic orbit. We find instead that a coherent summation over the infinity of periodic orbit contributions gives the desired spectrum.

Before we get to this point we have to recapitulate some basic notions of quantum mechanics; after having defined the main quantum objects of interest, the quantum propagator and the Green's function, we will relate the quantum propagation to the classical flow of the underlying dynamical system. We will then proceed to construct semiclassical approximations to the quantum propagator and the Green's function. A short rederivation of classical Hamiltonian dynamics starting from the Hamilton-Jacobi equation will be offered along the way. The derivation of the Gutzwiller trace formula and the semiclassical zeta function as a sum and as a product over periodic orbits will be given in chapter 24. In subsequent chapters we butress our case by applying and extyending the theory: a cycle expansion calculation of scattering resonances in a 3-disk billiard in chapter **??**, the spectrum of helium in chapter 25, and the incorporation of diffraction effects in chapter 26.

23.1 Quantum mechanics: A brief review

We start with a review of standard quantum mechanical concepts prerequisite to the derivation of the semiclassical trace formula.

In coordinate representation the time evolution of a quantum mechanical wave function is governed by the Schrödinger equation

$$i\hbar\frac{\partial}{\partial t}\psi(q,t) = \hat{H}(q,\frac{\hbar}{i}\frac{\partial}{\partial q})\psi(q,t), \tag{23.1}$$

where the Hamilton operator $\hat{H}(q,-i\hbar\partial_q)$ is obtained from the classical Hamiltonian by substitution $p \to -i\hbar\partial_q$. Most of the Hamiltonians we shall consider here are of form

$$H(q,p) = T(p) + V(q)\,, \qquad T(p) = p^2/2m\,, \tag{23.2}$$

describing dynamics of a particle in a d-dimensional potential $V(q)$. For time independent Hamiltonians we are interested in finding stationary solutions of the Schrödinger equation of the form

$$\psi_n(q,t) = e^{-iE_nt/\hbar}\phi_n(q), \tag{23.3}$$

where E_n are the eigenenergies of the system obtained by solving the eigenvalue equation $\hat{H}\phi_n(q) = E_n\phi_n(q)$. For bound systems the spectrum is discrete and the eigenfunctions form an orthonormal

$$\int d^dq\,\phi_n(q)\phi_m^*(q) = \delta_{nm} \tag{23.4}$$

and complete

$$\sum_n \phi_n(q)\phi_n^*(q') = \delta(q-q')\,. \tag{23.5}$$

set of functions in a Hilbert space. For simplicity we will assume that the system is bound, although most of the results will be applicable to open systems, where one has complex resonances instead of real energies, and the spectrum has continuous components. ☞ chapter ??

A given wave function can be expanded in the energy eigenbasis

$$\psi(q,t) = \sum_n c_n e^{-iE_nt/\hbar}\phi_n(q)\,, \tag{23.6}$$

where the expansion coefficient c_n is given by the projection of the initial wave function $\psi(q,0)$ onto the nth eigenstate

$$c_n = \int d^dq\,\phi_n^*(q)\psi(q,0). \tag{23.7}$$

By substituting (23.7) into (23.6), we can cast the evolution of a wave function into a multiplicative form

$$\psi(q,t) = \int d^dq' K(q,q',t)\psi(q',0)\,,$$

with the kernel

$$K(q,q',t) = \sum_n \phi_n(q)\,e^{-iE_nt/\hbar}\phi_n^*(q') \tag{23.8}$$

called the quantum evolution operator, or the *propagator*. Applied twice, first for time t_1 and then for time t_2, it propagates the initial wave function from q' to q'', and then from q'' to q

$$K(q,q',t_1+t_2) = \int dq''\,K(q,q'',t_2)K(q'',q',t_1) \tag{23.9}$$

forward in time, hence the name "propagator". In non-relativistic quantum mechanics the range of q'' is infinite, meaning that the wave can propagate at any speed; in relativistic quantum mechanics this is rectified by restricting the propagation to the forward light cone.

Since the propagator is a linear combination of the eigenfunctions of the Schrödinger equation, it also satisfies the Schrödinger equation

$$i\hbar\frac{\partial}{\partial t}K(q,q',t) = \hat{H}(q,\frac{i}{\hbar}\frac{\partial}{\partial q})K(q,q',t)\,, \tag{23.10}$$

and is thus a wave function defined for $t \geq 0$; from the completeness relation (23.5) we obtain the boundary condition at $t = 0$:

$$\lim_{t\to 0_+} K(q,q',t) = \delta(q-q')\,. \tag{23.11}$$

The propagator thus represents the time evolution of a wave packet which starts out as a configuration space delta-function localized in the point q' at the initial

time $t = 0$.

For time independent Hamiltonians the time dependence of the wave functions is known as soon as soon as the eigenenergies E_n and eigenfunctions ϕ_n have been determined. With time dependence rendered "trivial", it makes sense to focus on obtained from the propagator via a Laplace transformation

$$G(q,q',E+i\epsilon) = \frac{1}{i\hbar}\int_0^\infty dt\, e^{\frac{i}{\hbar}Et-\frac{\epsilon}{\hbar}t}K(q,q',t) = \sum_n \frac{\phi_n(q)\phi_n^*(q')}{E-E_n+i\epsilon}\,. \quad (23.12)$$

Here ϵ is a small positive number, ensuring the existence of the integral. The eigenenergies show up as poles in the Green's function with residues corresponding to the wave function amplitudes. If one is only interested in the spectrum, one may restrict the considerations to the (formal) trace of the Green's function,

$$\mathrm{tr}\, G(q,q',E) = \int d^dq\, G(q,q,E) = \sum_n \frac{1}{E-E_n}\,, \quad (23.13)$$

where E is complex, with a positive imaginary part, and we have used the eigenfunction orthonormality (23.4). This trace is formal, since in general the sum in (23.13) is divergent. We shall return to this point in sects. 24.1.1 and 24.1.2.

A a useful characterization of the set of eigenvalues is given in terms of the *density of states*, with a delta function peak at each eigenenergy, fig. 23.1(a),

$$d(E) = \sum_n \delta(E-E_n). \quad (23.14)$$

Using the identity

23.1 on p. 483

$$\delta(E-E_n) = -\lim_{\epsilon\to+0}\frac{1}{\pi}\mathrm{Im}\,\frac{1}{E-E_n+i\epsilon} \quad (23.15)$$

we can express the density of states in terms of the trace of the Green's function, that is

$$d(E) = \sum_n \delta(E-E_n) = -\lim_{\epsilon\to 0}\frac{1}{\pi}\mathrm{Im}\,\mathrm{tr}\, G(q,q',E+i\epsilon). \quad (23.16)$$

sect. 24.1.1

This relation is the reason why we chose to describe the quantum spectrum in terms of the density of states. As we shall see, a semiclassical formula for right

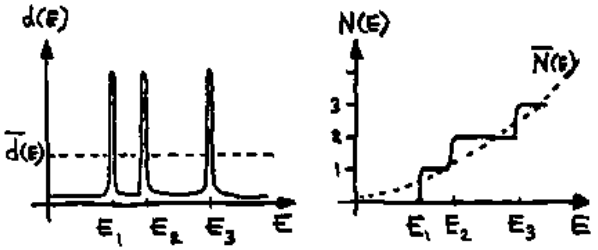

Figure 23.1: Schematic picture of **a)** the density of states $d(E)$, and **b)** the spectral staircase function $N(E)$. The dashed lines denote the mean density of states $\bar{d}(E)$ and the average number of states $\bar{N}(E)$ discussed in more detail in sect. 17.1.

hand side of this relation will yield the quantum spectrum in terms of periodic orbits.

The density of states can be written as the derivative $d(E) = \mathrm{d}N(E)/\mathrm{d}E$ of another useful quantity, the *spectral staircase* function

$$N(E) = \sum_n \Theta(E-E_n) \quad (23.17)$$

which counts the number of eigenenergies below E, fig. 23.1(b). Here Θ is the Heaviside function

$$\Theta(x) = 1 \quad \text{if } x > 0; \quad \Theta(x) = 0 \quad \text{if } x < 0\,. \quad (23.18)$$

This completes our lightning review of quantum mechanics.

23.2 Semiclassical evolution

Semiclassical approximations to quantum mechanics are valid in the regime where the de Broglie wavelength $\lambda \sim \hbar/p$ of a particle with momentum p is much *shorter* than the length scales across which the potential of the system changes significantly. In the short wavelength approximation the particle is a point-like object bouncing off potential walls the same way it does in the classical mechanics. The real novelty of quantum mechanics is the interference of the point-like particle with other versions of itself travelling along different classical trajectories, a feat impossible in classical mechanics. The short wavelength –

remark 23.1

or semiclassical – formalism is developed by formally taking the limit $\hbar \to 0$ in quantum mechanics in such a way that quantum quantities go to their classical counterparts.

The mathematical formulation of the semiclassical approximation starts out with a rewrite of the wave function

$$\psi(q,t) = A(q,t)e^{iR(q,t)/\hbar}\,, \tag{23.19}$$

in terms of a pair of real functions $R(q,t)$ and $A(q,t)$, its phase and magnitude. The time evolution of the phase and the magnitude of ψ follows from the Schrödinger equation (23.1)

23.2 on p. 483

$$\left(i\hbar\frac{\partial}{\partial t} + \frac{\hbar^2}{2m}\frac{\partial^2}{\partial q^2} - V(q)\right)\psi(q,t) = 0\,. \tag{23.20}$$

Take for concreteness a Hamiltonian $\hat{H}$ of form (23.2), assume $A \neq 0$,and separate out the real and the imaginary parts we get two equations; the real part governs the time evolution of the phase

$$\frac{\partial R}{\partial t} + \frac{1}{2m}\left(\frac{\partial R}{\partial q}\right)^2 + V(q) - \frac{\hbar^2}{2m}\frac{1}{A}\frac{\partial^2}{\partial q^2}A = 0\,, \tag{23.21}$$

and the imaginary part giving the time evolution of the amplitude

23.3 on p. 483

$$\frac{\partial A}{\partial t} + \frac{1}{m}\sum_{i=1}^{d}\frac{\partial A}{\partial q_i}\frac{\partial R}{\partial q_i} + \frac{1}{2m}A\frac{\partial^2 R}{\partial q^2} = 0\,. \tag{23.22}$$

23.4 on p. 483

23.5 on p. 483

In this way a linear PDE for a complex wave function is converted into a set of coupled non-linear PDE's of real-valued functions R and A. The coupling term in (23.21) is, however, of order $\hbar^2$ and thus small in the semiclassical limit $\hbar \to 0$. Now we make the *Wentzel-Kramers-Brillouin* (WKB) *ansatz*: we assume the magnitude $A(q,t)$ varies slowly compared to the phase $R(q,t)/\hbar$, so we drop the $\hbar$-dependent term. In this approximation the phase $R(q,t)$ and the corresponding "momentum field" $\frac{\partial R}{\partial q}(q,t)$ can be determined from the amplitude independent equation

$$\frac{\partial R}{\partial t} + H\left(q, \frac{\partial R}{\partial q}\right) = 0\,. \tag{23.23}$$

We recognize this as the classical *Hamilton-Jacobi equation*. We will refer to this step as the *semiclassical approximation* to wave mechanics, and from now on work only within this approximation.

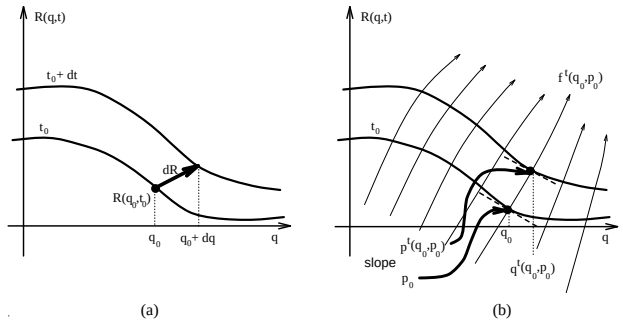

Figure 23.2: (a) A phase $R(q,t)$ plotted as a function of the position q for two infinitesimally close times. (b) The phase $R(q,t)$ transported by a swarm of "particles"; The Hamilton's equations (23.28) construct $R(q,t)$ by transporting $q_0 \to q(t)$ and the slope of $R(q_0,t_0)$, that is $p_0 \to p(t)$.

23.2.1 Hamilton's equations

> William Rowan Hamilton was born in 1805. At three he could read English; by four he began to read Latin, Greek and Hebrew, by ten he read Sanskrit, Persian, Arabic, Chaldee, Syrian and sundry Indian dialects. At age seventeen he began to think about optics, and worked out his great principle of "Characteristic Function".
>
> Turnbull, *Lives of Mathematicians*

If you feel that you already understand the Hamilton-Jacobi theory, you can safely skip this section.

The wave equation (23.1) describes how the wave function ψ evolves with time, and if you think of ψ as an (infinite dimensional) vector, position q plays a role of an index. In one spatial dimension the phase R plotted as a function of the position q for two different times looks something like fig. 23.2(a): The phase $R(q,t_0)$ deforms smoothly with time into the phase $R(q,t)$ at time t. Hamilton's idea was to let a swarm of particles transport R and its slope $\partial R/\partial q$ at q at initial time $t = t_0$ to a corresponding $R(q,t)$ and its slope at time t, fig. 23.2(b). For notational convenience, define

$$p_i = p_i(q,t) := \frac{\partial R}{\partial q_i}\,, \quad i = 1,2,\ldots,d\,. \tag{23.24}$$

We saw earlier that (23.21) reduces in the semiclassical approximation to the Hamilton-Jacobi equation (23.23). To make life simple, we shall assume through-

out this chapter that the Hamilton's function $H(q,p)$ does not depend explicitly on time t, that is the energy is conserved.

To start with, we also assume that the function $R(q,t)$ is smooth and well defined for every q at the initial time t. This is true for sufficiently short times; as we will see later R develops folds and becomes multi-valued as t progresses. Consider now the variation of the function $R(q,t)$ with respect to independent infinitesimal variations of the time and space coordinates dt and dq, fig. 23.2(a)

$$dR = \frac{\partial R}{\partial t}dt + \frac{\partial R}{\partial q}dq\,. \tag{23.25}$$

Dividing through by dt and substituting (23.23) we obtain the total derivative of $R(q,t)$ with respect to time *along as yet arbitrary direction* $\dot{q}$, that is,

$$\frac{dR}{dt}(q,\dot{q},t) = -H(q,p) + \dot{q}\cdot p\,. \tag{23.26}$$

Note that the "momentum" $p = \partial R/\partial q$ is a well defined function of q and t. In order to integrate $R(q,t)$ with the help of (23.26) we also need to know how $p = \partial R/\partial q$ changes along $\dot{q}$. Varying p with respect to independent infinitesimal variations dt and dq and substituting the Hamilton-Jacobi equation (23.23) yields

$$d\frac{\partial R}{\partial q} = \frac{\partial^2 R}{\partial q \partial t}dt + \frac{\partial^2 R}{\partial q^2}dq = -\left(\frac{\partial H}{\partial q} + \frac{\partial H}{\partial p}\frac{\partial p}{\partial q}\right)dt + \frac{\partial p}{\partial q}dq\,.$$

Note that $H(q,p)$ depends on q also through $p(q,t) = \partial R/\partial q$, hence the $\frac{\partial H}{\partial p}$ term in the above equation. Dividing again through by dt we get the time derivative of $\partial R/\partial q$, that is,

$$\dot{p}(q,\dot{q},t) + \frac{\partial H}{\partial q} = \left(\dot{q} - \frac{\partial H}{\partial p}\right)\frac{\partial p}{\partial q}\,. \tag{23.27}$$

Time variation of p depends not only on the yet unknown $\dot{q}$, but also on the second derivatives of R with respect to q with yet unknown time dependence. However, if we *choose* $\dot{q}$ (which was arbitrary, so far) such that the right hand side of the above equation vanishes, we can calculate the function $R(q,t)$ along a specific trajectory $(q(t),p(t))$ given by integrating the ordinary differential equations

$$\dot{q} = \frac{\partial H(q,p)}{\partial p}, \qquad \dot{p} = -\frac{\partial H(q,p)}{\partial q} \tag{23.28}$$

with initial conditions

$$q(t_0) = q', \qquad p(t_0) = p' = \frac{\partial R}{\partial q}(q',t_0). \tag{23.29}$$

☞ sect. 5.1

We recognize (23.28) as the Hamilton's equations of motion of classical mechanics.

$\dot{q}$ is no longer an independent function, and the phase $R(q,t)$ can now be computed by integrating equation (23.26) along the trajectory $(q(t),p(t))$

$$\begin{aligned} R(q,t) &= R(q',t_0) + R(q,t;q',t_0) \\ R(q,t;q',t_0) &= \int_{t_0}^{t} d\tau\,[\dot{q}(\tau)\cdot p(\tau) - H(q(\tau),p(\tau))]\,, \end{aligned} \tag{23.30}$$

with the initial conditions (23.29). In this way the Hamilton-Jacobi *partial* differential equation (23.21) is solved by integrating a set of *ordinary* differential equations, the Hamilton's equations. In order to determine $R(q,t)$ for arbitrary q and t we have to find a q' such that the trajectory starting in $(q', p' = \partial_q R(q',t_0))$ reaches q in time t and then compute R along this trajectory, see fig. 23.2(b). Erudite reader has already noticed that the integrand of (23.30) is known as the Lagrangian, and that a variational principle lurks somewhere, but we shall not make much fuss about that here.

Throughout this chapter we assume that the energy is conserved, and that the only time dependence of $H(q,p)$ is through $(q(\tau),p(\tau))$, so the value of $R(q,t;q',t_0)$ does not depend on t_0, but only on the elapsed time $t - t_0$. To simplify notation we will set $t_0 = 0$ and write

$$R(q,q',t) = R(q,t;q',0)\,.$$

The initial momentum of the particle must coincide with the initial momentum of the trajectory connecting q' and q:

$$p' = \frac{\partial}{\partial q'}R(q',0) = -\frac{\partial}{\partial q'}R(q,q',t). \tag{23.31}$$

23.6 on p. 483

Function $R(q,q',t)$ is known as the *Hamilton's principal function*.

23.7 on p. 483

To summarize: Hamilton's achievement was to trade in the Hamilton-Jacobi *partial* differential equation (23.23) for the evolution of a wave front for a finite number of *ordinary* differential equations of motion which increment the initial phase $R(q,0)$ by the integral (23.30) along the phase space trajectory $(q(\tau),p(\tau))$.

23.2.2 Action

Before proceeding, we note in passing a few facts about Hamiltonian dynamics that will be needed for the construction of semiclassical Green's functions. If the energy is conserved, the $\int H(q,p)d\tau$ integral in (23.30) is simply Et. The first term, or the *action*

$$S(q,q',E) = \int_0^t d\tau\, \dot{q}(\tau)\cdot p(\tau) = \int_{q'}^{q} dq\cdot p \tag{23.32}$$

is integrated along a trajectory from q' to q with a given energy E. By (23.30) the action is the Legendre transform of Hamilton's principal function

$$S(q,q',E) = R(q,q',t) + Et\,. \tag{23.33}$$

The time of flight t along the trajectory connecting $q' \to q$ with fixed energy E is given by

$$\frac{\partial}{\partial E} S(q,q',E) = t\,. \tag{23.34}$$

The way to think about the formula (23.33) for action is that the time of flight is a function of the energy, $t = t(q,q',E)$. The left hand side is explicitly a function of E; the right hand side is an implicit function of E through energy dependence of the flight time t.

Going in the opposite direction, the energy of a trajectory $E = E(q,q',t)$ connecting $q' \to q$ with a given time of flight t is given by the derivative of Hamilton's principal function

$$\frac{\partial}{\partial t} R(q,q',t) = -E\,, \tag{23.35}$$

and the second variations of R and S are related in the standard way of Legendre transforms:

$$\frac{\partial^2}{\partial t^2} R(q,q',t) \frac{\partial^2}{\partial E^2} S(q,q',E) = -1\,. \tag{23.36}$$

A geometric visualization of what the phase evolution looks like is very helpful in understanding the origin of topological indices to be introduced in what follows. Given an initial phase $R(q,t_0)$, the gradient $\partial_q R$ defines a d-dimensional ☞ sect. 23.2.4

Lagrangian manifold $(q,\, p = \partial_q R(q))$ in the full $2d$ dimensional phase space (q,p). The defining property of this manifold is that any contractable loop γ in it has zero action,

$$0 = \oint_\gamma dq\cdot p,$$

a fact that follows from the definition of p as a gradient, and the Stokes theorem. Hamilton's equations of motion preserve this property and map a Lagrangian manifold into a Lagrangian manifold time t later. This fact is called the Poincaré-Cartan theorem.

Returning back to the main line of our argument: we show next that the velocity field given by the Hamilton's equations together with the continuity equation determines the amplitude of the wave function.

23.2.3 Density evolution

To obtain the full solution of the Schrödinger equation (23.1), we also have to integrate (23.22). Already Schrödinger noted that if one defines

$$\rho = \rho(q,t) \coloneqq A^2 = \psi^*\psi$$

evaluated along the trajectory $(q(t),p(t))$, the amplitude equation (23.22) is equivalent to the continuity equation (7.36) after multiplying (23.22) by $2A$, that is

$$\frac{\partial \rho}{\partial t} + \frac{\partial}{\partial q_i}(\rho v_i) = 0\,. \tag{23.37}$$

Here, $v_i = \dot{q}_i = p_i/m$ denotes a velocity field, which is in turn determined by the phase $R(q,t)$ or equivalently by the Lagrangian manifold $(q(t),p(t) = \partial_q R(q,t))$,

$$v = \frac{1}{m}\frac{\partial}{\partial q} R(q,t).$$

As we already know how to solve the Hamilton-Jacobi equation (23.23), we can also solve for the density evolution as follows:

The density $\rho(q)$ can be visualized as the density of a configuration space flow $q(t)$ of a swarm of hypothetical particles; the trajectories $q(t)$ are solutions

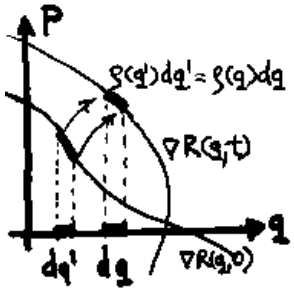

Figure 23.3: Density evolution of an initial surface $(q', p' = \partial_q R(q', 0)$ into $(q(t), p(t))$ surface time t later, sketched in 1 dimension. While the number of trajectories and the phase space Liouville volume are conserved, the density of trajectories projected on the q coordinate varies; trajectories which started in dq' at time zero end up in the interval dq.

of Hamilton's equations with initial conditions given by $(q(0) = q', p(0) = p' = \partial_q R(q', 0))$.

If we take a small configuration space volume $d^d q$ around some point q at time t, then the number of particles in it is $\rho(q,t)d^d q$. They started initially in a small volume $d^d q'$ around the point q' of the configuration space. For the moment, we assume that there is only one solution, the case of several paths will be considered below. The number of particles at time t in the volume is the same as the number of particles in the initial volume at $t = 0$,

$$\rho(q(t), t)d^d q = \rho(q', 0)d^d q' \,,$$

see fig. 23.3. The ratio of the initial and the final volumes can be expressed as

$$\rho(q(t), t) = \left|\det \mathbf{j}(q, q', t)\right| \rho(q', 0), \tag{23.38}$$

where $\mathbf{j}$ stands for the configuration space Jacobian ☞ sect. 7.2

$$\mathbf{j}(q, q', t) = \frac{\partial q'_l}{\partial q_k} \,. \tag{23.39}$$

As we know how to compute trajectories $(q(t), p(t))$, we know how to compute this jacobian and, by (23.38), the density $\rho(q(t), t)$ at time t.

23.2.4 Semiclassical wave function

Now we have all ingredients to write down the semiclassical wave function at time t. Consider first the case when our initial wave function can be written in

terms of single-valued functions $A(q', 0)$ and $R(q', 0)$. For sufficiently short times, $R(q,t)$ will remain a single-valued function of q, and every $d^d q$ configuration space volume element keeps its orientation. The evolved wave function is in the semiclassical approximation then given by

$$\begin{aligned} \psi_{sc}(q,t) &= A(q,t)e^{iR(q,t)/\hbar} = \sqrt{\det \mathbf{j}(q,q',t))}\, A(q',0)e^{i(R(q',0)+R(q,q',t))/\hbar} \\ &= \sqrt{\det \mathbf{j}(q,q',t)}\, e^{iR(q,q',t)/\hbar}\, \psi(q',0) \,. \end{aligned}$$

As the time progresses the Lagrangian manifold $\partial_q R(q,t)$ can develop folds, so for longer times the value of the phase $R(q,t)$ is not necessarily unique; in general more than one trajectory will connect points q and q' with different phases $R(q,q',t)$ accumulated along these paths, see fig. 23.4.

Whenever the Lagrangian manifold develops a fold, the density of the phase space trajectories in the fold projected on the configuration coordinates diverges. Presence of a fold is signaled by the divergence of an eigenvalue of the Jacobian $\mathbf{j}$ from (23.39). The projection of a simple fold, or of an envelope of a family of phase space trajectories, is called a *caustic*; this expression comes from the Greek word for "capable of burning", evoking the luminous patterns that one observes on the bottom of a swimming pool.

We thus expect in general a collection of different trajectories from q' to q which we will index by j, with different phase increments $R_j(q,q',t)$. The hypothetical particles of the density flow at a given configuration space point can move with different momenta $p = \partial_q R_j(q,t)$. This is not an ambiguity, since in the full (q,p) phase space each particle follows its own trajectory with a unique momentum.

The folding also changes the orientation of the pieces of the Lagrangian manifold $(q, \partial_q R(q,t))$ with respect to the initial manifold, so the eigenvalues of the Jacobian determinant change sign at each fold crossing. We can keep track of the signs by writing the Jacobian determinant as

$$\det \mathbf{j}^j(q,q',t) = e^{-i\pi m_j(q,q',t)} |\det \mathbf{j}^j(q,q',t)|,$$

where $m_j(q,q',t)$ counts the number of sign changes of the Jacobian determinant on the way from q' to q along the trajectory indexed with j, see fig. 23.4. We shall refer to the integer $m_j(q,q',t)$ as the *topological or Morse index* of the trajectory. So in general the semiclassical approximation to the wave function is thus a sum over possible trajectories that start in q' and end in q in time t

$$\psi_{sc}(q,t) = \sum_j |\det \mathbf{j}^j(q,q',t)|^{1/2} e^{iR_j(q,q',t)/\hbar - i\pi m_j(q,q',t)/2} \psi(q'_j, 0) \,, \tag{23.40}$$

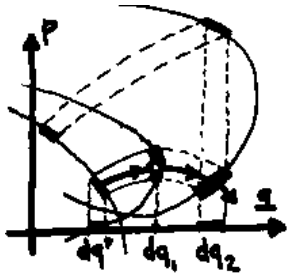

Figure 23.4: Folding of the Lagrangian surface $(q, \partial_q R(q,t))$. The inital surface $(q', p' = \partial_q R(q',0))$ is mapped into the surface $(q(t), p(t))$ some time t later; this surface may develop a fold at $q = q_1$; the volume element dq_1 in the neighborhood of the folding point which steams from some inital volume element dq' is proportional to $\sqrt{dq'}$ instead of dq' at the fold. The Jacobian (23.39), $\partial q'/\partial q$, diverges like $1/\sqrt{q_1 - q(t)}$ when computed along the trajectory going trough the folding point at q_1. After the folding the orientation of the interval dq' has changed when being mapped into dq_2; in addition the function R, as well as its derivative which defines the Lagrangian manifold, becomes multi-valued. Distinct trajectories starting from different initial points q' can now reach the same final point q_2.

each contribution weighted by corresponding density, phase increment and the topological indexphase increment and the topological index.

That the correct topological index is obtained by simply counting the number of eigenvalue sign changes and taking the square root is not obvious - the careful argument requires that quantum wave functions evaluated across the folds remain single valued.

23.3 Semiclassical propagator

We saw in sect. 23.1 that the evolution of an initial wave function $\psi(q,0)$ is completely determined by the propagator (23.8). As $K(q,q',t)$ itself satisfies the Schrödinger equation (23.10), we can treat it as a wave function parameterized by the configuration point q'. In order to obtain a semiclassical approximation to the propagator we follow now the ideas developed in the last section. There is, however, one small complication: the initial condition (23.11) demands that the propagator at $t = 0$ is a δ-function at $q = q'$, that is, the amplitude is infinite at q' and the phase is not well defined. Our hypothetical cloud of particles is thus initially localized at $q = q'$ with *any* initial velocity. This is in contrast to the situation in the previous section where we assumed that the particles at a given point q have well defined velocity (or a discrete set of velocities) given by $\dot{q} = \partial_p H(q,p)$. We will now derive at a semiclassical expression for $K(q,q',t)$ by considering the propagator for short times first, and extrapolating from there to arbitrary times t.

For infinitesimally short times dt away from the singular point $t = 0$ we

assume that it is again possible to write the propagator in terms of a well defined phase and amplitude, that is

$$K(q,q',dt) = A(q,q',dt)e^{\frac{i}{\hbar}R(q,q',dt)}\,.$$

As all particles start at $q = q'$, $R(q,q',dt)$ will be of the form (23.30), that is

$$R(q,q',dt) = p\dot{q}dt - H(q,p)dt\,, \tag{23.41}$$

with $\dot{q} \approx (q - q')/dt$. For Hamiltonians of the form (23.2) we have $\dot{q} = p/m$, which leads to

$$R(q,q',dt) = \frac{m(q-q')^2}{2dt} - V(q)dt\,.$$

Inserting this into our ansatz for the propagator we obtain

$$K_{sc}(q,q',dt) \approx A(q,q',dt)e^{\frac{i}{\hbar}\left(\frac{m}{2dt}(q-q')^2 - V(q)dt\right)}\,. \tag{23.42}$$

For infinitesimal times we can neglecting the term $-V(q)dt$, so $K_{sc}(q,q',dt)$ is a d-dimensional gaussian with width $\sigma^2 = i\hbar dt/m$. This gaussian is a finite width approximation to the Dirac delta function if $A = (m/2\pi i\hbar dt)^{d/2}$, with $A(q,q',dt)$ fixed by the Dirac delta function normalization condition. The correctly normalized propagator for short times dt is therefore

23.8 on p. 483

$$K_{sc}(q,q',dt) \approx \left(\frac{m}{2\pi i\hbar dt}\right)^{d/2} e^{\frac{i}{\hbar}\left(\frac{m(q-q')^2}{2dt} - V(q)dt\right)}\,. \tag{23.43}$$

The short time dynamics of the Lagrangian manifold $(q, \partial_q R)$ which corresponds to the quantum propagator can now be deduced from (23.41); one obtains

$$\frac{\partial R}{\partial q} = p \approx \frac{m}{dt}(q - q')\,,$$

that is the particles start for short times on a Lagrangian manifold which is a plane in phase space, see fig. 23.5. Note, that for $dt \to 0$, this plane is given by the condition $q = q'$, that is, particles start on a plane parallel to the momentum axis. As we have already noted. all particles start at $q = q'$ but with different

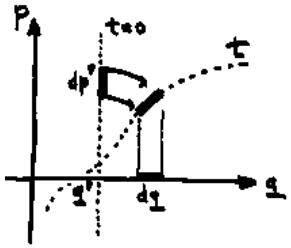

Figure 23.5: Evolution of the semiclassical propagator. The configuration which corresponds to the initial conditions of the propagator is a Lagrangian manifold $q = q'$, that is, a plane parallel to the p axis. The hypothetical particles are thus initially all placed at q' but take on all possible momenta p'. The Jacobian matrix C (23.46) relates an initial volume element in momnetum space dp' to a final configuration space volume dq.

velocities for $t = 0$. The slope of the Lagrangian plane for a short finite time is given as

$$\frac{\partial p_i}{\partial q_j} = -\frac{\partial^2 R}{\partial q_j \partial q'_i} = -\frac{\partial p'_i}{\partial q_j} = \frac{m}{dt}\delta_{ij}\,.$$

The prefactor $(m/dt)^{d/2}$ in (23.43) can therefore be interpreted as the determinant of the Jacobian of the transformation from final position coordinates q to initial momentum coordinates p', that is

$$K_{sc}(q, q', dt) = \frac{1}{(2\pi i\hbar)^{d/2}}|\det C|^{1/2} e^{iR(q,q',dt)/\hbar}, \tag{23.44}$$

where

$$C(q, q', dt)_{ij} = \left.\frac{\partial p'_j}{\partial q_i}\right|_{t,q'} = -\frac{\partial^2 R(q, q', dt)}{\partial q_i \partial q'_j} \tag{23.45}$$

The subscript $\cdots|_t$ indicates that the partial derivatives are to be evaluated with t, q' fixed.

The propagator in (23.44) that has been obtained for short times is, however, already more or less in its final form. We only have to evolve our short time approximation of the propagator according to (23.40)

$$K_{sc}(q'', q', t' + dt) = \sum_j |\det \mathbf{j}_j(q'', q, t')|^{1/2} e^{iR_j(q'',q,t')/\hbar - i\pi m_j(q'',q,t')/2} K(q_j, q'_j, dt)\,,$$

and we included here already the possibility that the phase becomes multi-valued, that is, that there is more than one path from q' to q''. The topological index $m_j = m_j(q'', q', t)$ is the number of singularities in the Jacobian along the trajectory j

from q' to q''. We can write $K_{sc}(q'', q', t' + dt)$ in closed form using the fact that $R(q'', q, t') + R(q, q', dt) = R(q'', q', t' + dt)$ and the multiplicativity of Jacobian determinants, that is

$$\begin{aligned}\det \mathbf{j}(q'', q, t) \det C(q, q', t) &= \det \left.\frac{\partial q}{\partial q''}\right|_t \det \left.\frac{\partial p'}{\partial q}\right|_{q',dt} \\ &= \det \left.\frac{\partial p'}{\partial q''}\right|_{q',t'+dt} = \det C(q'', q', t' + dt)\end{aligned} \tag{23.46}$$

The final form of the semiclassical or *Van Vleck propagator*, is thus

$$K_{sc}(q, q', t) = \sum_j \frac{1}{(2\pi i\hbar)^{d/2}}|\det C_j(q, q', t)|^{1/2} e^{iR_j(q,q',t)/\hbar - im_j\pi/2}\,. \tag{23.47}$$

This Van Vleck propagator is the essential ingredient of the semiclassical quantization to follow.

The apparent simplicity of the semiclassical propagator is deceptive. The wave function is not evolved simply by multiplying by a complex number of magnitude $\sqrt{\det \partial q'/\partial q}$ and phase $R(q, q', t)$; the more difficult task in general is to find the trajectories connecting q' and q in a given time t.

In addition, we have to treat the approximate propagator (23.47) with some care. Unlike the full quantum propagator which satisfies the group property (23.9) exactly the semiclassical propagator performs this only approximately, that is

$$K_{sc}(q, q', t_1 + t_2) \approx \int dq''\, K_{sc}(q, q'', t_2) K_{sc}(q'', q', t_1)\,. \tag{23.48}$$

The connection can be made explicit by the stationary phase approximation, which we will discuss in sect. 23.4.1. Approximating the integral in (23.48) by integrating only over regions near points q'' at which the phase is stationary, leads to the stationary phase condition

$$\frac{\partial R(q, q'', t_2)}{\partial q''_i} + \frac{\partial R(q'', q, t_1)}{\partial q''_i} = 0. \tag{23.49}$$

Classical trajectories contribute whenever the final momentum for a path from q' to q'' and the initial momentum for a path from q'' to q coincide. We will treat the method of stationary phase in more detail in sect. 23.4.1. Unlike the classical evolution of sect. 8.2, the semiclassical evolution is not an evolution by linear operator multiplication, but evolution supplemented by a stationary phase condition $p_{out} = p_{in}$ that matches up the classical momenta at each evolution step.

?? on p. ??

23.3.1 Free particle propagator

To develop some intuition about the above formalism, consider the case of a free particle. For a free particle the potential energy vanishes, the kinetic energy is $\frac{m}{2}\dot{q}^2$, and the Hamilton's principal function (23.30) is

$$R(q,q',t) = \frac{m(q-q')^2}{2t}\,. \tag{23.50}$$

The matrix $C(q,q',t)$ from (23.45) can be evaluated explicitly, and the Van Vleck propagator is

$$K_{sc}(q,q',t) = \left(\frac{m}{2\pi i\hbar t}\right)^{d/2} e^{im(q-q')^2/2\hbar t}\,, \tag{23.51}$$

identical to the short times propagator (23.43), with $V(q)=0$. This case is rather exceptional: for a free particle the semiclassical propagator turns out to be the exact quantum propagator $K(q,q',t)$, as can be checked by substitution in the Schrödinger equation (23.20). The Feynman path integral formalism uses this fact to construct an exact quantum propagator by integrating the free particle propagator (with $V(q)$ treated as constant for short times) along all possible (not necessary classical) paths from q' to q, see also remark 23.3.

23.9 on p. 484
23.10 on p. 484
23.11 on p. 484

23.4 Semiclassical Green's function

So far we have derived semiclassical formulas for the time evolution of wave functions, that is, we obtained approximate solutions to the time dependent Schrödinger equation (23.1). Even though we assumed in the calculation a time independent Hamiltonian of the special form (23.2), the derivation leads to the same final result (23.47) were one to consider more complicated or explicitly time dependent Hamiltonians. The propagator is thus important when we are interested in finite time quantum mechanical effects. For time independent Hamiltonians, the time dependence of the propagator as well as of wave functions is, however, essentially given in terms of the energy eigen-spectrum of the system, as in (23.6). It is therefore adventageous to switch from a time representation to an energy representation, that is from the propagator (23.8) to the energy dependent Green's function (23.12). A semiclassical approximation of the Green's function $G_{sc}(q,q',E)$ is given by the Laplace transform (23.12) of the Van Vleck propagator $K_{sc}(q,q',t)$:

$$G_{sc}(q,q',E) = \frac{1}{i\hbar}\int_0^\infty dt\, e^{iEt/\hbar} K_{sc}(q,q',t)\,. \tag{23.52}$$

The expression as it stands is not very useful; in order to evaluate the integral at least approximately we need the method of stationary phase next which we introduce next.

23.4.1 Method of stationary phase

Semiclassical approximations are often based on saddlepoint evaluations of integrals of the type

$$I = \int d^d x\, A(x)\, e^{is\Phi(x)} \tag{23.53}$$

where s is assumed to be a large, real parameter and $\Phi(x)$ is a real-valued function. For large s the phase oscillates rapidly and "averages to zero" everywhere except at the *extremal points* $\Phi'(x_0)=0$, $\Phi''(x_0)\neq 0$. The method of approximating the integral by its values at extremal points is therefore often called *method of stationary phase*. Restricting ourselves to one-dimensional integrals first, we expand $\Phi(x_0+\delta x)$ around x_0 to second order in δx, and write

$$I = \int dx\, A(x)\, e^{is(\Phi(x_0)+\frac{1}{2}\Phi''(x_0)\delta x^2+\ldots)}\,.$$

If $A(x)$ varies slowly around x_0 compared to the exponential function we may retain the leading term in an expansion of the amplitude and up to quadratic terms in the phase approximate the integral I by

$$I \approx A(x_0)e^{is\Phi(x_0)}\int_{-\infty}^{\infty} dx\, e^{is\Phi''(x_0)\frac{x^2}{2}} = A(x_0)\left(\frac{2\pi}{s|\Phi''(x_0)|}\right)^{1/2} e^{\frac{\pm i\pi}{4}}\,, \tag{23.54}$$

where $\pm$ corresponds to positive/negative sign of $\Phi''(x_0)$. The integral (23.54) is known as a *Fresnel integral*. Generalizing this method to d dimensions, consider stationary phase points fulfilling

23.12 on p. 484

$$\frac{d}{dx_i}\Phi(x)\bigg|_{x=x_0} = 0 \quad \forall i = 1,\ldots d\,.$$

An expansion of the phase up to second order involves now the symmetric matrix of second derivatives of $\Phi(x)$, that is

$$D_{ij}(x_0) = \frac{\partial^2}{\partial x_i \partial x_j}\Phi(x)\bigg|_{x=x_0}\,.$$

After choosing a suitable coordinate system which diagonalises D, we can approximate the d-dimensional integral by d one-dimensional Fresnel integrals; the stationary phase estimate of (23.53) is then

$$I \approx \sum_{x_0} (2\pi i/s)^{d/2} |\det D(x_0)|^{-1/2} A(x_0)\, e^{is\Phi(x_0) - \frac{i\pi}{2} m(x_0)}\,, \tag{23.55}$$

where the sum runs over all stationary phase points x_0 of $\Phi(x)$ and $m(x_0)$ counts the number of negative eigenvalues of $\mathbf{D}(x_0)$.

23.13 on p. 484

The stationary phase approximation is all that is needed for the semiclassical approximation, with the proviso that D in (23.55) has no zero eigenvalues.

23.14 on p. 484

23.15 on p. 485

23.4.2 Long trajectories

When evaluating the integral (23.52) approximately we have to distinguish between two types of contributions: those coming from stationary points of the phase and those coming from infinitesimally short times. The first type of contributions can be obtained by stationary phase approximation and will be treated in this section. The latter originate from the singular behavior of the propagator for $t \to 0$ where the assumption that the amplitude changes slowly compared to the phase is no longer valid. The short time contributions therefore have to be treated separately, which we will do in sect. 23.4.3.

The stationary phase points t^* of the integrand in (23.52) are given by the condition

$$\frac{\partial}{\partial t} R(q,q',t^*) + E = 0\,. \tag{23.56}$$

We recognize this condition as the solution of (23.35), the time $t^* = t^*(q,q',E)$ in which a particle of energy E starting out in q' reaches q. Taking into account the second derivative of the phase evaluated at the stationary phase point,

$$R(q,q',t) + Et = R(q,q',t^*) + \frac{1}{2}(t-t^*)^2 \frac{\partial^2}{\partial t^2} R(q,q',t^*) + \cdots$$

the stationary phase approximation of the integral corresponding to a specific branch j of the Van Vleck propagator (23.47) yields

$$G_j(q,q',E) = \frac{1}{i\hbar(2i\pi\hbar)^{(d-1)/2}} \left| \det C_j \left(\frac{\partial^2 R_j}{\partial t^2} \right)^{-1} \right|^{1/2} e^{\frac{i}{\hbar} S_j - \frac{i\pi}{2} m_j}\,, \tag{23.57}$$

where $m_j = m_j(q,q',E)$ now includes a possible additional phase arising from the time stationary phase integration (23.54), and $C_j = C_j(q,q',t^*)$, $R_j = R_j(q,q',t^*)$ are evaluated at the transit time t^*. We re-express the phase in terms of the energy dependent action (23.33)

$$S(q,q',E) = R(q,q',t^*) + Et^*\,, \qquad \text{with} \quad t^* = t^*(q,q',E)\,, \tag{23.58}$$

the Legendre transform of the Hamilton's principal function. Note that the partial derivative of the action (23.58) with respect to q_i

$$\frac{\partial S(q,q',E)}{\partial q_i} = \frac{\partial R(q,q',t^*)}{\partial q_i} + \left(\frac{\partial R(q,q',t)}{\partial t^*} + E \right) \frac{\partial t}{\partial q_i}.$$

is equal to

$$\frac{\partial S(q,q',E)}{\partial q_i} = \frac{\partial R(q,q',t^*)}{\partial q_i}, \tag{23.59}$$

due to the stationary phase condition (23.56), so the definition of momentum as a partial derivative with respect to q remains unaltered by the Legendre transform from time to energy domain.

23.17 on p. 485

Next we will simplify the amplitude term in (23.57) and rewrite it as an explicit function of the energy. Consider the $[(d+1)\times(d+1)]$ matrix

$$D(q,q',E) = \begin{pmatrix} \frac{\partial^2 S}{\partial q' \partial q} & \frac{\partial^2 S}{\partial q' \partial E} \\ \frac{\partial^2 S}{\partial q \partial E} & \frac{\partial^2 S}{\partial E^2} \end{pmatrix} = \begin{pmatrix} -\frac{\partial p'}{\partial q} & -\frac{\partial p'}{\partial E} \\ \frac{\partial t}{\partial q} & \frac{\partial t}{\partial E} \end{pmatrix}, \tag{23.60}$$

where $S = S(q,q',E)$ and we used (23.31–23.34) here to obtain the left hand side of (23.60). The minus signs follow from observing from the definition of (23.32) that $S(q,q',E) = -S(q',q,E)$. Note that D is nothing but the Jacobian matrix of the coordinate transformation $(q,E) \to (p',t)$ for fixed q'. We can therefore use the multiplication rules of determinants of Jacobians, which are just ratios of volume elements, to obtain

$$\begin{aligned} \det D &= (-1)^{d+1} \left\| \frac{\partial(p',t)}{\partial(q,E)} \right\|_{q'} = (-1)^{d+1} \left\| \frac{\partial(p',t)}{\partial(q,t)} \frac{\partial(q,t)}{\partial(q,E)} \right\|_{q'} \\ &= (-1)^{d+1} \left\| \frac{\partial p'}{\partial q} \right\|_{t,q'} \left\| \frac{\partial t}{\partial E} \right\|_{q',q} = -\det C \left(\frac{\partial^2 R}{\partial t^2} \right)^{-1}. \end{aligned}$$

23.18 on p. 485

We use here the notation $\|.\|_{q',t}$ for a Jacobian determinant with partial deriva-

tives evaluated at t, q' fixed, and likewise for other subscripts. Using the relation (23.36) which relates the term $\frac{\partial t}{\partial E}$ to $\partial_t^2 R$ we can write the determinant of D as a product of the Van Vleck determinant (23.45) and the amplitude factor arising from the stationary phase approximation. The amplitude in (23.57) can thus be interpreted as the determinant of a Jacobian of a coordinate transformation which includes time and energy as independent coordinates. This causes the increase in the dimensionality of the matrix D relative to the Van Vleck determinant (23.45).

We can now write down the semiclassical approximation of the contribution of the jth trajectory to the Green's function (23.57) in explicitly energy dependent form:

$$G_j(q,q',E) = \frac{1}{i\hbar(2i\pi\hbar)^{(d-1)/2}} \left|\det D^j\right|^{1/2} e^{\frac{i}{\hbar}S_j - \frac{i\pi}{2}m_j} \,. \tag{23.61}$$

However, for no purposes this is still not the most convenient form of the Green's function.

The trajectory contributing to $G_j(q,q',E)$ is constrained to a given energy E, and will therefore be on a phase space manifold of constant energy, that is $H(q,p) = E$. Writing this condition as partial differential equation for $S(q,q',E)$, that is

$$H(q, \frac{\partial S}{\partial q}) = E \,,$$

one obtains

$$\begin{aligned} \frac{\partial}{\partial q_i'} H(q,p) &= 0 = \frac{\partial H}{\partial p_j}\frac{\partial p_j}{\partial q_i'} = \dot{q}_j \frac{\partial^2 S}{\partial q_j \partial q_i'} \\ \frac{\partial}{\partial q_i} H(q',p') &= 0 = \frac{\partial^2 S}{\partial q_i \partial q_j'}\dot{q}_j' \,, \end{aligned} \tag{23.62}$$

that is the sub-matrix $\partial^2 S/\partial q_i \partial q_j'$ has (left- and right-) eigenvectors corresponding to an eigenvalue 0. In the local coordinate system

$$\mathbf{q} = (q_\parallel, q_{\perp 1}, q_{\perp 2}, \cdots, q_{\perp(d-1)}) \,, \qquad \text{with} \quad \dot{\mathbf{q}} = (\dot{q}, 0, 0, \cdots, 0)$$

in which the longitudinal coordinate axis $q_\parallel$ points along the velocity vector $\dot{q}$, the matrix of variations of $S(q,q',E)$ has a column and a row of zeros as (23.62) takes form

$$\dot{q}\frac{\partial^2 S}{\partial q_\parallel \partial q_i'} = \frac{\partial^2 S}{\partial q_i \partial q_\parallel'}\dot{q}' = 0 \,.$$

The initial and final velocities are non-vanishing except for points $|\dot{q}| = 0$. These are the turning points (where all energy is potential), and we assume that neither q nor q' is a turning point (in our application - periodic orbits - we can always chose $q = q'$ not a truning point). In the local coordinate system with one axis along the trajectory and all other perpendicular to it the determinant of (23.60) is of the form

$$\det D(q,q',E) = (-1)^{d+1} \begin{Vmatrix} 0 & 0 & \frac{\partial^2 S}{\partial E \partial q_\parallel'} \\ 0 & \frac{\partial^2 S}{\partial q_\perp \partial q_\perp'} & * \\ \frac{\partial^2 S}{\partial q_\parallel \partial E} & * & * \end{Vmatrix} \,. \tag{23.63}$$

The corner entries can be evaluated using (23.34)

$$\frac{\partial^2 S}{\partial q_\parallel \partial E} = \frac{\partial}{\partial q_\parallel} t = \frac{1}{\dot{q}} \,, \qquad \frac{\partial^2 S}{\partial E \partial q_\parallel'} = \frac{1}{\dot{q}'} \,.$$

As the $q_\parallel$ axis points along the velocity direction, velocities $\dot{q}$, $\dot{q}'$ are by construction almost always positive non-vanishing numbers. In this way the determinant of the $[(d+1)\times(d+1)]$ dimensional matrix $D(q,q',E)$ can essentially be reduced to the determinant of a $[(d-1)\times(d-1)]$ dimensional *transverse* matrix $D_\perp(q,q',E)$

$$\begin{aligned} \det D(q,q',E) &= \frac{1}{\dot{q}\dot{q}'} \det D_\perp(q,q',E) \\ D_\perp(q,q',E)_{ik} &= -\frac{\partial^2 S(q,q',E)}{\partial q_{\perp i} \partial q_{\perp k}'} \,. \end{aligned} \tag{23.64}$$

Putting everything together we obtain the jth trajectory contribution to the semiclassical Green's function

23.19 on p. 485

$$G_j(q,q',E) = \frac{1}{i\hbar(2\pi\hbar)^{(d-1)/2}} \frac{1}{|\dot{q}\dot{q}'|^{1/2}} \left|\det D_\perp^j\right|^{1/2} e^{\frac{i}{\hbar}S_j - \frac{i\pi}{2}m_j} \,, \tag{23.65}$$

where the topological index $m_j = m_j(q,q',E)$ now counts the number of changes of sign of $\det D_\perp^j$ along the trajectory j which connects q' to q at energy E. The velocities $\dot{q}$, $\dot{q}'$ also depend on (q,q',E) and the trajectory j. While in the case of the propagator the initial momentum variations $\delta p'$ are unrestricted, for the Green's function the $(\delta q', \delta p')$ variations are restricted to the constant energy shell; the appearance of the $1/\dot{q}\dot{q}'$ weights in the Green's function can be traced to this constraint.

23.4.3 Short trajectories

The stationary phase method cannot be used when t^* is small, both because we cannot extend the integration in (23.54) to $-\infty$, and because the amplitude of $K(q,q',t)$ is divergent. In this case we have to evaluate the integral involving the short time form of the exact quantum mechanical propagator (23.43)

$$G_0(q,q',E) = \frac{1}{i\hbar}\int_0^\infty dt \left(\frac{m}{2\pi i\hbar t}\right)^{d/2} e^{\frac{i}{\hbar}(\frac{m(q-q')^2}{2t} - V(q)t + Et)}.$$

By introducing a dimensionless variable $\tau = t\sqrt{2m(E-V(q))}/m|q-q'|$, the integral can be rewritten as

$$G_0(q,q',E) = \frac{m}{i\hbar^2(2\pi i)^{d/2}}\left(\frac{\sqrt{2m(E-V)}}{\hbar|q-q'|}\right)^{\frac{d}{2}-1}\int_0^\infty \frac{d\tau}{\tau^{d/2}} e^{\frac{i}{2\hbar}S_0(q,q',E)(\tau+1/\tau)},$$

where $S_0(q,q',E) = \sqrt{2m(E-V)}|q-q'|$ is the short distance form of the action. Using the integral representation of the Hankel function of first kind

$$H_\nu^+(z) = -\frac{i}{\pi}e^{-i\nu\pi/2}\int_0^\infty e^{\frac{1}{2}iz(\tau+1/\tau)}\tau^{-\nu-1}d\tau$$

we can write the short distance form of the Green's function as

$$G_0(q,q',E) \approx -\frac{im}{2\hbar^2}\left(\frac{\sqrt{2m(E-V)}}{2\pi\hbar|q-q'|}\right)^{\frac{d-2}{2}} H^+_{\frac{d-2}{2}}(S_0(q,q',E)/\hbar). \qquad (23.66)$$

There is nothing sacred about the Hankel function - it is merely a useful observation, as for special functions the short wavelength asymptotics comes for free and can be found in standard reference books. The short distance Green's function approximation is valid when $S_0(q,q',E) \leq \hbar$.

Commentary

Remark 23.1 Limit $\hbar \to 0$. The semiclassical limit "$\hbar \to 0$" discussed in sect. 23.2 is a shorthand notation for the limit in which typical quantities like the actions R or S in semiclassical expressions for the propagator or the Green's function become large compared to $\hbar$. In the world that we live in the quantity $\hbar$ is a fixed physical constant whose value [6] is $1.054571596(82)\,10^{-34}$ Js.

Remark 23.2 Madelung's fluid dynamics. A very different interpretation of (23.21–23.22) has been given by Madelung [2], and then built upon by Bohm [4] and others [32, 5]. Keeping the $\hbar$ dependent term in (23.21), the ordinary differential equations driving the flow (23.28) have to be altered; if the Hamiltonian can be written as kinetic plus potential term $V(q)$ as in (23.2), the $\hbar^2$ term modifies the p equation of motion as

$$\dot{p_i} = -\frac{\partial}{\partial q_i}\left(V(q) + Q(q,t)\right), \qquad (23.67)$$

where, for the example at hand,

$$Q(q,t) = -\frac{\hbar^2}{2m}\frac{1}{\sqrt{\rho}}\frac{\partial^2}{\partial q^2}\sqrt{\rho} \qquad (23.68)$$

interpreted by Bohm [4] as the "quantum potential". Madelung observed that Hamilton's equation for the momentum (23.67) can be rewritten as

$$\frac{\partial v_i}{\partial t} + \left(v\cdot\frac{\partial}{\partial q}\right)v_i = -\frac{1}{m}\frac{\partial V}{\partial q_i} - \frac{1}{m\rho}\frac{\partial}{\partial q_j}\sigma_{ij}, \qquad (23.69)$$

where $\sigma_{ij} = \frac{\hbar^2\rho}{4m}\frac{\partial^2 \ln\rho}{\partial q_i \partial q_j}$ is the "pressure" stress tensor, $v_i = p_i/m$, and $\rho = A^2$ as defined [32] in sect. 23.2.3. We recall that the Eulerian $\frac{\partial}{\partial t} + \frac{\partial q_i}{\partial t}\frac{\partial}{\partial q_i}$ is the ordinary derivative of Lagrangian mechanics, that is $\frac{d}{dt}$. For comparison, the Euler equation for classical hydrodynamics is

$$\frac{\partial v_i}{\partial t} + \left(v\cdot\frac{\partial}{\partial q}\right)v_i = -\frac{1}{m}\frac{\partial V}{\partial q_i} - \frac{1}{m\rho}\frac{\partial}{\partial q_j}(p\delta_{ij}),$$

where $p\delta_{ij}$ is the pressure tensor.

The classical dynamics corresponding to quantum evolution is thus that of an "hypothetical fluid" experiencing $\hbar$ and ρ dependent stresses. The "hydrodynamic" interpretation of quantum mechanics has, however, not been very fruitful in practice.

Remark 23.3 Path integrals. The semiclassical propagator (23.47) can also be derived from Feynman's path integral formalism. Dirac was the first to discover that in the short-time limit the quantum propagator (23.51) is exact. Feynman noted in 1946 that one can construct the exact propagator of the quantum Schrödinger equation by formally summing over all possible (and emphatically not classical) paths from q' to q, .

Gutzwiller started from the path integral to rederive Van Vleck's semiclassical expression for the propagator; Van Vleck's original derivation is very much in the spirit of what has presented in this chapter. He did, however, not consider the possibility of the formation of caustics or folds of Lagrangian manifolds and thus did not include the topological phases in his semiclassical expression for the propagator. Some 40 years later Gutzwiller [22] added the topolagical indices when deriving the semiclassical propagator from Feynman's path integral by stationary phase conditions.

Résumé

The aim of the semiclassical or short-wavelength methods is to approximate a solution of the Schrödinger equation with a semi-classical wave function

$$\psi_{sc}(q,t) = \sum_j A_j(q,t) e^{iR_j(q,t)/\hbar} ,$$

accurate to the leading order in $\hbar$. Here the sum is over all classical trajectories that connect the initial point q' to the final point q in time t. "Semi–" refers to $\hbar$, the quantum unit of phase in the exponent. The quantum mechanics enters only through this atomic scale, in units of which the variation of the phase across the classical potential is assumed to be large. "–classical" refers to the rest - both the amplitudes $A_j(q,t)$ and the phases $R_j(q,t)$ - which are determined by the classical Hamilton-Jacobi equations.

In the semiclassical approximation the quantum time evolution operator is given by the *semiclassical propagator*

$$K_{sc}(q,q',t) = \frac{1}{(2\pi i\hbar)^{d/2}} \sum_j \left\|\partial p'/\partial q\right\|_j^{1/2} e^{\frac{i}{\hbar}R_j - \frac{i\pi}{2}m_j} ,$$

where the topological index $m_j(q,q',t)$ counts the number of the direction reversal along the jth classical trajectory that connects $q' \to q$ in time t. Until very recently it was not possible to resolve quantum evolution on quantum time scales (such as one revolution of electron around a nucleus) - physical measurements are almost always done at time scales asymptotically large compared to the intrinsic quantum time scale. Formally this enformtion is extracted by means of a Laplace transform of the propagator which yields the energy dependent *semiclassical Green's function*

$$G_{sc}(q,q',E) = G_0(q,q',E) + \frac{1}{i\hbar(2\pi i\hbar)^{\frac{(d-1)}{2}}} \sum_j \frac{\left\|\partial p'_\perp/\partial q_\perp\right\|_j^{1/2}}{\left|\dot{q}\dot{q}'\right|_j^{1/2}} e^{i\frac{R_j}{\hbar} - im_j\frac{\pi}{2}} \quad (23.70)$$

where $G_0(q,q',E)$ is the contribution of short trajectories with $S_0(q,q',E) \leq \hbar$, while the sum is over the contributions of long trajectories (23.65) going from q' to q with fixed energy E, with $S_j(q,q',E) \gg \hbar$.

References

[23.1] A. Einstein, "On the Quantum Theorem of Sommerfeld and Epstein," p. 443, English translation of "Zum Quantensatz von Sommerfeld und Epstein", *Verh. Deutsch. Phys. Ges.* **19**, 82 (1917), in *The Collected Papers of Albert Einstein*, Vol. **6**: *The Berlin Years: Writings, 1914-1917*, A. Engel, transl. and E. Schucking, ed. (Princeton University Press, Princeton, New Jersey 1997).

[23.2] E. Madelung, *Zeitschr. fr Physik* **40**, 332 (1926).

[23.3] E. Schrödinger, *Annalen der Physik* **79**, 361, 489; **80**, 437; **81**, 109 (1926).

[23.4] D. Bohm, *Phys. Rev.* **85**, 166 (1952).

[23.5] P.R. Holland, *The quantum theory of motion - An account of the de Broglie-Bohm casual interpretation of quantum mechanics* (Cambridge Univ. Press, Cambridge 1993).

[23.6] `http://physics.nist.gov/cgi-bin/cuu`

Exercises

Exercise 23.1 **Dirac delta function, Lorentzian representation.** *Derive Eq. (23.15).*

Exercise 23.2 **WKB ansatz.** *Try to show that no other ansatz gives a meaningful definition of the momentum in the $\hbar \to 0$ limit.*

Exercise 23.3 **1-dimensional harmonic oscillator.** *Take a 1-dimensional harmonic oscillator $U(q) = \frac{1}{2}kq^2$. Take a WKB wave function of form $A(q,t) = a(t)$ and $R(q,t) = r(t) + b(t)q + c(t)q^2$, where $r(t), a(t), b(t)$ and $c(t)$ are time dependent coefficients. Derive ordinary differential equations by using (23.21) and (23.22) and solve them.*

Exercise 23.4 **1-dimensional linear potential.** *Take a 1-dimensional linear potential $U(q) = -Fq$. Take a WKB wave function of form $A(q,t) = a(t)$ and $R(q,t) = r(t) + b(t)q + c(t)q^2$, where $r(t), a(t), b(t)$ and $c(t)$ are time dependent coefficients. Derive and solve the ordinary differential equations from (23.21) and (23.22).*

Exercise 23.5 **d-dimensional quadratic potentials.** *Generalize the above method to general d-dimensional quadratic potentials.*

Exercise 23.6 **Free particle Hamilton's principal function.** *Calculate $R(q, q', t)$ for*

a) a d-dimensional free particle

b) a 3-dimensional particle in constant magnetic field

c) a 1-dimensional harmonic oscillator.

Exercise 23.7 **Time evolution of R.** *Calculate the time evolution of $R(q,0) = a + bq + cq^2$ for a 1-dimensional harmonic oscillator using (23.30) and (23.31).*

Exercise 23.8 **Dirac delta function, gaussian representation.** *Consider the gaussian distribution function*

$$\delta_\sigma(z) = \frac{1}{\sqrt{2\pi\sigma^2}} e^{-z^2/2\sigma^2} .$$

Show that in $\sigma \to 0$ limit this is the Dirac delta function (??).

Exercise 23.9 **d-dimensional free particle propagator.** *Verify the results in sect. 23.3.1; show explicitely that (23.51), the semiclassical Van Vleck propagator in d dimensions, solves the Schrödinger's equation.*

Exercise 23.10 **Charged particle in constant magnetic field.** *Calculate the semiclassical propagator for a charged particle in constant magnetic field in 3 dimensions. Verify that the semiclassical expression coincides with the exact solution.*

Exercise 23.11 **1-dimensional harmonic oscillator propagator.** *Calculate the semiclassical propagator for a 1-dimensional harmonic oscillator and verify that it is identical to the exact quantum propagator.*

Exercise 23.12 **Fresnel integral.** *Show that*

$$\int_{-\infty}^{\infty} dx\, e^{iax^2/2} = \left(\frac{2\pi}{|a|}\right)^{1/2} e^{\frac{i\pi m}{4}} \tag{23.71}$$

where $m = a/|a|$ is the sign of a.

Exercise 23.13 **d-dimensional gaussian integrals.** *Show that the gaussian integral in d-dimensions is given by*

$$\frac{1}{(2\pi)^{d/2}} \int d^d x e^{-\frac{1}{2}x^T\cdot M^{-1}\cdot x + x\cdot J} \;=\; |\det M|^{\frac{1}{2}}\, e^{\frac{1}{2}J^T\cdot M\cdot J}\,, \tag{23.72}$$

where M is a real positive definite $[d\times d]$ matrix, that is a matrix with strictly positive eigenvalues. x, J are d-dimensional vectors, on x^T is the transpose of x.

Exercise 23.14 **Stationary phase approximation.** *All semiclassical approximations are based on saddlepoint evaluations of integrals of type*

$$I = \int d^d x A(x) e^{i\Phi(x)/\hbar} \tag{23.73}$$

for small values of $\hbar$. Obtain the stationary phase estimate

$$I \approx \sum_n A(x_n) e^{i\Phi(x_n)/\hbar} \frac{(2\pi i\hbar)^{d/2}}{\sqrt{\det \mathbf{D}^2\Phi(x_n)}},$$

where $\mathbf{D}^2\Phi(x_n)$ denotes the second derivative matrix.

Exercise 23.15 **Sterling formula for $n!$.** *Compute an approximate value of $n!$ for large n with the help of stationary phase approximation. Hint: $n! = \int_0^\infty dt\, t^{n-1} e^{-t}$.*

Exercise 23.16 **Airy function for large arguments.** *Important contributions as stationary phase points may arise from extremal points where the first non-zero term in a Taylor expansion of the phase is of third or higher order. Such situations occur, for example, at bifurcation points or in diffraction effects, (such as waves near sharp corners, waves creeping around obstacles). In such calculations one meets Airy functions integrals of the form*

$$Ai(x) = \frac{1}{2\pi} \int_{-\infty}^{+\infty} dy\, e^{i(xy - \frac{y^3}{3})} \,. \tag{23.74}$$

Calculate the Airy function $Ai(x)$ by stationary phase approximation. What happens when considering the limit $x \to 0$. Estimate for which value of x the stationary phase approximation breaks down. Give it a go.

Exercise 23.17 **Free particle action.** *Calculate the energy dependent action for a free particle, a charged particle in a constant magnetic field and for the harmonic oscillator.*

Exercise 23.18 **A usefull determinant identity.** *Show that the following two determinants equal each other:*
$A[(n+1) \times (n+?)] determinant$

$$\det\left(M'_n\right) = \overset{n+1}{\begin{bmatrix} x_{1,1} & \dots & x_{1,n} & y_1 \\ \vdots & \ddots & \vdots & \vdots \\ x_{n,1} & \dots & x_{n,n} & y_n \\ z_1 & \dots & z_n & E \end{bmatrix}}_{n+1} \tag{23.75}$$

and the $[n \times n]$ determinant:

$$E \det\left(M_n\right) = E \overset{n}{\begin{bmatrix} x_{1,1} - y_1 z_1 E^{-1} & \dots & x_{1,n} - y_1 z_n E^{-1} \\ \vdots & \ddots & \vdots \\ x_{n,1} - y_n z_1 E^{-1} & \dots & x_{n,n} - y_n z_n E^{-1} \end{bmatrix}}_{n} \tag{23.76}$$

Exercise 23.19 **Free particle semiclassical Green's functions.** *Calculate the semiclassical Green's functions for the systems of exercise 23.17.*

Chapter 24

Semiclassical quantization

(G. Vattay, G. Tanner and P. Cvitanović)

> If there exist fewer than ℓ integrals of type (14), as is the case, for example, according to POINCARÉ in the three-body problem, then the p_i are not expressible by the q_i and the quantum condition of SOMMERFELD-EPSTEIN fails also in the slightly generalized form that has been given here.
>
> A. Einstein

We derive here the Gutzwiller trace formula and the semiclassical zeta function, the central results of the semiclassical quantization of classically chaotic systems. In chapter **??** we will rederive these formulas for the case of scattering in open systems. Quintessential wave mechanics effects such as creeping, diffraction and tunneling will be taken up in chapter 26.

24.1 Trace formula

Our next task is to evaluate the Green's function trace (23.13) of the semiclassical approximation. The trace

$$\operatorname{tr} G_{sc}(E) = \int d^d q\, G_{sc}(q,q,E) = \operatorname{tr} G_0(E) + \sum_j \int d^d q\, G_j(q,q,E)$$

receives contributions from "long" classical trajectories which start and end in q after finite time, and the "zero length" trajectories whose lengths approach zero as $q' \to q$.

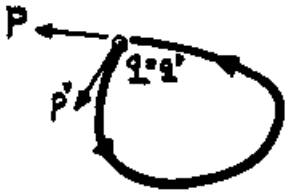

Figure 24.1: A returning trajectory in configuration space. The orbit is periodic in the full phase space only if the initial and the final momenta of a returning trajectory coincide as well.

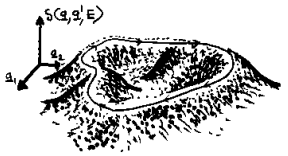

Figure 24.2: A romanticized sketch of $S_p(E) = S(q,q,E) = \oint p(q,E)dq$ landscape orbit. Unstable periodic orbits traverse isolated ridges and saddles of the mountainous landscape of the action $S(q_\parallel, q_\perp, E)$. Along a periodic orbit $S_p(E)$ is constant; in the transverse directions it generically changes quadratically.

First we work out the contributions coming from the finite time *returning* classical orbits, that is trajectories that originate and end at a given configuration point q. As we are identifying q with q', taking of a trace involves (still another!) stationary phase condition in the $q' \to q$ limit,

$$\left.\frac{\partial S_j(q,q',E)}{\partial q_i}\right|_{q'=q} + \left.\frac{\partial S_j(q,q',E)}{\partial q'_i}\right|_{q'=q} = 0\,,$$

meaning that the initial and final momenta (23.59) of contributing trajectories should coincide

$$p_j(q,q,E) - p'_j(q,q,E) = 0\,, \qquad q \in j\text{th periodic orbit}\,, \tag{24.1}$$

so the trace receives contributions only from those long classical trajectories which are *periodic* in the full phase space.

For a returning orbit the natural coordinate system is the intrinsic one, with $q_\parallel$ axis pointing in the $\dot q$ direction along the orbit, and $q_\perp$, the rest of the coordinates transverse to $\dot q$. The jth periodic orbit contribution to the trace of the semiclassical Green's function in the intrinsic coordinates is

$$\operatorname{tr} G_j(E) = \frac{1}{i\hbar(2\pi\hbar)^{(d-1)/2}} \oint_j \frac{dq_\parallel}{\dot q} \int_j d^{d-1}q_\perp |\det D_\perp^j|^{1/2} e^{\frac{i}{\hbar}S_j - \frac{i\pi}{2}m_j}\,,$$

where the integration in $q_\parallel$ goes from 0 to L_j, the geometric length of small tube around the orbit in the configuration space. As always, in the stationary phase

approximation we worry only about the fast variations in the phase $S_j(q_\parallel, q_\perp, E)$, and assume that the density varies smoothly and is well approximated by its value $D^j_\perp(q_\parallel, 0, E)$ on the classical trajectory, $q_\perp = 0$. The topological index $m(q_\parallel, q_\perp, E)$ is an integer which generically does not change in the infinitesimal neighborhood of an isolated periodic orbit.

The transverse integration is again carried out by the stationary phase method, with the phase stationary on the periodic orbit, $q_\perp = 0$. The result of the transverse integration can depend only on the parallel coordinate

$$\mathrm{tr}\, G_j(E) = \frac{1}{i\hbar} \oint \frac{dq_\parallel}{\dot q} \left| \frac{\det D_{\perp j}(q_\parallel, 0, E)}{\det D'_{\perp j}(q_\parallel, 0, E)} \right|^{1/2} e^{\frac{i}{\hbar} S_j - \frac{i\pi}{2} m_j},$$

where the new determinant in the denominator, $\det D'_{\perp j} =$

$$\det \left(\frac{\partial^2 S(q,q',E)}{\partial q_{\perp i} \partial q_{\perp j}} + \frac{\partial^2 S(q,q',E)}{\partial q'_{\perp i} \partial q_{\perp j}} + \frac{\partial^2 S(q,q',E)}{\partial q_{\perp i} \partial q'_{\perp j}} + \frac{\partial^2 S(q,q',E)}{\partial q'_{\perp i} \partial q'_{\perp j}} \right),$$

is the determinant of the second derivative matrix coming from the stationary phase integral in transverse directions.

The ratio $D_{\perp j}/D'_{\perp j}$ is here to enforce the periodic boundary condition for the semiclassical Green's function evaluated on a periodic orbit. It can be given a meaning in terms of the monodromy matrix of the periodic orbit by following observations

$$\begin{aligned} \det D_\perp &= \left\| \frac{\partial p'_\perp}{\partial q_\perp} \right\| = \left\| \frac{\partial (q'_\perp, p'_\perp)}{\partial (q_\perp, q'_\perp)} \right\| \\ \det D'_\perp &= \left\| \frac{\partial p_\perp}{\partial q_\perp} - \frac{\partial p'_\perp}{\partial q_\perp} + \frac{\partial p_\perp}{\partial q'_\perp} - \frac{\partial p'_\perp}{\partial q'_\perp} \right\| = \left\| \frac{\partial (p_\perp - p'_\perp, q_\perp - q'_\perp),}{\partial (q_\perp, q'_\perp)} \right\| . \end{aligned}$$

Defining the $2(d-1)$-dimensional transverse vector $x_\perp = (q_\perp, p_\perp)$ in the full phase space we can express the ratio

$$\begin{aligned} \frac{\det D'_\perp}{\det D_\perp} &= \left\| \frac{\partial (p_\perp - p'_\perp, q_\perp - q'_\perp)}{\partial (q'_\perp, p'_\perp)} \right\| = \left\| \frac{\partial (x_\perp - x'_\perp)}{\partial x'_\perp} \right\| \\ &= \det\, (\mathbf{J} - \mathbf{1}) \ , \end{aligned} \tag{24.2}$$

in terms of the monodromy matrix $\mathbf{J}$ for a surface of section transverse to the orbit within the constant energy $E = H(q,p)$ shell.

The classical periodic orbit action $S_j(E) = \oint p(q_\parallel, E) dq_\parallel$ does not depend on the starting point $q_\parallel$ along the orbit, see fig. 24.2. The eigenvalues of the monodromy matrix are independent of where $\mathbf{J}_j$ is evaluated along the orbit, so $\det(1 - \mathbf{J}_j)$ can also be taken out of the the $q_\parallel$ integral

$$\mathrm{tr}\, G_j(E) = \frac{1}{i\hbar} \sum_j \frac{1}{|\det(1 - \mathbf{J}_j)|^{1/2}} e^{r\left(\frac{i}{\hbar} S_j - \frac{i\pi}{2} m_j\right)} \oint \frac{dq_\parallel}{\dot q_\parallel} .$$

Here we have assumed that $\mathbf{J}_j$ has no marginal eigenvalues. The determinant of the monodromy matrix, the action $S_p(E) = \oint p(q_\parallel, E) dq_\parallel$ and the topological index are all classical invariants of the periodic orbit, independent of $q_\parallel$. The integral in the parallel direction we now do exactly.

First we take into account the fact that any repeat of a periodic orbit is also a periodic orbit. The action and the topological index are additive along the trajectory, so for rth repeat they simply get multiplied by r. The monodromy matrix of the rth repeat of a prime cycle p is (by the chain rule for derivatives) $\mathbf{J}_p^r$, where $\mathbf{J}_p$ is the prime cycle monodromy matrix. Let us denote the time period of the prime cycle p, the single, shortest traversal of a periodic orbit by T_p. The remaining integral can be carried out by change of variables $dt = dq_\parallel/\dot q(t)$

$$\int_0^{L_j} \frac{dq_\parallel}{\dot q(t)} = \int_0^{T_p} dt = T_p,$$

as the spatial integral corresponds to a single traversal. If you do not see why this is so, rethink the derivation of the classical trace formula (11.19) - that derivation takes only three pages of text. Regrettably, in the quantum case we do not know of an hones derivation that takes less 30 pages. The final result, the *Gutzwiller trace formula*

$$\mathrm{tr}\, G_{sc}(E) = \mathrm{tr}\, G_0(E) + \frac{1}{i\hbar} \sum_p T_p \sum_{r=1}^{\infty} \frac{1}{|\det(1 - \mathbf{J}_p^r)|^{1/2}} e^{r\left(\frac{i}{\hbar} S_p - \frac{i\pi}{2} m_p\right)}, \tag{24.3}$$

an expression for the trace of the semiclassical Green's function in terms of periodic orbits is beautiful in its simplicity and elegance.

The topological index $m_p(E)$ counts the number of changes of sign of the matrix of second derivatives evaluated along the prime periodic orbit p. By now we have gone through so many stationary phase approximations that you have surely lost track of what the total $m_p(E)$ actually is. The rule is this: The topological index of a closed curve in a 2-d phase space is the sum of the number

of times the partial derivatives $\frac{\partial p_i}{\partial q_i}$ for each dual pair (q_i, p_i), $i = 1, 2, \ldots, d$ (no sum on i) change their signs as one goes once around the curve.

We still have to evaluate $\mathrm{tr}\, G_0(E)$, the contribution coming from the infinitesimal trajectories. The real part of $\mathrm{tr}\, G_0(E)$ is infinite in the $q' \to q$ limit, so it makes no sense to write it down explicitly here. However, the imaginary part is finite, and plays an important role in the density of states formula, which we derive next.

24.1.1 Semiclassical density of states

The semiclassical contribution to the density of states (23.13) is given by the imaginary part of the Gutzwiller trace formula (24.3) multiplied with $-1/\pi$. The contribution coming from the zero length trajectories is the imaginary part of (23.66) for $q' \to q$ integrated over the configuration space

$$d_0(E) = -\frac{1}{\pi}\int d^d q\, \mathrm{Im}\, G_0(q,q,E),$$

$$\mathrm{Im}\, G_0(q,q,E) = -\lim_{q'\to q} \frac{m}{2\hbar^2}\left(\frac{\sqrt{2m(E-V)}}{2\pi\hbar|q-q'|}\right)^{\frac{d-2}{2}} J^+_{\frac{d-2}{2}}(S_0(q,q',E)/\hbar).$$

where $G_0(q,q',E)$ is the short time Green's function (23.66). Using the Bessel function $J^+_\nu = \mathrm{Im}\, H^+_\nu$ asymptotic estimate

$$J_\nu(z) \approx \frac{1}{\Gamma(\nu+1)}\left(\frac{z}{2}\right)^\nu \text{ for } |z| << 1.$$

we obtain the zero length trajectories contribution to the density of states

$$d_0(E) = \frac{m}{\hbar^d 2^{d-1}\pi^{d/2}\Gamma(d/2)}\int_{V(q)<E} d^d q\, [2m(E-V(q))]^{(d-2)/2}\,. \tag{24.4}$$

The result is the same as (**??**), the average density estimate $\bar{d}(E)$. The initial wild guess is indeed correct, and the semiclassical density of states is a sum of the average density of states and the oscillation of the density of states around the average, $d_{sc}(E) = \bar{d}(E) + d_{osc}(E)$, where

$$d_{osc}(E) = \frac{1}{\pi\hbar}\sum_p T_p \sum_{r=1}^{\infty} \frac{\cos(rS_p(E)/\hbar - r m_p \pi/2)}{|\det\,(1-\mathbf{J}_p^r)|^{1/2}} \tag{24.5}$$

follows from the trace formula (24.3).

24.1.2 Regularization of the trace

The real part of the $q' \to q$ zero length Green's function (23.66) is ultraviolet divergent in dimensions $d > 1$, and so is its formal trace (23.13). The short distance behavior of the real part of the Green's function can be extracted from the real part of (23.66) by using the Bessel function expansion for small z

$$Y_\nu(z) \approx \begin{cases} -\frac{1}{\pi}\Gamma(\nu)\left(\frac{z}{2}\right)^{-\nu} & \text{for } \nu \neq 0 \\ \frac{2}{\pi}(\ln(z/2)+\gamma) & \text{for } \nu = 0 \end{cases},$$

where $\gamma = 0.577...$ is the Euler constant. The real part of the Green's function for short distance is dominated by the singular part

$$G_{sing}(|q-q'|,E) = \begin{cases} -\frac{m}{2\hbar^2\pi^{\frac{d}{2}}}\Gamma((d-2)/2)\frac{1}{|q-q'|^{d-2}} & \text{for } d \neq 2 \\ \frac{m}{2\pi\hbar^2}(\ln(2m(E-V)|q-q'|/2\hbar)+\gamma) & \text{for } d = 2 \end{cases}.$$

The *regularized* Green's function

$$G_{reg}(q,q',E) = G(q,q',E) - G_{sing}(|q-q'|,E)$$

is obtained by subtracting the $q' \to q$ ultraviolet divergence. For the regularized Green's function the Gutzwiller trace formula is

$$\mathrm{tr}\, G_{reg}(E) = -i\pi\bar{d}(E) + \frac{1}{i\hbar}\sum_p T_p \sum_{r=1}^{\infty} \frac{e^{r(\frac{i}{\hbar}S_p(E) - \frac{i\pi}{2}m_p(E))}}{|\det\,(1-\mathbf{J}_p^r)|^{1/2}}\,. \tag{24.6}$$

Now you stand where Gutzwiller stood in 1990. You hold the trace formula in your hands. You have no clue how good is the $\hbar \to 0$ approximation, how to take care of the sum over an infinity of periodic orbits, and whether the formula converges at all.

24.2 Semiclassical spectral determinant

> The theoreticians now work with an audacity unheard of in earlier times, at present no physical law is considered assured beyond doubt, each and every physical truth is open to dispute. It often looks as if the time of chaos again is drawing near in theoretical physics.
>
> M. Planck, *Phys. Zeitschr.* **11**, 922 (1910)

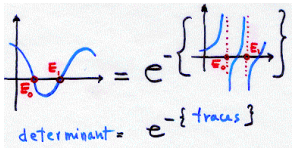

Figure 24.3: A sketch of how spectral determinants convert poles into zeros: The trace shows $1/(E-E_n)$ type singularities at the eigenenergies while the spectral determinant goes smoothly through zeroes.

The problem with trace formulas is that they diverge where we need them, at the individual energy eigenvalues. What to do? Much of the quantum chaology literature responds to the challenge of wrestling the trace formulas by replacing the delta functions in the density of states (23.14) by gaussians. But there is no need to do this - we can compute the eigenenergies without any further ado by remembering that the smart way to determine the eigenvalues of linear operators is by determining zeros of their characteristic determinants.

A better way to compute energy levels is to construct the spectral determinant whose zeroes yield the eigenenergies, $\det{}_{sc}(H-E_n)=0$. A first guess might be that the spectral determinant is the Hadamard product of form

$$f(E)=\prod_n (E-E_n),$$

but this product is not well defined, since for fixed E we multiply larger and larger numbers $(E-E_n)$. This problem is dealt with by *regularization*, discussed below in appendix 24.1.2. Here we offer an impressionistic sketch of regularization.

The logarithmic derivative of $f(E)$ is the formal trace of the Green's function

$$-\frac{d}{dE}\ln f(E)=\sum_n \frac{1}{E-E_n}=\mathrm{tr}\, G(E).$$

This quantity, not surprisingly, is divergent again. This relation however opens a way to derive a convergent version of $f(E)$, by replacing the trace with the regularized trace

$$-\frac{d}{dE}\ln\det{}_{sc}(\hat{(}H)-E)(E)=\mathrm{tr}\, G_{reg}(E).$$

The regularized trace still has $1/(E-E_n)$ poles at the semiclassical eigenenergies, poles which can be generated only if $\det{}_{sc}(\hat{(}H)-E)(E)$ has a zero at $E=E_n$, see fig. 24.3. By integrating and exponentiating we obtain

$$\det{}_{sc}(\hat{(}H)-E)(E)=\exp\left(-\int^E dE'\,\mathrm{tr}\, G_{reg}(E')\right)$$

Now we can use (24.6) and integrate the terms coming from periodic orbits, using the relation (23.34) between the action and the period of a periodic orbit, $dS_p(E)=T_p(E)dE$, and the relation (23.17) between the density of states and the spectral staircase, $d\bar{N}(E)=\bar{d}(E)dE$. We obtain the *semiclassical zeta function*

$$\det{}_{sc}(\hat{(}H)-E)(E)=e^{i\pi\bar{N}(E)}\exp\left(-\sum_p\sum_{r=1}^{\infty}\frac{1}{r}\frac{e^{ir(S_p/\hbar-m_p\pi/2)}}{|\det\,(1-\mathbf{J}_p^r)|^{1/2}}\right)\ . \quad (24.7)$$

We already know from the study of classical evolution operator spectra of chapter 12 that this can be evaluated by means of cycle expons of chapter 15. As always, the cycle action S_p, the topological index m_p and the monodromy matrix $\mathbf{J}_p$ eigenvalues are cycle invariants that depend only on the energy E.

24.3 One-dimensional systems

It has been a long trek, a stationary phase upon stationary phase. Let us check whether the result makes sense even in the simplest case, for quantum mechanics in one configuration dimension.

In one dimension the semiclassical density of states follows from the one-dimensional form of the oscillating density (24.5) and of the average density (**??**)

$$d(E)=\frac{T_p(E)}{2\pi\hbar}+\sum_r\frac{T_p(E)}{\pi\hbar}\cos(rS_p(E)/\hbar-rm_p(E)\pi/2). \quad (24.8)$$

The classical particle oscillates in a single potential well with period $T_p(E)$. There is no monodromy matrix to evaluate, as in one dimension there is only the parallel coordinate, and no transverse directions. The r repetition sum in (24.8) can be rewritten by using the Fourier series expansion of a delta spike train

$$\sum_{n=-\infty}^{\infty}\delta(x-n)=\sum_{k=-\infty}^{\infty}e^{i2\pi kx}=1+\sum_{k=1}^{\infty}2\cos(2\pi kx).$$

We obtain

$$d(E)=\frac{T_p(E)}{2\pi\hbar}\sum_n\delta(S_p(E)/2\pi\hbar-m_p(E)/4-n). \quad (24.9)$$

This expression can be simplified by using the relation (23.34) between T_p and S_p, and the identity (7.7) $\delta(x-x^*) = |f'(x)|\delta(f(x))$, where x^* is the only zero of the function $f(x^*) = 0$ in the interval under consideration. We obtain

$$d(E) = \sum_n \delta(E - E_n),$$

where the energies E_n are the zeroes of the arguments of delta functions in (24.9)

$$S_p(E_n)/2\pi\hbar = n + m_p(E)/4.$$

These are precisely the *Bohr-Sommerfeld quantized energies* E_n satisfying the condition

$$S_p(E_n)/2\pi = \frac{1}{2\pi}\oint p(q,E_n)dq = \hbar\left(n + \frac{m_p(E)}{4}\right). \tag{24.10}$$

In this way the trace formula recovers the well known 1-dimensional quantization rule. In one dimension, the average of states can be expressed from the quantization condition. At $E = E_n$ the exact number of states is n, while the average number of states is $n - 1/2$ since the staircase function $N(E)$ has a unit jump in this point

$$\bar{N}(E) = n - \frac{1}{2} = S_p(E)/2\pi\hbar - m_p(E)/4 - \frac{1}{2}. \tag{24.11}$$

The 1-dimensional spectral determinant follows from (24.7) by dropping the monodromy matrix part and using (24.11)

$$\det{}_{sc}(\hat{(}H) - E)(E) = e^{-\frac{i}{2\hbar}S_p + \frac{i\pi}{2}m_p} e^{-\sum_r \frac{1}{r} e^{\frac{i}{\hbar}rS_p - \frac{i\pi}{2}rm_p}}. \tag{24.12}$$

Summation yields a logarithm by $\sum_r t^r/r = -\ln(1-t)$ and we get

$$\begin{aligned}\det{}_{sc}(\hat{(}H) - E)(E) &= e^{-\frac{i}{2\hbar}S_p + \frac{im_p}{4} + \frac{i\pi}{2}}(1 - e^{\frac{i}{\hbar}S_p - i\frac{m_p}{2}}) \\ &= 2\sin\left(S_p(E)/\hbar - m_p(E)/4\right).\end{aligned}$$

So in one dimension, where there is only one periodic orbit for a given energy E, nothing is gained by going from the trace formula to the spectral determinant. The spectral determinant is a real function for real energies, and its zeros are again the Bohr-Sommerfeld quantized eigenenergies (24.10).

24.4 Two-dimensional systems

For flows in two configuration dimensions the monodromy matrix $\mathbf{J}_p$ has two eigenvalues Λ_p and $1/\Lambda_p$, as explained in sect. 5.1.1. Isolated periodic orbits can be elliptic or hyperbolic. Here we discuss only the hyperbolic case, when the eigenvalues are real and their absolute value is not equal to one. The determinant appearing in the trace formulas can be written in terms of the expanding eigenvalue as

$$|\det\left(1 - \mathbf{J}_p^r\right)|^{1/2} = |\Lambda_p^r|^{1/2}\left(1 - 1/\Lambda_p^r\right),$$

and its inverse can be expanded as a geometric series

$$\frac{1}{|\det\left(1 - \mathbf{J}_p^r\right)|^{1/2}} = \sum_m \frac{1}{|\Lambda_p^r|^{1/2}\Lambda_p^{mr}}.$$

With the 2-dimensional expression for the average density of states (**??**) the spectral determinant becomes

$$\begin{aligned}\det{}_{sc}(\hat{(}H) - E)(E) &= e^{i\frac{m_A E}{2\hbar^2}} \exp\left(-\sum_p \sum_{r=1}^{\infty}\sum_{k=0}^{\infty} \frac{e^{irS_p/\hbar - irm_p\pi/2}}{r|\Lambda_p^r|^{1/2}\Lambda_p^{kr}}\right) \\ &= e^{i\frac{m_A E}{2\hbar^2}} \prod_p \prod_{k=0}^{\infty}\left(1 - \frac{1}{|\Lambda_p|^{1/2}\Lambda_p^k} e^{\frac{i}{\hbar}S_p - \frac{i\pi}{2}m_p}\right).\end{aligned} \tag{24.13}$$

Résumé

Spectral determinants and dynamical zeta functions arise both in classical and quantum mechanics because in both the dynamical evolution can be described by the action of linear evolution operators on infinite-dimensional vector spaces. In quantum mechanics the periodic orbit theory arose from studies of semiconductors, and the unstable periodic orbits have been measured in experiments on the very paradigm of Bohr's atom, the hydrogen atom, this time in strong external fields.

In practice, most " quantum chaos" calculations take the stationary phase approximation to quantum mechanics (the Gutzwiller trace formula, possibly improved by including tunneling periodic trajectories, diffraction corrections, *etc.*) as the point of departure. Once the stationary phase approximation is made,

what follows is *classical* in the sense that all quantities used in periodic orbit calculations - actions, stabilities, geometrical phases - are classical quantities. The problem is then to understand and control the convergence of classical periodic orbit formulas.

While various periodic orbit formulas are formally equivalent, practice shows that some are preferable to others. Three classes of periodic orbit formulas are frequently used:

Trace formulas. In classical dynamics trace formulas (**??**) hide under a variety of appelations such as the $f-\alpha$ or multifractal formalism; in quantum mechanics they are known as the Gutzwiller trace formulas. The trace of the semiclassical Green's function

$$\mathrm{tr}\, G_{sc}(E) = \int d^d q\, G_{sc}(q,q,E).$$

is given by a sum over the periodic orbits (24.6).

While easiest to derive, in calculations the trace formulas are hard to use for anything other than the leading eigenvalue estimates, as they tend to be divergent in the region of physical interest.

Zeros of *Ruelle or dynamical zeta functions*

$$1/\zeta(s) = \prod_p (1-t_p), \quad t_p = \frac{1}{\sqrt{\Lambda_p}} e^{\frac{i}{\hbar}S_p - i\pi m_p/2}$$

yield, in combination with cycle expansions, the semiclassical estimates of *quantum* resonances. For hyperbolic systems the dynamical zeta functions have good convergence and are a useful tool for determination of classical and quantum mechanical averages.

Selberg-type zeta functions, Fredholm determinants, spectral determinants, functional determinants are the natural objects for spectral calculations, with convergence better than for dynamical zeta functions, but with less transparent cycle expansions. The 2-dimensional Selberg-type zeta function (24.13)

$$\det{}_{sc}(\hat{(}H) - E)(E) = \prod_p \prod_{k=0}^{\infty} \left(1 - \frac{e^{iS_p/\hbar - i\pi m_p/2}}{|\Lambda_p|^{1/2}\Lambda_p^k}\right)$$

is a typical example. Most periodic orbit calculations are based on cycle expansions of such determinants.

As we have assumed that the periodic orbits are isolated, and do not form families (as is the case for integrable systems or in KAM tori of systems with mixed phase space), the formulas are valid only for the hyperbolic and elliptic periodic orbits.

For the deterministic dynamical flows and number theory, zeta functions are exact. The quantum-mechanical ones, derived by the Gutzwiller approach, are at best only the stationary phase approximations to the exact quantum spectral determinants, and for quantum mechanics an important conceptual problem arises already at the level of derivation of the semiclassical formulas; how accurate are they, and can the periodic orbit theory be systematically improved?

References

[24.1] M. Jammer, *The Conceptual Development of Quantum mechanics* (McGraw-Hill, New York 1966).

[24.2] J. Mehra and H. Rechtenberg, *The Historical Development of the Quantum Theory* (Springer, New York 1982).

[24.3] J.W.S. Rayleigh, *The Theory of Sound* (Macmillan, London 1896; reprinted by Dover, New York 1945).

[24.4] Young, (180?).

[24.5] Airy, (1838).

[24.6] Stokes, (1847).

[24.7] Gouy, (1899).

[24.8] Jefferies, (1920).

[24.9] J.B. Keller, *Ann. Phys. (N.Y.)* **4**, 180 (1958).

[24.10] J.B. Keller and S.I. Rubinow, *Ann. Phys. (N.Y.)* **9**, 24 (1960).

[24.11] J.B. Keller, "A geometrical theory of diffraction", in *Calculus of variations and its applications*, *Proc. of Symposia in appl. math.* **8**, (McGraw-Hill, New York, 1958).

[24.12] J.B. Keller, *Calculus of Variations***27**, (1958).

[24.13] V.P. Maslov, *Théorie des Perturbations et Métodes Asymptotiques* (Dunod, Paris, 1972).

[24.14] V.P. Maslov and M.V. Fedoriuk, *Semi-Classical Approximation in Quantum Mechanics* (Reidel, Boston 1981).

[24.15] V.I. Arnold, *Functional Anal. Appl.* **1**, 1 (1967).

[24.16] J.E. Marsden and T.S. Ratiu, *Introduction to Mechanics and Symmetry* (Springer-Verlag, New York, 1994).

[24.17] N. Bleistein and R.A. Handelsman, *Asymptotic Expansions of Integrals* (Dover, New York 1986).

[24.18] R.G. Littlejohn, J. Stat. Phys. **68**, 7 (1992).

[24.19] L.D. Landau and E.M. Lifshitz, *Mechanics* (Pergamon, London, 1959).

[24.20] R.G. Littlejohn, *"Semiclassical structure of trace formulas"*, in G. Casati and B. Chirikov, eds., *Quantum Chaos*, (Cambridge University Press, Cambridge 1994).

[24.21] V.I. Arnold, *Ordinary Differential Equations* (MIT Press, Cambridge, Mass. 1978).

[24.22] M.C. Gutzwiller, *J. Math. Phys.* **8**, 1979 (1967); **10**, 1004 (1969); **11**, 1791 (1970); **12**, 343 (1971).

[24.23] M.C. Gutzwiller, *J. Math. Phys.* **12**, 343 (1971)

[24.24] M.C. Gutzwiller, *Physica* **D5**, 183 (1982)

[24.25] M.C. Gutzwiller, *J. Phys. Chem.* **92**, 3154 (1984).

[24.26] A. Voros, *J. Phys.* **A 21**, 685 (1988).

[24.27] P. Cvitanović and P.E. Rosenqvist, in G.F. Dell'Antonio, S. Fantoni and V.R. Manfredi, eds., *From Classical to Quantum Chaos, Soc. Italiana di Fisica Conf. Proceed.* **41**, pp. 57-64 (Ed. Compositori, Bologna 1993).

[24.28] A. Wirzba, *CHAOS* **2**, 77 (1992).

[24.29] P. Cvitanović, G. Vattay and A. Wirzba, *"Quantum fluids and classical determinants"*, in H. Friedrich and B. Eckhardt., eds., *Classical, Semiclassical and Quantum Dynamics in Atoms – in Memory of Dieter Wintgen*, *Lecture Notes in Physics* **485** (Springer, New York 1997), `chao-dyn/9608012`.

[24.30] E.B. Bogomolny, CHAOS **2**, 5 (1992).

[24.31] E.B. Bogomolny, *Nonlinearity* **5**, 805 (1992).

[24.32] E. Schrödinger, *Annalen der Physik* **79**, 361, 489; **80**, 437, **81**, 109 (1926).

[24.33] E.A. Spiegel

[24.34] M. Kline, *Mathematical Thought from Ancient to Modern Times* (Oxford Univ. Press, Oxford 1972); on Monge and theory of characteristics - chapter 22.7.

[24.35] E.T. Bell, *Men of Mathematics* (Penguin, London 1937).

[24.36] R.P. Feynman, *Statistical Physics* (Addison Wesley, New York 1990).

[24.37] Goldstein, *Mechanics*, chapter 9.

[24.38] G. Tanner and D. Wintgen, *CHAOS* **2**, 53 (1992).

[24.39] P. Cvitanović and F. Christiansen, *CHAOS* **2**, 61 (1992).

[24.40] M.V. Berry and J.P. Keating, *J. Phys.* **A 23**, 4839 (1990).

[24.41] H.H. Rugh, *"Generalized Fredholm determinants and Selberg zeta functions for Axiom A dynamical systems"*, *Ergodic Theory Dynamical Systems* **16**, 805 (1996).

[24.42] B. Eckhard and G. Russberg, Phys. Rev. **E 47**, 1578 (1993).

[24.43] D. Ruelle, *Statistical Mechanics, Thermodynamical Formalism* (Addison-Wesley, Reading MA, 1987).

[24.44] P. Szépfalusy, T. Tél, A. Csordás and Z. Kovács, Phys. Rev. **A 36**, 3525 (1987).

[24.45] H.H. Rugh, Nonlinearity **5**, 1237 (1992) and H.H. Rugh, *Ph.D. Thesis* (Niels Bohr Institute, 1993).

[24.46] P. Cvitanović, P.E. Rosenqvist, H.H. Rugh and G. Vattay, *Scattering Theory - special issue*, CHAOS (1993).

[24.47] E.J. Heller, S. Tomsovic and A. Sepúlveda CHAOS **2**, *Periodic Orbit Theory - special issue*, 105, (1992).

[24.48] V.I. Arnold, *Geometrical Methods in the Theory of Ordinary Differential Equations*, (SpringerVerlag, New York 1983).

[24.49] R. Dashen, B. Hasslacher and A. Neveu , "Nonperturbative methods and extended hadron models in field theory. 1. Semiclassical functional methods.", *Phys. Rev.* **D10**, 4114 (1974).

[24.50] V.I. Arnold, *Geometrical Methods in the Theory of Ordinary Differential Equations* (Springer, New York 1983).

Exercises

Exercise 24.1 **Volume of d-dimensional sphere.** *Show that the volume of a d-dimensional sphere of radius r equals $\pi^{d/2} r^d/\Gamma(1+d/2)$. Show that $\Gamma(1+d/2) = \Gamma(d/2)d/2$.*

Exercise 24.2 **Monodromy matrix from second variations of the action.** *Show that*

$$D_{\perp j}/D'_{\perp j} = (\mathbf{1} - \mathbf{J}) \tag{24.14}$$

Exercise 24.3 **Jacobi gymnastics.** *Prove that the ratio of determinants in (M.28) can be expressed as*

$$\frac{\det D'_{\perp j}(q_\parallel, 0, E)}{\det D_{\perp j}(q_\parallel, 0, E)} = \det \begin{pmatrix} I - \mathbf{J}_{qq} & -\mathbf{J}_{qp} \\ -\mathbf{J}_{pq} & I - \mathbf{J}_{pp} \end{pmatrix} = \det (1 - \mathbf{J}_j) \,, \tag{24.15}$$

where $\mathbf{J}_j$ is the monodromy matrix of the periodic orbit.

Exercise 24.4 **Quantum two-disk scattering.** *Compute the quasiclassical spectral determinant*

$$Z(\varepsilon) = \prod_{p,j,l} \left(1 - \frac{t_p}{\Lambda_p^{j+2l}}\right)^{j+1}$$

for the two disk problem. Use the geometry

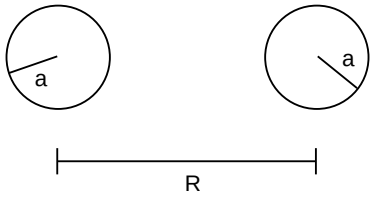

The full quantum mechanical version of this problem can be solved by finding the zeros in k for the determinant of the matrix

$$M_{m,n} = \delta_{m,n} + \frac{(-1)^n}{2} \frac{J_m(ka)}{H_n^{(1)}(ka)} \left(H_{m-n}^{(1)}(kR) + (-1)^n H_{m+n}^{(1)}(kR) \right) \,,$$

where J_n is the nth Bessel function and $H_n^{(1)}$ is the Hankel function of the first kind. Find the zeros of the determinant closest to the origin by solving $\det M(k) = 0$. (Hints: notice the structure $M = I + A$ to approximate the determinant; read chapter ??; or read Chaos **2**, *79 (1992))*

Exercise 24.5 **Pinball topological index.** *Upgrade your pinball simulator so that it compute the topological index for each orbit it finds.*

Exercise 24.6 **Transport equations.** *Write the wave-function in the asymptotic form*

$$\psi(q,t) = e^{\frac{i}{\hbar}R(x,t) + \frac{i}{\hbar}\varepsilon t} \sum_{n\geq 0} (i\hbar)^n A_n(x,t) \,.$$

Derive the transport equations for the A_n by substituting this into the Schrödinger equation and then collecting terms by orders of $\hbar$. Notice that equation for $\dot{A}_n$ only requires knowledge of A_{n-1} and R.

Exercise 24.7 **Zero length orbits.** *Derive the classical trace (11.1) rigorously and either add the $t \to 0_+$ zero length contribution to the trace formula, or show that it vanishes. Send us a reprint of* Phys. Rev. Lett. *with the correct derivation.*

Chapter 25

Helium atom

> "But," Bohr protested, "nobody will believe me unless I can explain every atom and every molecule." Rutherford was quick to reply, "Bohr, you explain hydrogen and you explain helium and everybody will believe the rest."
> John Archibald Wheeler (1986)

(G. Tanner)

So far much has been said about 1-dimensional maps, game of pinball and other curious but rather idealized dynamical systems. If you have became impatient and started wondering what good are the methods learned so far in solving real physical problems, we have good news for you. We will show in this chapter that the concepts of symbolic dynamics, unstable periodic orbits, and cycle expansions are essential tools to understand and calculate classical and quantum mechanical properties of nothing less than the helium, a dreaded three-body Coulomb problem.

This sounds almost like one step too much at a time; we all know how rich and complicated the dynamics of the three-body problem is – can we really jump from three static disks directly to three charged particles moving under the influence of their mutually attracting or repelling forces? It turns out, we can, but we have to do it with care. The full problem is indeed not accessible in all its detail, but we are able to analyze a somewhat simpler subsystem – collinear helium. This system plays an important role in the classical dynamics of the full three-body problem and its quantum spectrum.

The main work in reducing the quantum mechanics of helium to a semiclassical treatment of collinear helium lies in understanding why we are allowed to do so. We will not worry about this too much in the beginning; after all, 80 years and many failed attempts separate Heisenberg, Bohr and others in the 1920ties

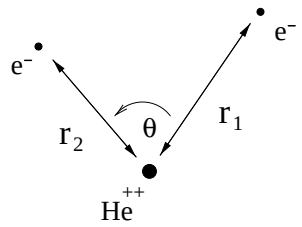

Figure 25.1: Coordinates for the helium three body problem in the plane.

from the insights we have today on the role chaos plays for helium and its quantum spectrum. We will introduce collinear helium in sect. 25.1 and discuss its dynamics in some detail. We will learn how to integrate and find periodic orbits and how to determine the relevant eigenvalues of the Jacobian matrix. We will explain in sect. 25.2 why a quantization of the collinear dynamics in helium will enable us to find parts of the full helium spectrum; we then set up the semiclassical spectral determinant and evaluate its cycle expansion. A full quantum justification of this treatment of helium is briefly discussed in sect. 25.2.1.

25.1 Classical dynamics of collinear helium

The full classical helium system consists of two electrons of mass m_e and charge $-e$ moving about a positively charged nucleus of mass m_{he} and charge $+2e$.

The helium electron-nucleus mass ratio $m_{he}/m_e = 1836$ is so large that we may work in the infinite nucleus mass approximation $m_{he} = \infty$, fixing the nucleus at the origin. Finite nucleus mass effects can be taken into account without any substantial difficulty. We are now left with two electrons moving in three spatial dimensions around the origin. The total angular momentum of the combined electron system is still conserved. In the special case of angular momentum $L = 0$, the electrons move in a fixed plane containing the nucleus. The three body problem can then be written in terms of three independent coordinates only, the electron-nucleus distances r_1 and r_2 and the inter-electron angle Θ, see fig. 25.1.

25.2 on p. 529

This looks like something we can lay our hands on; the problem has been reduced to three degrees of freedom, six phase space coordinates in all, and the total energy is conserved. But let us go one step further; the electrons are attracted by the nucleus but repelled by each other. They will tend to stay as far away from each other as possible, preferably on opposite sides of the nucleus. It is thus worth having a closer look at the situation where the three particles are all on a line with the nucleus being somewhere between the two electrons. If we, in addition, let the electrons have momenta pointing towards the nucleus as in fig. 25.2, then there is no force acting on the electrons perpendicular to the

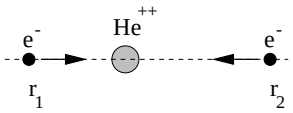

Figure 25.2: Collinear helium, with the two electrons on opposite sides of the nucleus.

common interparticle axis. That is, if we start the classical system on the dynamical subspace $\Theta = \pi$, $\frac{d}{dt}\Theta = 0$, the three particles will remain in this *collinear configuration* for all times.

25.1.1 Scaling

In what follows we will restrict the dynamics to this collinear subspace. It is a system of two degrees of freedom with the Hamiltonian

$$H = \frac{1}{2m_e}\left(p_1^2 + p_2^2\right) - \frac{2e}{r_1} - \frac{2e}{r_2} + \frac{e}{r_1 + r_2} = E\,, \tag{25.1}$$

where E is the total energy. We will first consider the dependence of the dynamics on the energy E. A simple analysis of potential versus kinetic energy tells us that if the energy is positive both electrons can escape to $r_i \to \infty$, $i = 1, 2$. More interestingly, a single electron can still escape even if E is negative, carrying away an unlimited amount of kinetic energy, as the total energy of the remaining inner electron has no lower bound. Not only that, but one electron *will* escape eventually for almost all starting conditions. The overall dynamics thus depends critically on whether $E > 0$ or $E < 0$. But how does the dynamics change otherwise with varying energy? Fortunately, not at all. Helium dynamics remains invariant under a change of energy up to a simple scaling transformation; a solution of the equations of motion at a fixed energy $E_0 = -1$ can be transformed into a solution at an arbitrary energy $E < 0$ by scaling the coordinates as

$$r_i(E) = \frac{e^2}{(-E)}\, r_i, \quad p_i(E) = \sqrt{-m_e E}\, p_i, \quad i = 1, 2\,,$$

together with a time transformation $t(E) = e^2 m_e^{1/2} (-E)^{-3/2}\, t$. We include the electron mass and charge in the scaling transformation in order to obtain a non–dimensionalized Hamiltonian of the form

$$H = \frac{p_1^2}{2} + \frac{p_2^2}{2} - \frac{2}{r_1} - \frac{2}{r_2} + \frac{1}{r_1 + r_2} = -1\,. \tag{25.2}$$

The case of negative energies chosen here is the most interesting one for us. It exhibits chaos, unstable periodic orbits and is responsible for the bound states and resonances of the quantum problem treated in sect. 25.2.

There is another classical quantity important for a semiclassical treatment of quantum mechanics, and which will also feature prominently in the discussion in the next section; this is the classical action (23.32) which scales with energy as

$$S(E) = \oint \mathrm{d}\mathbf{q}(E) \cdot \mathbf{p}(E) = \frac{e^2 m_e^{1/2}}{(-E)^{1/2}}\, S, \tag{25.3}$$

with S being the action obtained from (25.2) for $E = -1$, and coordinates $\mathbf{q} = (r_1, r_2)$, $\mathbf{p} = (p_1, p_2)$. For the Hamiltonian (25.2), the period of a cycle and its action are related by (23.34), $T_p = \frac{1}{2} S_p$.

25.1.2 Regularization of two–body collisions

Next, we have a closer look at the singularities in the Hamiltonian (25.2). Whenever two bodies come close to each other, accelerations become large, numerical routines require lots of small steps, and numerical precision suffers. No numerical routine will get us through the singularity itself, and in collinear helium electrons have no option but to collide with the nucleus. Hence a *regularization* of the differential equations of motions is a necessary prerequisite to any numerical work on such problems, both in celestial mechanics (where a spaceship executes close approaches both at the start and its destiantion) and in quantum mechanics (where much of semiclassical physics is dominated by returning classical orbits that probe the quantum wave function at the nucleus).

There is a fundamental difference between two–body collisions $r_1 = 0$ or $r_2 = 0$, and the triple collision $r_1 = r_2 = 0$. Two–body collisions can be regularized, with the singularities in equations of motion removed by a suitable coordinate transformation together with a time transformation preserving the Hamiltonian structure of the equations. Such regularization is not possible for the triple collision, and solutions of the differential equations can not be continued through the singularity at the origin. As we shall see, the chaos in collinear helium originates from this singularity of triple collisions.

A regularization of the two–body collisions is achieved by means of the Kustaanheimo–Stiefel (KS) transformation, which consists of a coordinate dependent time transformation which stretches the time scale near the origin, and a canonical transformation of the phase space coordinates. In order to motivate the method, we apply it first to the 1-dimensional Kepler problem

$$H = \frac{1}{2}p^2 - \frac{2}{x} = E\,. \tag{25.4}$$

To warm up, consider the $E = 0$ case, starting at $x = 0$ at $t = 0$. Even though the equations of motion are singular at the intial point, we can immediately integrate

$$\frac{1}{2}\dot{x}^2 - \frac{2}{x} = 0$$

by means of separation of variables

$$\sqrt{x}dx = \sqrt{2}dt\,, \qquad x = (9/2)^{\frac{1}{3}}\, t^{\frac{2}{3}}\,, \tag{25.5}$$

and observe that the solution is not singular. The aim of regularization is to compensate for the infinite acceleration at the origin by introducing a fictitious time, in terms of which the passage through the origin is smooth.

A time transformation $dt = f(q,p)d\tau$ for a system described by a Hamiltonian $H(q,p) = E$ leaves the Hamiltonian structure of the equations of motion unaltered, if the Hamiltonian itself is transformed into $\mathcal{H}(q,p) = f(q,p)(H(q,p) - E)$. For the 1– dimensional Coulomb problem with (25.4) we choose the time transformation $dt = xd\tau$ which lifts the $|x| \to 0$ singularity in (25.4) and leads to a new Hamiltonian

$$\mathcal{H} = \frac{1}{2}xp^2 - 2 - Ex = 0. \tag{25.6}$$

The solution (25.5) is now parametrized by the fictitous time $d\tau$ through a pair of equations

$$x = \frac{1}{2}\tau^2\,, \qquad t = \frac{1}{6}\tau^3\,.$$

The equations of motion are, however, still singular as $x \to 0$:

$$\frac{d^2x}{d\tau^2} = -\frac{1}{2x}\frac{dx}{d\tau} + xE\,.$$

Appearance of the square root in (25.5) now suggests a canonical transformation of form

$$x = Q^2\,, \quad p = \frac{P}{2Q} \tag{25.7}$$

which maps the Kepler problem into that of a harmonic oscillator with Hamiltonian

$$H(Q,P) = \frac{1}{8}P^2 - EQ^2 = 2, \tag{25.8}$$

with all singularities completely removed.

We now apply this method to collinear helium. The basic idea is that one seeks a higher-dimensional generalization of the "square root removal" trick (25.7), by introducing a new vector Q with property $r = |Q|^2$. In this simple 1-dimensional example the KS transformation can be implemented by

$$r_1 \;=\; Q_1^2\,, \qquad r_2 = Q_2^2\,, \qquad p_1 = \frac{P_1}{2Q_1}\,, \qquad p_2 = \frac{P_2}{2Q_2} \tag{25.9}$$

25.1 on p. 529

and reparametrization of time by $d\tau = dt/r_1r_2$. The singular behavior in the original momenta at r_1 or $r_2 = 0$ is again compensated by stretching the time scale at these points. The Hamiltonian structure of the equations of motions with respect to the new time τ is conserved, if we consider the Hamiltonian

$$H_{ko} = \frac{1}{8}(Q_2^2P_1^2 + Q_1^2P_2^2) - 2R_{12}^2 + Q_1^2Q_2^2\left(1 + \frac{1}{R_{12}^2}\right) = 0 \tag{25.10}$$

with $R_{12} = (Q_1^2 + Q_2^2)^{1/2}$. The equations of motion now have the form

$$\begin{aligned} \dot{P}_1 &= 2Q_1\left[2 - \frac{P_2^2}{8} - Q_2^2\left(1 + \frac{Q_2^2}{R_{12}^4}\right)\right]; \qquad \dot{Q}_1 = \frac{1}{4}P_1Q_2^2 \\ \dot{P}_2 &= 2Q_2\left[2 - \frac{P_1^2}{8} - Q_1^2\left(1 + \frac{Q_1^2}{R_{12}^4}\right)\right]; \qquad \dot{Q}_2 = \frac{1}{4}P_2Q_1^2. \end{aligned} \tag{25.11}$$

Individual electron–nucleus collisions at $r_1 = Q_1^2 = 0$ or $r_2 = Q_2^2 = 0$ no longer pose a problem to a numerical integration routine. The equations (25.11) are singular only at the triple collision $R_{12} = 0$, that is, when both electrons hit the nucleus at the same time.

The new coordinates and the Hamiltonian (25.10) are very useful when calculating trajectories for collinear helium; they are, however, less intuitive as a visualization of the three-body dynamics. We will therefore refer to the old coordinates r_1, r_2 when discussing the dynamics and the periodic orbits.

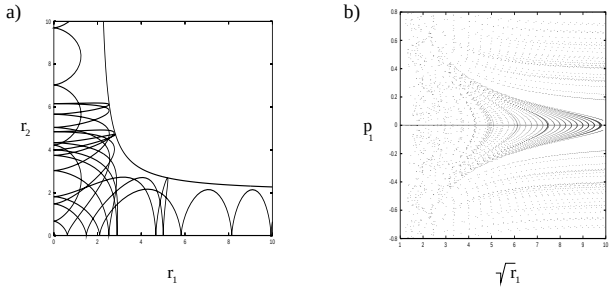

Figure 25.3: a) A typical trajectory in the $r_1 - r_2$ plane; the trajectory enters here along the r_1 axis and escapes to infinity along the r_2 axis; b) Poincaré map (r_2=0) for collinear helium. Strong chaos prevails for small r_1 near the nucleus.

25.1.3 Chaos, symbolic dynamics and periodic orbits

Let us have a closer look at the dynamics in collinear helium. The electrons are attracted by the nucleus. During an electron–nucleus collision momentum is transferred between the inner and outer electron. The inner electron has a maximal screening effect on the charge of the nucleus, diminishing the attractive force on the outer electron. This electron – electron interaction is negligible if the outer electron is far from the nucleus at a collision and the overall dynamics is regular like in the 1-dimensional Kepler problem.

Things change drastically if both electrons approach the nucleus nearly simultaneously. The momentum transfer between the electrons depends now sensitively on how the particles approach the origin. Intuitively, these nearly missed triple collisions render the dynamics chaotic. A typical trajectory is plotted in fig. 25.3(a) where we used r_1 and r_2 as the relevant axis. The dynamics can also be visualized in a Poincaré surface of section, see fig. 25.3(b). We plot here the coordinate and momentum of the outer electron whenever the inner particle hits the nucleus, that is, r_1 or $r_2 = 0$. As the unstructured gray region of the Poincaré section for small r_1 illustrates, the dynamics is chaotic whenever the outer electron is close to the origin during a collision. Conversely, regular motions dominate whenever the outer electron is far from the nucleus. As one of the electrons escapes for almost any starting condition, the system is unbounded: one electron (say electron 1) can escape, with an arbitrary amount of kinetic energy taken by the fugative. The remaining electron is trapped in a Kepler ellipse with total energy in the range $[-1, -\infty]$. There is no energy barrier which would separate the bound from the unbound regions of the phase space. From general kinematic arguments one deduces that the outer electron will not return when $p_1 > 0$, $r_2 \leq 2$ at $p_2 = 0$, the turning point of the inner electron. Only if the two electrons approach the nucleus almost symmetrically along the line $r_1 = r_2$, and

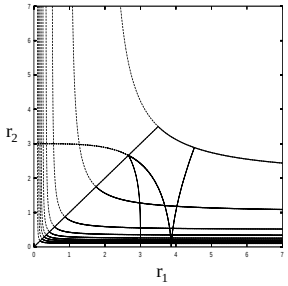

Figure 25.4: The cycle 011 in the fundamental domain $r_1 \geq r_2$ (full line) and in the full domain (dashed line).

pass close to the triple collision can the momentum transfer between the electrons be large enough to kick one of the particles out completely. In other words, the electron escape originates from the near triple collisions.

The collinear helium dynamics has some important properties which we now list.

Reflection symmetry

The Hamiltonian (25.1) is invariant with respect to electron–electron exchange; this symmetry corresponds to the mirror symmetry of the potential along the line $r_1 = r_2$, fig. 25.4. As a consequence, we can restrict ourselves to the dynamics in the *fundamental domain* $r_1 \geq r_2$ and treat a crossing of the diagonal $r_1 = r_2$ as a hard wall reflection. The dynamics in the full domain can then be reconstructed by unfolding the trajectory through back-reflections. As explained in chapter 19, the dynamics in the fundamental domain is the key to the factorization of spectral determinants, to be implemented here in (25.22). Note also the similarity between the fundamental domain of the collinear potential fig. 25.4, and the fundamental domain fig. 9.5(b) in the 3–disk system, a simpler problem with the same binary symbolic dynamics.

in depth:
sect. 19.6, p. 369

Symbolic dynamics

We have already made the claim that the triple collisions render the collinear helium fully chaotic. We have no proof of the assertion, but the analysis of the symbolic dynamics lends further credence to the claim.

The potential in (25.2) forms a ridge along the line $r_1 = r_2$. One can show that a trajectory passing the ridge must go through at least one two-body collision $r_1 = 0$ or $r_2 = 0$ before coming back to the diagonal $r_1 = r_2$. This suggests a *binary* symbolic dynamics corresponding to the dynamics in the fundamental domain $r_1 \geq r_2$; the symbolic dynamics is linked to the Poincaré map $r_2 = 0$ and the symbols 0 and 1 are defined as

0: if the trajectory is not reflected from the line $r_1 = r_2$ between two collisions with the nucleus $r_2 = 0$;

1: if a trajectory is reflected from the line $r_1 = r_2$ between two collisions with the nucleus $r_2 = 0$.

Empirically, the symbolic dynamics is complete for a Poincaré map in the fundamental domain, that is, there exists a one-to-one correspondence between binary symbol sequences and collinear trajectories in the fundamental domain, with exception of the $\overline{0}$ cycle.

Periodic orbits

The existence of a binary symbolic dynamics makes it easy to count the number of periodic orbits in the fundamental domain, as in sect. 10.5.2. However, mere existence of these cycles does not suffice to calculate semiclassical spectral determinants. We need to determine their phase space trajectories and calculate their periods, topological indices and stabilities. A restriction of the periodic orbit search to a suitable Poincaré surface of section, e.g. $r_2 = 0$ or $r_1 = r_2$, leaves us in general with a 2-dimensional search. Methods to find periodic orbits in multi-dimensional spaces have been described in chapter 14. They depend sensitively on good starting guesses. A systematic search for all orbits can be achieved only after combining multi-dimensional Newton methods with interpolation algorithms based on the binary symbolic dynamics phase space partitioning. All cycles up to symbol length 16 (some 8000 primitive cycles) have been computed by such methods, with some examples shown in fig. 25.5. All numerical evidence indicates that the dynamics of collinear helium is hyperbolic, and that all periodic orbits are unstable.

Note that the fixed point $\overline{0}$ cycle is not in this list. The $\overline{0}$ cycle would correspond to the situation where the outer electron sits at rest infinitely far from the nucleus while the inner electron bounces back and forth into the nucleus. The orbit is the limiting case of an electron escaping to infinity with zero kinetic energy. The orbit is in the regular (that is separable) limit of the dynamics and is thus marginally stable. The existence of this orbit is also related to intermittent behavior generating the quasi–regular dynamics for large r_1 that we have already noted in fig. 25.3(b).

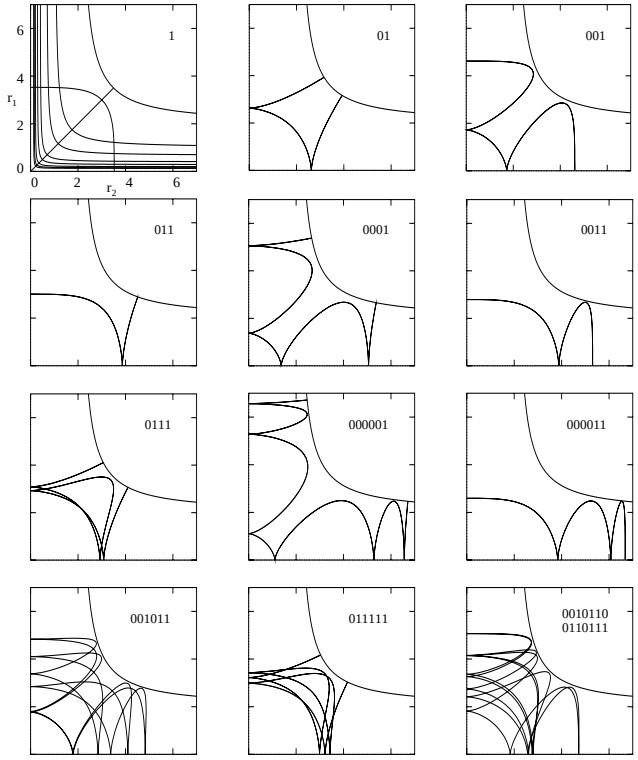

Figure 25.5: Some of the shortest cycles in collinear helium. The classical collinear electron motion is bounded by the potential barrier $-1 = -2/r_1 - 2/r_2 + 1/(r_1 + r_2)$ and the condition $r_i \geq 0$. The orbits are shown in the full r_1–r_2 domain, the itineraries refers to the dynamics in the $r_1 \geq r_2$ fundamental domain. The last figure, the 14-cycle 00101100110111, is an example of a typical cycle with no symmetry.

Search algorithm for an arbitrary periodic orbit is quite cumbersome to program. There is, however, a class of periodic orbits, orbits with symmetries, which can be easily found by a one-parameter search. The only symmetry left for the dynamics in the fundamental domain is time reversal symmetry; a time reversal symmetric periodic orbit is an orbit whose trajectory in phase space is mapped onto itself when changing $(p_1, p_2) \to (-p_1, -p_2)$, by reversing the direction of the momentum of the orbit. Such an orbit must be a "libration" or self-retracing cycle, an orbit that runs back and forth along the same path in the (r_1, r_2) plane. The cycles $\overline{1}$, $\overline{01}$ and $\overline{001}$ in fig. 25.5 are examples of self-retracing cycles. Luckily, the shortest cycles that we desire most ardently have this symmetry.

Why is this observation helpful? A self-retracing cycle must start perpendicular to the boundary of the fundamental domain, that is, on either of the axis $r_2 = 0$ or $r_1 = r_2$, or on the potential boundary $-\frac{2}{r_1} - \frac{2}{r_2} + \frac{1'}{r_1+r_2} = -1$. By shooting off trajectories perpendicular to the boundaries and monitoring the orbits returning to the boundary with the right symbol length we will find time reversal symmetric cycles by varying the starting point on the boundary as the only parameter. But how can we tell whether a given cycle is self-retracing or not? All the relevant information is contained in the itineraries; a cycle is self-retracing if its itinerary is invariant under time reversal symmetry (that is read backwards) and a suitable number of cyclic permutations. All binary strings up to length 5 fulfill this condition. The symbolic dynamics contains even more information; we can tell at which boundary the total reflection occurs. One finds that an orbit starts out perpendicular

- to the diagonal $r_1 = r_2$ if the itinerary is time reversal invariant and has an odd number of 1's; an example is the cycle $\overline{001}$ in fig. 25.5;
- to the axis $r_2 = 0$ if the itinerary is time reversal invariant and has an even number of symbols; an example is the cycle $\overline{0011}$ in fig. 25.5;
- to the potential boundary if the itinerary is time reversal invariant and has an odd number of symbols; an example is the cycle $\overline{011}$ in fig. 25.5.

All cycles up to symbol length 5 are time reversal invariant, the first two non-time reversal symmetric cycles are cycles $\overline{00101 1}$ and $\overline{00110 1}$ in fig. 25.5. Their determination would require a two-parameter search. The two cycles are mapped onto each other by time reversal symmetry, that is, they have the same trace in the r_1–r_2 plane, but they trace out distinct cycles in the full phase space.

We are ready to integrate trajectories for classical collinear helium with the help of the equations of motions (25.11) and to find all cycles up to length 5. There is only one thing not yet in place; we need the governing equations for the matrix elements of the Jacobian matrix along a trajectory in order to calculate stability indices. We will provide the main equations in the next section, with the details of the derivation relegated to the appendix C.2.

25.5 on p. 529

25.1.4 Local coordinates, Jacobian matrix

In this section, we will derive the equations of motion for the Jacobian matrix along a collinear helium trajectory. The Jacobian matrix is 4-dimensional; the two trivial eigenvectors corresponding to the conservation of energy and displacements along a trajectory can, however, be projected out by suitable orthogonal coordinates transformations, see appendix C. We will give the transformation to local coordinates explicitly, here for the regularized coordinates (25.9), and state the resulting equations of motion for the reduced $[2 \times 2]$ Jacobian matrix.

The vector locally parallel to the trajectory is pointing in the direction of the phase space velocity (5.4)

$$v_m = \dot{x}_m(t) = \omega_{mn} \frac{\partial H}{\partial x_n} = (H_{P_1}, H_{P_2}, -H_{Q_1}, -H_{Q_2})^T,$$

with $H_{Q_i} = \frac{\partial H}{\partial Q_i}$, and $H_{P_i} = \frac{\partial H}{\partial P_i}$, $i = 1{,}2$. The vector perpendicular to a trajectory $x(t) = (Q_1(t), Q_2(t), P_1(t), P_2(t))$ and to the energy manifold is given by the gradient of the Hamiltonian (25.10)

$$\gamma = \nabla H = (H_{Q_1}, H_{Q_2}, H_{P_1}, H_{P_2})^T .$$

By symmetry $v_m \gamma_m = \omega_{mn} \frac{\partial H}{\partial x_n} \frac{\partial H}{\partial x_m}$, so the two vectors are orthogonal.

Next, we consider the orthogonal matrix

$$\begin{aligned} \mathbf{O}_{\gamma(t)} &= (\gamma_1, \gamma_2, \gamma/R, v) \qquad (25.12) \\ &= \begin{pmatrix} -H_{P_2}/R & H_{Q_2} & H_{Q_1}/R & H_{P_1} \\ H_{P_1}/R & -H_{Q_1} & H_{Q_2}/R & H_{P_2} \\ -H_{Q_2}/R & -H_{P_2} & H_{P_1}/R & -H_{Q_1} \\ H_{Q_1}/R & H_{P_1} & H_{P_2}/R & -H_{Q_2} \end{pmatrix} \end{aligned}$$

with $R = |\nabla H|^2 = (H_{Q_1}^2 + H_{Q_2}^2 + H_{P_1}^2 + H_{P_2}^2)$, which provides a transformation to local phase space coordinates centered on the trajectory $x(t)$ along the two vectors (γ, v). The vectors $\gamma_{1,2}$ are phase space vectors perpendicular to the trajectory and to the energy manifold in the 4-dimensional phase space of collinear helium. The Jacobian matrix (4.5) rotated to the local coordinate system by $\mathbf{O}$ then has the form

25.6 on p. 530

$$\mathbf{m} = \begin{pmatrix} m_{11} & m_{12} & * & 0 \\ m_{21} & m_{22} & * & 0 \\ 0 & 0 & 1 & 0 \\ * & * & * & 1 \end{pmatrix}, \quad \mathbf{J} = \mathbf{O}^{\mathbf{T}} \mathbf{m} \mathbf{O} \sigma$$

The linearized motion perpendicular to the trajectory on the energy manifold is described by the $[2 \times 2]$ matrix $\mathbf{m}$; the 'trivial' directions correspond to unit eigenvalues on the diagonal in the 3rd and 4th column and row.

The equations of motion for the reduced Jacobian matrix $\mathbf{m}$ are given by

$$\dot{\mathbf{m}} = \mathrm{l}(t)\mathbf{m}(t), \tag{25.13}$$

with $\mathbf{m}(0) = \mathbf{1}$. The matrix l depends on the trajectory in phase space and has the form

$$\mathrm{l} = \begin{pmatrix} l_{11} & l_{12} & * & 0 \\ l_{21} & l_{22} & * & 0 \\ 0 & 0 & 0 & 0 \\ * & * & * & 0 \end{pmatrix},$$

where the relevant matrix elements l_{ij} are given by

$$\begin{aligned} l_{11} &= \frac{1}{R}[2H_{Q_1Q_2}(H_{Q_2}H_{P_1} + H_{Q_1}H_{P_2}) \\ &\quad +(H_{Q_1}H_{P_1} - H_{Q_2}H_{P_2})(H_{Q_1Q_1} - H_{Q_2Q_2} - H_{P_1P_1} + H_{P_2P_2})] \\ l_{12} &= -2H_{Q_1Q_2}(H_{Q_1}H_{Q_2} - H_{P_1}H_{P_2}) \\ &\quad +(H_{Q_1}^2 + H_{P_2}^2)(H_{Q_2Q_2} + H_{P_1P_1}) + (H_{Q_2}^2 + H_{P_1}^2)(H_{Q_1Q_1} + H_{P_2P_2}) \\ l_{21} &= \frac{1}{R^2}[2(H_{Q_1P_2} + H_{Q_2P_1})(H_{Q_2}H_{P_1} + H_{Q_1}H_{P_8}) \\ &\quad -(H_{P_1}^2 + H_{P_2}^2)(H_{Q_1Q_1} + H_{Q_2Q_2}) - (H_{Q_1}^2 + H_{Q_2}^2)(H_{P_1P_1} + H_{P_2P_2})] \\ l_{22} &= -l_{11}\,. \end{aligned} \tag{25.14}$$

Here $H_{Q_iQ_j}$, $H_{P_iP_j}$, $i, j = 1, 2$ are the second partial derivatives of H with respect to the coordinates Q_i, P_i, evaluated at the phase space coordinate of the classical trajectory.

25.1.5 Getting ready

Now everything is in place: the regularized equations of motion can be implemented in a Runge–Kutta or any other integration scheme to calculate trajectories. We have a symbolic dynamics and know how many cycles there are and how to find them (at least up to symbol length 5). We know how to compute the Jacobian matrix whose eigenvalues enter the semiclassical spectral determinant (24.7). By (23.34) the action S_p is proportional to the period of the orbit, $S_p = 2T_p$.

p	$S_p/2\pi$	$\ln\lvert\Lambda_p\rvert$	σ_p	m_p
1	1.82900	0.6012	0.5393	2
01	3.61825	1.8622	1.0918	4
001	5.32615	3.4287	1.6402	6
011	5.39451	1.8603	1.6117	6
0001	6.96677	4.4378	2.1710	8
0011	7.04134	2.3417	2.1327	8
0111	7.25849	3.1124	2.1705	8
00001	8.56618	5.1100	2.6919	10
00011	8.64306	2.7207	2.6478	10
00101	8.93700	5.1562	2.7291	10
00111	8.94619	4.5932	2.7173	10
01011	9.02689	4.1765	2.7140	10
01111	9.07179	3.3424	2.6989	10
000001	10.13872	5.6047	3.2073	12
000011	10.21673	3.0323	3.1594	12
000101	10.57067	6.1393	3.2591	12
000111	10.57628	5.6766	3.2495	12
001011	10.70698	5.3251	3.2519	12
001101	10.70698	5.3251	3.2519	12
001111	10.74303	4.3317	3.2332	12
010111	10.87855	5.0002	3.2626	12
011111	10.91015	4.2408	3.2467	12

Table 25.1: Action S_p (in units of 2π), Lyapunov exponent $|\Lambda_p|/T_p$ for the motion in the collinear plane, winding number σ_p for the motion perpendicular to the collinear plane, and the topological index m_p for all fundamental domain cycles up to topological length 6.

There is, however, still a slight complication. Collinear helium is an invariant 4-dimensional subspace of the full helium phase space. If we restrict the dynamics to angular momentum equal zero, we are left with 6 phase space coordinates. That is not a problem when computing periodic orbits, they are oblivious to the other dimensions. However, the Jacobian matrix does pick up extra contributions. When we calculate the Jacobian matrix for the full problem, we must also allow for displacements out of the collinear plane, so the full Jacobian matrix for dynamics for $L = 0$ angular momentum is 6 dimensional. Fortunately, the linearized dynamics in and off the collinear helium subspace decouple, and the Jacobian matrix can be written in terms of two distinct $[2\times 2]$ matrices, with trivial eigendirections providing the remaining two dimensions. The submatrix related to displacements off the linear configuration characterizes the linearized dynamics in the additional degree of freedom, the Θ-coordinate in fig. 25.1. It turns out that the linearized dynamics in the Θ coordinate is stable, corresponding to a bending type motion of the two electrons. We will need the stability exponents for all degrees of freedom in evaluating the semiclassical spectral determinant in sect. 25.2.

The numerical values of the actions, stability exponents, stability angles, and topological indices for the shortest cycles are listed in table 25.1.4. These numbers, needed for the semiclassical quantization implemented in the next section, an also be helpful in checking your own calculations.

25.2 Semiclassical quantization of collinear helium

Before we get down to a serious calculation of the helium quantum energy levels let us have a brief look at the overall structure of the spectrum. This will give us a preliminary feel for which parts of the helium spectrum are accessible with the help of our collinear model – and which are not. In order to keep the discussion as simple as possible and to concentrate on the semiclassical aspects of our calculations we offer here only a rough overview. For a guide to more detailed accounts see remark 25.4.

25.2.1 Structure of helium spectrum

We start by recalling Bohr's formula for the spectrum of hydrogen like one-electron atoms. The eigenenergies form a Rydberg series

$$E_N = -\frac{e^4 m_e}{\hbar^2}\frac{Z^2}{2N^2}\,, \tag{25.15}$$

where Ze is the charge of the nucleus and m_e is the mass of the electron. Through the rest of this chapter we adopt the atomic units $e = m_e = \hbar = 1$.

The simplest model for the helium spectrum is obtained by treating the two electrons as independent particles moving in the potential of the nucleus neglecting the electron–electron interaction. Both electrons are then bound in hydrogen like states; the inner electron will see a charge $Z = 2$, screening at the same time the nucleus, the outer electron will move in a Coulomb potential with effective charge $Z - 1 = 1$. In this way obtain a first estimate for the total energy

$$E_{N,n} = -\frac{2}{N^2} - \frac{1}{2n^2} \qquad \text{with} \quad n > N. \tag{25.16}$$

This double Rydberg formula contains already most of the information we need to understand the basic structure of the spectrum. The (correct) ionizations thresholds $E_N = -\frac{2}{N^2}$ are obtained in the limit $n \to \infty$, yielding the ground and excited states of the helium ion He^+. We will therefore refer to N as the principal quantum number. We also see that all states $E_{N,n}$ with $N \geq 2$ lie above the first ionization threshold for $N = 1$. As soon as we switch on electron-electron interaction these states are no longer bound states; they turn into resonant states which decay into a bound state of the helium ion and a free outer electron. This might not come as a big surprise if we have the classical analysis of the previous section in mind: we already found that one of the classical electrons will almost always escape after some finite time. More remarkable is the fact that the first, $N = 1$ series consists of true bound states for all n, an effect which can only be understood by quantum arguments.

The hydrogen-like quantum energies (25.15) are highly degenerate; states with different angular momentum but the same principal quantum number N share the same energy. We recall from basic quantum mechanics of hydrogen atom that the possible angular momenta for a given N span $l = 0, 1 \ldots N-1$. How does that affect the helium case? Total angular momentum L for the helium three-body problem is conserved. The collinear helium is a subspace of the classical phase space for $L = 0$; we thus expect that we can only quantize helium states corresponding to the total angular momentum zero, a subspectrum of the full helium spectrum. Going back to our crude estimate (25.16) we may now attribute angular momenta to the two independent electrons, l_1 and l_2 say. In order to obtain total angular momentum $L = 0$ we need $l_1 = l_2 = l$ and $l_{z1} = -l_{z2}$, that is, there are N different states corresponding to $L = 0$ for fixed quantum numbers N, n. That means that we expect N different Rydberg series converging to each ionization threshold $E_N = -2/N^2$. This is indeed the case and the N different series can be identified also in the exact helium quantum spectrum, see fig. 25.6. The degeneracies between the different N Rydberg series corresponding to the same principal quantum number N, are removed by the electron-electron interaction. We thus already have a rather good idea of the coarse structure of the spectrum.

In the next step, we may even speculate which parts of the $L = 0$ spectrum can be reproduced by the semiclassical quantization of collinear helium. In the

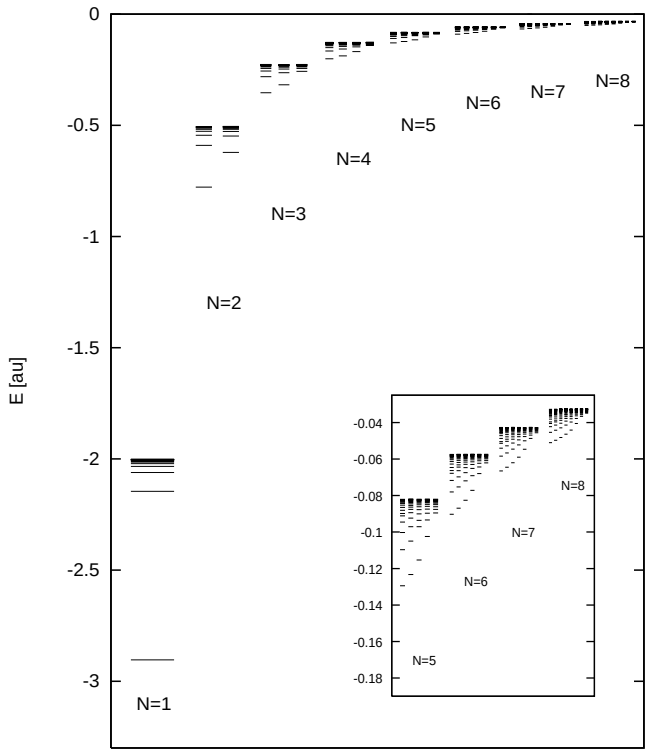

Figure 25.6: The exact quantum helium spectrum for $L = 0$. The energy levels denoted by bars have been obtained from full 3-dimensional quantum calculations [3].

collinear helium, both classical electrons move back and forth along a common axis through the nucleus, so each has zero angular momentum. We therefore expect that collinear helium describes the Rydberg series with $l = l_1 = l_2 = 0$. These series are the energetically lowest states for fixed (N, n), corresponding to the Rydberg series on the outermost left side of the spectrum in fig. 25.6. We will see in the next section that this is indeed the case and that the collinear model holds down to the $N = 1$ bound state series, including even the ground state of helium! We will also find a semiclassical quantum number corresponding to the angular momentum l and show that the collinear model describes states for moderate angular momentum l as long as $l \ll N$. .

☞ remark 25.4

25.2.2 Semiclassical spectral determinant for collinear helium

Nothing but lassitude can stop us now from calculating our first semiclassical eigenvalues. The only thing left to do is to set up the spectral determinant in terms of the periodic orbits of collinear helium and to write out the first few terms of its cycle expansion with the help of the binary symbolic dynamics. The semiclassical spectral determinant (24.7) has been written as product over all cycles of the classical systems. The energy dependence in collinear helium enters the classical dynamics only through simple scaling transformations described in sect. 25.1.1 which makes it possible to write the semiclassical spectral determinant in the form

$$\det\left(\hat{H}-E\right)_{sc} = \exp\left(-\sum_p \sum_{r=1}^{\infty} \frac{1}{r} \frac{e^{ir(sS_p - m_p\frac{\pi}{2})}}{(-\det\left(1-\mathbf{J}^r_{p\perp}\right))^{1/2} |\det\left(1-\mathbf{J}^r_{p\parallel}\right)|^{1/2}}\right) , \quad (25.17)$$

with the energy dependence absorbed into the variable

$$s = \frac{e^2}{\hbar}\sqrt{\frac{m_e}{-E}} ,$$

obtained by using the scaling relation (25.3) for the action. As explained in sect. 25.1.4, the fact that the $[4 \times 4]$ Jacobian matrix decouples into two $[2 \times 2]$ submatrices corresponding to the dynamics *in* the collinear space and *perpendicular* to it makes it possible to write the denominator in terms of a product of two determinants. Stable and unstable degrees of freedom enter the trace formula in different ways, reflected by the absence of the modulus sign and the minus sign in front of $\det\left(1-\mathbf{J}_{\perp}\right)$. The topological index m_p corresponds to the unstable dynamics in the collinear plane. Note that the factor $e^{i\pi\bar{N}(E)}$ present in (24.7) is absent in (25.17). Collinear helium is an open system, that is the eigenenergies are resonances corresponding to the complex zeros of the semiclassical spectral determinant and the mean energy staircase $\bar{N}(E)$ not defined. In order to obtain

a spectral determinant as an infinite product of the form (24.13) we may proceed as in (12.9) by expanding the determinants in (25.17) in terms of the eigenvalues of the corresponding Jacobian matrices. The matrix representing displacements perpendicular to the collinear space has eigenvalues of the form $\exp(\pm 2\pi i\sigma)$, reflecting stable linearized dynamics. σ is the full winding number along the orbit in the stable degree of freedom, multiplicative under multiple repetitions of this orbit .The eigenvalues corresponding to the unstable dynamics along the collinear axis are paired as $\{\Lambda, 1/\Lambda\}$ with $|\Lambda| > 1$ and real. As in (12.9) and (24.13) we may thus write

$$\begin{aligned}
&\left[-\det\left(1-\mathbf{J}^r_\perp\right)\left|\det\left(1-\mathbf{J}^r_\parallel\right)\right|\right]^{-1/2} \qquad (25.18)\\
&= \left[-(1-\Lambda^r)(1-\Lambda^{-r})\left|(1-e^{2\pi i r\sigma})(1-e^{-2\pi i r\sigma})\right|\right]^{-1/2}\\
&= \sum_{k,\ell=0}^{\infty} \frac{1}{|\Lambda^r|^{1/2}\Lambda^{rk}} e^{-ir(\ell+1/2)\sigma}\,.
\end{aligned}$$

The $\pm$ sign corresponds to the hyperbolic/inverse hyperbolic periodic orbits with positive/negative eigenvalues Λ. Using the relation (25.19) we see that the sum over r in (25.17) is the expansion of the logarithm, so the semiclassical spectral determinant can be rewritten as a product over dynamical zeta functions, as in (12.9):

$$\det\left(\hat{H}-E\right)_{sc} = \prod_{k=0}^{\infty}\prod_{m=0}^{\infty}\zeta^{-1}_{k,m} = \prod_{k=0}^{\infty}\prod_{m=0}^{\infty}\prod_{p}(1-t_p^{(k,m)})\,, \qquad (25.19)$$

where the cycle weights are given by

$$t_p^{(k,m)} = \frac{1}{|\Lambda|^{1/2}\Lambda^k} e^{i\left(sS_p - m_p\frac{\pi}{2} - 4\pi(\ell+1/2)\sigma_p\right)}\,, \qquad (25.20)$$

and m_p is the topological index for the motion in the collinear plane which equals twice the topological length of the cycle. The two independent directions perpendicular to the collinear axis lead to a twofold degeneracy in this degree of freedom which accounts for an additional factor 2 in front of the winding number σ. The values for the actions, winding numbers and stability indices of the shortest cycles in collinear helium are listed in table 25.1.4.

The integer indices ℓ and k play very different roles in the semiclassical spectral determinant (25.19). A linearized approximation of the flow along a cycle corresponds to a harmonic approximation of the potential in the vicinity of the trajectory. Stable motion corresponds to a harmonic oscillator potential, unstable motion to an inverted harmonic oscillator. The index ℓ which contributes

as a phase to the cycle weights in the dynamical zeta functions can therefore be interpreted as a harmonic oscillator quantum number; it corresponds to vibrational modes in the Θ coordinate and can in our simplified picture developed in sect. 25.2.1 be related to the quantum number $l = l_1 = l_2$ representing the single particle angular momenta. Every distinct ℓ value corresponds to a full spectrum which we obtain from the zeros of the semiclassical spectral determinant $1/\zeta_\ell$ keeping ℓ fixed. The harmonic oscillator approximation will eventually break down with increasing off-line excitations and thus increasing ℓ. The index k corresponds to 'excitations' along the unstable direction and can be identified with local resonances of the inverted harmonic oscillator centered on the given orbit. The cycle contributions $t_p^{(k,m)}$ decrease exponentially with increasing k. Higher k terms in an expansion of the determinant give corrections which become important only for large negative imaginary s values. As we are interested only in the leading zeros of (25.19), that is the zeros closest to the real energy axis, it is sufficient to take only the $k = 0$ terms into account.

Next, let us have a look at the discrete symmetries discussed in sect. 25.1.3. Collinear helium has a C_2 symmetry as it is invariant under reflection across the $r_1 = r_2$ line corresponding to the electron-electron exchange symmetry. As explained in sects. 19.1.2 and 19.5, we may use this symmetry to factorize the semiclassical spectral determinant. The spectrum corresponding to the states symmetric or antisymmetric with respect to reflection can be obtained by writing the dynamical zeta functions in the symmetry factorized form

$$1/\zeta^{(\ell)} = \prod_a (1-t_a)^2 \prod_{\tilde{s}}(1-t_{\tilde{s}}^2)\,. \qquad (25.21)$$

Here, the first product is taken over all asymmetric prime cycles, that is cycles that are not self-dual under the C_2 symmetry. Such cycles come in pairs, as two equivalent orbits are mapped into each other by the symmetry transformation. The second product runs over all self-dual cycles; these orbits cross the axis $r_1 = r_2$ twice at a right angle. The self-dual cycles close in the fundamental domain $r_1 \le r_2$ already at half the period compared to the orbit in the full domain, and the cycle weights $t_{\tilde{s}}$ in (25.21) are the weights of fundamental domain cycles. The C_2 symmetry now leads to the factorization of (25.21) $1/\zeta = \zeta_+^{-1}\zeta_-^{-1}$, with

$$\begin{aligned}
1/\zeta_+^{(\ell)} &= \prod_a (1-t_a)\prod_{\tilde{s}}(1-t_{\tilde{s}})\,,\\
1/\zeta_-^{(\ell)} &= \prod_a (1-t_a)\prod_{\tilde{s}}(1+t_{\tilde{s}})\,, \qquad (25.22)
\end{aligned}$$

setting $k = 0$ in what follows. The symmetric subspace resonances are given by the zeros of $1/\zeta_+^{(\ell)}$, antisymmetric resonances by the zeros of $1/\zeta_-^{(\ell)}$, with the

two dynamical zeta functions defined as products over orbits in the fundamental domain. The symmetry properties of an orbit can be read off directly from its symbol sequence, as explained in sect. 25.1.3. An orbit with an odd number of 1's in the itinerary is self-dual under the C_2 symmetry and enters the spectral determinant in (25.22) with a negative or a positive sign, depending on the symmetry subspace under consideration.

25.2.3 Cycle expansion results

So far we have established a factorized form of the semiclassical spectral determinant and have thereby picked up two *good quantum numbers*; the quantum number m has been identified with an excitation of the bending vibrations, the exchange symmetry quantum number ± 1 corresponds to states being symmetric or antisymmetric with respect to the electron-electron exchange. We may now start writing down the binary cycle expansion (15.5) and determine the zeros of spectral determinant. There is, however, still another problem: there is no cycle 0 in the collinear helium. The symbol sequence $\overline{0}$ corresponds to the limit of an outer electron fixed with zero kinetic energy at $r_1 = \infty$, the inner electron bouncing back and forth into the singularity at the origin. This introduces intermittency in our system, a problem discussed in chapter 18. We note that the behavior of cycles going far out in the channel r_1 or $r_2 \to \infty$ is very different from those staying in the near core region. A cycle expansion using the binary alphabet reproduces states where both electrons are localized in the near core regions: these are the lowest states in each Rydberg series. The states converging to the various ionization thresholds $E_N = -2/N^2$ correspond to eigenfunctions where the wave function of the outer electron is stretched far out into the ionization channel $r_1, r_2 \to \infty$. To include those states, we have to deal with the dynamics in the limit of large r_1, r_2. This turns out to be equivalent to switching to a symbolic dynamics with an infinite alphabet. With this observation in mind, we may write the cycle expansion (....) for a binary alphabet without the $\overline{0}$ cycle as

☞ remark 25.5

$$1/\zeta^{\ell}(s) = 1 \quad -t_1^{(\ell)} - t_{01}^{(\ell)} - [t_{001}^{(\ell)} + t_{011}^{(\ell)} - t_{01}^{(\ell)} t_1^{(\ell)}] \\ -[t_{0001}^{(\ell)} + t_{0011}^{(\ell)} - t_{001}^{(\ell)} t_1^{(\ell)} + t_{0111}^{(\ell)} - t_{011}^{(\ell)} t_1^{(\ell)}] - \dots \,. \qquad (25.23)$$

The weights $t_p^{(\ell)}$ are given in (25.19), with contributions of orbits and composite orbits of the same total symbol length collected within square brackets. The cycle expansion depends only on the classical actions, stability indices and winding numbers, given for orbits up to length 6 in table 25.1.4. To get reacquainted with the cycle expansion formula (25.23), consider a truncation of the series after the

first term

$$1/\zeta^{(\ell)}(s) \approx 1 - t_1 \,.$$

The quantization condition $1/\zeta^{(\ell)}(s) = 0$ leads to

$$E_{m,N} = -\frac{(S_1/2\pi)^2}{[m + \frac{1}{2} + 2(N + \frac{1}{2})\sigma_1]^2}, \qquad m, N = 0, 1, 2, \dots \,, \qquad (25.24)$$

with $S_1/2\pi = 1.8290$ for the action and $\sigma_1 = 0.5393$ for the winding number, see table 25.1.4, the 1 cycle in the fundamental domain. This cycle can be described as the *asymmetric stretch* orbit, see fig. 25.5. The additional quantum number N in (25.24) corresponds to the principal quantum number defined in sect. 25.2.1. The states described by the quantization condition (25.24) are those centered closest to the nucleus and correspond therefore to the lowest states in each Rydberg series (for a fixed m and N values), in fig. 25.6. The simple formula (25.24) gives already a rather good estimate for the ground state of helium! Results obtained from (25.24) are tabulated in table 25.2, see the 3rd column under $j = 1$ and the comparison with the full quantum calculations.

In order to obtain higher excited quantum states, we need to include more orbits in the cycle expansion (25.23), covering more of the phase space dynamics further away from the center. Taking longer and longer cycles into account, we indeed reveal more and more states in each N-series for fixed m. This is illustrated by the data listed in table 25.2 for symmetric states obtained from truncations of the cycle expansion of $1/\zeta_+$.

25.7 on p. 530

Results of the same quality are obtained for antisymmetric states by calculating the zeros of $1/\zeta_-^{(\ell)}$. Repeating the calculation with $\ell = 1$ or higher in (25.22) reveals states in the Rydberg series which are to the right of the energetically lowest series in fig. 25.6.

Commentary

Remark 25.1 Sources. The full 3-dimensional Hamiltonian after elimination of the center of mass coordinates, and an account of the finite nucleus mass effects is given in ref. [2]. The general two–body collision regularizing Kustaanheimo–Stiefel transformation [5], a generalization of Levi-Civita's [13] Pauli matrix two–body collision regularization for motion in a plane, is due to Kustaanheimo [12] who realized that the correct

N	n	$j=1$	$j=4$	$j=8$	$j=12$	$j=16$	$-E_{\rm qm}$
1	1	3.0970	2.9692	2.9001	2.9390	2.9248	2.9037
2	2	0.8044	0.7714	0.7744	0.7730	0.7727	0.7779
2	3	—	0.5698	0.5906	0.5916	0.5902	0.5899
2	4	—	—	—	0.5383	0.5429	0.5449
3	3	0.3622	0.3472	0.3543	0.3535	0.3503	0.3535
3	4	—	—	0.2812	0.2808	0.2808	0.2811
3	5	—	—	0.2550	0.2561	0.2559	0.2560
3	6	—	—	—	0.2416	0.2433	0.2438
4	4	0.2050	0.1962	0.1980	0.2004	0.2012	0.2010
4	5	—	0.1655	0.1650	0.1654	0.1657	0.1657
4	6	—	—	0.1508	0.1505	0.1507	0.1508
4	7	—	—	0.1413	0.1426	0.1426	0.1426

Table 25.2: Collinear helium, real part of the symmetric subspace resonances obtained by a cycle expansion (25.23) up to cycle length j. The exact quantum energies [3] are in the last column. The states are labeled by their principal quantum numbers. A dash as an entry indicates a missing zero at that level of approximation.

higher-dimensional generalization of the "square root removal" trick (25.7), by introducing a vector Q with property $r = |Q|^2$, is the same as Dirac's trick of getting linear equation for spin 1/2 fermions by means of spinors. Vector spaces equipped with a product and a known satisfy $|Q \cdot Q| = |Q|^2$ define *normed algebras*. They appear in various physical applications - as quaternions, octonions, spinors. The technique was originally developed in celestial mechanics [6] to obtain numerically stable solutions for planetary motions. The basic idea was in place as early as 1931, when H. Hopf [14] used a KS transformation in order to illustrate a Hopf's invariant. The KS transformation for the collinear helium was introduced in ref. [2].

Remark 25.2 Complete binary symbolic dynamics. No stable periodic orbit and no exception to the binary symbolic dynamics of the collinear helium cycles have been found in numerical investigations. A proof that all cycles are unstable, that they are uniquely labelled by the binary symbolic dynamcis, and that this dynamics is complete is, however, still missing. The conjectured Markov partition of the phase space is given by the triple collision manifold, that is by those trajectories which start in or end at the singular point $r_1 = r_2 = 0$. See also ref. [2].

Remark 25.3 Spin and particle exchange symmetry. In our presentation of collinear helium we have completely ignored all dynamical effects due to the spin of the particles involved, such as the electronic spin-orbit coupling. Electrons are fermions and that determines the symmetry properties of the quantum states. The total wave function, including the spin

degrees of freedom, must be antisymmetric under the electron-electron exchange transformation. That means that a quantum state symmetric in the position variables must have an antisymmetric spin wave function, i.e. the spins are antiparallel and the total spin is zero (singletstate). Antisymmetric states have symmetric spin wave function with total spin 1 (tripletstates). The threefold degeneracy of spin 1 states is lifted by the spin-orbit coupling.

Remark 25.4 Helium quantum numbers. The classification of the helium states in terms of single electron quantum numbers, sketched in sect. 25.2.1, prevailed until the 1960's; a growing discrepancy between experimental results and theoretical predictions made it necessary to refine this picture. In particular, the different Rydberg series sharing a given N-quantum number correspond, roughly speaking, to a quantization of the inter electronic angle Θ, see fig. 25.1, and can not be described in terms of single electron quantum numbers l_1, l_2. The fact that something is slightly wrong with the single electron picture laid out in sect. 25.2.1 is highlighted when considering the collinear configuration where both electrons are on the *same* side of the nucleus. As both electrons again have angular momentum equal to zero, the corresponding quantum states should also belong to single electron quantum numbers $(l_1, l_2) = (0, 0)$. However, the single electron picture breaks down completely in the limit $\Theta = 0$ where electron-electron interaction becomes the dominant effect. The quantum states corresponding to this classical configuration are distinctively different from those obtained from the collinear dynamics with electrons on different sides of the nucleus. The Rydberg series related to the classical $\Theta = 0$ dynamics are on the outermost rigth side in each N subspectrum in fig. 25.6, and contain the energetically highest states for given N, n quantum numbers, see also remark 25.5. A detailed account of the historical development as well as a modern interpretation of the spectrum can be found in ref. [1].

Remark 25.5 Beyond the unstable collinear helium subspace. The semiclassical quantization of the chaotic collinear helium subspace is discussed in refs. [7, 8, 9]. Classical and semiclassical considerations beyond what has been discussed in sect. 25.2 follow several other directions, all outside the main of this book.

A classical study of the dynamics of collinear helium where both electrons are on the same side of the nucleus reveals that this configuration is fully stable both in the collinear plane and perpendicular to it. The corresponding quantum states can be obtained with the help of an approximate EBK-quantization which reveals helium resonances with extremely long lifetimes (quasi - bound states in the continuum). These states form the energetically highest Rydberg series for a given principal quantum number N, see fig. 25.6. Details can be found in refs. [10, 11].

In order to obtain the Rydberg series structure of the spectrum, that is the succession of states converging to various ionization thresholds, we

need to take into account the dynamics of orbits which make large excursions along the r_1 or r_2 axis. In the chaotic collinear subspace these orbits are characterized by symbol sequences of form $(a0^n)$ where a stands for an arbitrary binary symbol sequence and 0^n is a succession of n 0's in a row. A summation of the form $\sum_{n=0}^{\infty} t_{a0^n}$, where t_p are the cycle weights in (25.19), and cycle expansion of indeed yield all Rydbergstates up the various ionization thresholds, see ref. [4].
For a comprehensive overview on spectra of two-electron atoms and semiclassical treatments ref. [1].

Résumé

We have covered a lot of ground starting with considerations of the classical properties of a three-body Coulomb problem, and ending with the semiclassical helium spectrum. We saw that the three-body problem restricted to the dynamics on a collinear appears to be fully chaotic; this implies that traditional semiclassical methods such as *WKB*quantization will not work and that we needed the full periodic orbit theory to obtain leads to the semiclassical spectrum of helium. As a piece of unexpected luck the symbolic dynamics is simple, and the semiclassical quantization of the collinear dynamics yields an important part of the helium spectrum, including the ground state, to a reasonable accuracy. A sceptic might say: "Why bother with all the semiclassical considerations? A straightforward numerical quantum calculation achieves the same goal with better precision." While this is true, the semiclassical analysis offers new insights into the *structure* of the spectrum. We discovered that the dynamics perpendicular to the collinear plane was stable, giving rise to an additional (approximate) quantum number ℓ. We thus understood the origin of the different Rydberg series depicted in fig. 25.6, a fact which is not at all obvious from a numerical solution of the quantum problem.

Having traversed the long road from the classical game of pinball all the way to a credible helium spectrum computation, we could declare victory and fold down this enterprise. Nevertheless, there is still much to think about - what about such quintessentially quantum effects as diffraction, tunnelling, ...? As we shall now see, the periodic orbit theory has still much of interest to offer.

References

[25.1] G. Tanner, J-M. Rost and K. Richter, Rev. Mod. Phys. **72**, 497 (2000).

[25.2] K. Richter, G. Tanner, and D. Wintgen, Phys. Rev. A **48**, 4182 (1993).

[25.3] Bürgers A., Wintgen D. and Rost J. M., J. Phys. B **28**, 3163 (1995).

[25.4] G. Tanner and D. Wintgen Phys. Rev. Lett. **75** 2928 (1995).

[25.5] P. Kustaanheimo and E. Stiefel, *J. Reine Angew. Math.* **218**, 204 (1965).

[25.6] E.L. Steifel and G. Scheifele, *Linear and regular celestial mechanics* (Springer, New York 1971).

[25.7] G.S. Ezra, K. Richter, G. Tanner and D. Wintgen, J. Phys. B **24**, L413 (1991).

[25.8] D. Wintgen, K. Richter and G. Tanner, CHAOS **2**, 19 (1992).

[25.9] R. Blümel and W. P. Reinhardt, *Directions in Chaos Vol 4*, eds. D. H. Feng and J.-M. Yuan (World Scientific, Hongkong), 245 (1992).

[25.10] K. Richter and D. Wintgen, J. Phys. B **24**, L565 (1991).

[25.11] D. Wintgen and K. Richter, Comments At. Mol. Phys. **29**, 261 (1994).

[25.12] P. Kustaanheimo, *Ann. Univ. Turku, Ser. AI.*, **73** (1964).

[25.13] T. Levi-Civita, *Opere mathematische* **2** (1956).

[25.14] H. Hopf, *Math. Ann.* **104** (1931).

Exercises

Exercise 25.1 **Kustaanheimo–Stiefel transformation.** *Check the Kustaanheimo–Stiefel regularization for collinear helium; derive the Hamiltonian (25.10) and the collinear helium equations of motion (25.11).*

Exercise 25.2 **Helium in the plane.** *Starting with the helium Hamiltonian in the infinite nucleus mass approximation $m_{he} = \infty$, and angular momentum $L = 0$, show that the three body problem can be written in terms of three independent coordinates only, the electron-nucleus distances r_1 and r_2 and the inter-electron angle Θ, see fig. 25.1.*

Exercise 25.3 **Helium trajectories.** *Do some trial integrations of the collinear helium equations of motion (25.11). Due to the energy conservation, only three of the phase space coordinates (Q_1, Q_2, P_1, P_2) are independent. Alternatively, you can integrate in 4 dimensions and use the energy conservation as a check on the quality of your integrator.*

The dynamics can be visualized as a motion in the original configuration space (r_1, r_2), $r_i \geq 0$ quadrant, or, better still, by an appropriately chosen 2-d Poincaré section, exercise 25.4. Most trajectories will run away, do not be surprised - the classical collinear helium is unbound. Try to guess approximately the shortest cycle of fig. 25.4.

Exercise 25.4 **A Poincaré section for collinear Helium.** *Construct a Poincaré section of fig. 25.3b that reduces the helium flow to a map. Try to delineate regions which correspond to finite symbol sequences, that is initial conditions that follow the same topological itinerary in the fig. 25.3a space for a finite number of bounces. Such rough partition can be used to initiate 2–dimensional Newton-Raphson method searches for helium cycles, exercise 25.5.*

Exercise 25.5 **Collinear helium cycles.** *The motion in the (r_1, r_2) plane is topologically similar to the pinball motion in a 3-disk system, except that the motion is in the Coulomb potential.*

Just as in the 3-disk system the dynamics is simplified if viewed in the fundamental domain, *in this case the region between r_1 axis and the $r_1 = r_2$ diagonal. Modify your integration routine so the trajectory bounces off the diagonal as off a mirror. Miraculously, the symbolic dynamics for the survivors again turns out to be binary, with 0 symbol signifying a bounce off the r_1 axis, and 1 symbol for a bounce off the diagonal. Just as in the 3-disk game of pinball, we thus know what cycles need to be computed for the cycle expansion (25.23).*

Guess some short cycles by requiring that topologically they correspond to sequences of bounces either returning to the same r_i axis or reflecting off the diagonal. Now either Use special symmetries of orbits such as self-retracing to find all orbits up to length 5 by a 1-dimensional Newton search.

Exercise 25.6 **Collinear helium cycle stabilities.** *Compute the eigenvalues for the cycles you found in exercise 25.5, as described in sect. 25.1.4. You may either integrate the reduced 2×2 matrix using equations (25.13) together with the generating function $\mathbb{1}$ given in local coordinates by (25.14) or integrate the full 4×4 Jacobian matrix, see sect. 17.1. Integration in 4 dimensions should give eigenvalues of the form $(1, 1, \Lambda_p, 1/\Lambda_p)$; The unit eigenvalues are due to the usual periodic orbit invariances; displacements along the orbit as well as perpendicular to the energy manifold are conserved; the latter one provides a check of the accuracy of your computation. Compare with table 25.1.4; you should get the actions and Lyapunov exponents right, but topological indices and stability angles we take on faith.*

Exercise 25.7 **Helium eigenenergies.** *Compute the lowest eigenenergies of singlet and triplet states of helium by substituting cycle data into the cycle expansion (25.23) for the symmetric and antisymmetric zeta functions (25.22). Probably the quickest way is to plot the magnitude of the zeta function as function of real energy and look for the minima. As the eigenenergies in general have a small imaginary part, a contour plot such as fig. 15.1, can yield informed guesses. Better way would be to find the zeros by Newton method, sect. 15.1.4. How close are you to the cycle expansion and quantum results listed in table 25.2? You can find more quantum data in ref. [3].*

Chapter 26

Diffraction distraction

(N. Whelan)

Diffraction effects characteristic to scattering off wedges are incorporated into the periodic orbit theory.

26.1 Quantum eavesdropping

As noted in chapter 25, the classical mechanics of the helium atom is undefined at the instant of a triple collision. This is a common phenomenon - there is often some singularity or discontinuity in the classical mechanics of physical systems. This discontinuity can even be helpful in classifying the dynamics. The points in phase space which have a past or future at the discontinuity form manifolds which divide the phase space and provide the symbolic dynamics. The general rule is that quantum mechanics smoothes over these discontinuities in a process we interpret as diffraction. We solve the local diffraction problem quantum mechanically and then incorporate this into our global solution. By doing so, we reconfirm the central leitmotif of this treatise: think locally - act globally.

While being a well-motivated physical example, the helium atom is somewhat involved. In fact, so involved that we do not have a clue how to do it. In its place we illustrate the concept of diffractive effects with a pinball game. There are various classes of discontinuities which a billiard can have. There may be a grazing condition such that some trajectories hit a smooth surface while others are unaffected - this leads to the creeping described in chapter **??**. There may be a vertex such that trajectories to one side bounce differently from those to the other side. There may be a point scatterer or a magnetic flux line such that we do not know how to continue classical mechanics through the discontinuities. In what follows, we specialize the discussion to the second example - that of vertices

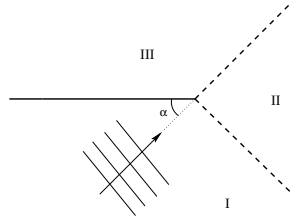

Figure 26.1: Scattering of a plane wave off a half line.

or wedges. To further simplify the discussion, we consider the special case of a half line which can be thought of as a wedge of angle zero.

We start by solving the problem of the scattering of a plane wave off a half line (see fig. 26.1). This is the local problem whose solution we will use to construct a global solution of more complicated geometries. We define the vertex to be the origin and launch a plane wave at it from an angle α. What is the total field? This is a problem solved by Sommerfeld in 1896 and our discussion closely follows his.

The total field consists of three parts - the incident field, the reflected field and the diffractive field. Ignoring the third of these for the moment, we see that the space is divided into three regions. In region I there is both an incident and a reflected wave. In region II there is only an incident field. In region III there is nothing so we call this the shadowed region. However, because of diffraction the field does enter this region. This accounts for why you can overhear a conversation if you are on the opposite side of a thick wall but with a door a few meters away. Traditionally such effects have been ignored in semi-classical calculations because they are relatively weak. However, they can be significant.

To solve this problem Sommerfeld worked by analogy with the full line case, so let us briefly consider that much simpler problem. There we know that the problem can be solved by images. An incident wave of amplitude A is of the form

$$v(r,\psi) = Ae^{-ikr\cos\psi} \tag{26.1}$$

where $\psi = \phi - \alpha$ and ϕ is the angular coordinate. The total field is then given by the method of images as

$$v_{\rm tot} = v(r,\phi-\alpha) - v(r,\phi+\alpha), \tag{26.2}$$

where the negative sign ensures that the boundary condition of zero field on the line is satisfied.

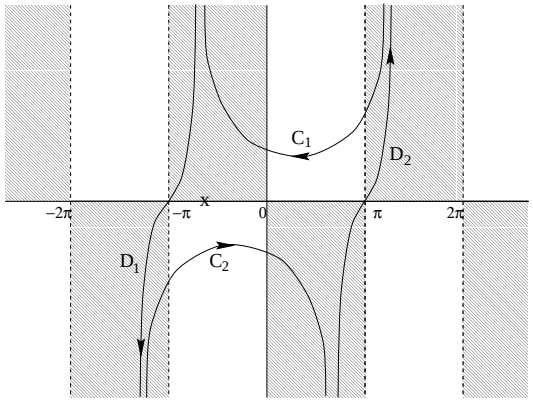

Figure 26.2: The contour in the complex β plane. The pole is at $\beta = -\psi$ (marked by $\times$ in the figure) and the integrand approaches zero in the shaded regions as the magnitude of the imaginary part of β approaches infinity.

Sommerfeld then argued that $v(r,\psi)$ can also be given a complex integral representation

$$v(r,\psi) = A\int_C d\beta f(\beta,\psi)e^{-ikr\cos\beta}. \tag{26.3}$$

This is certainly correct if the function $f(\beta,\psi)$ has a pole of residue $1/2\pi i$ at $\beta = -\psi$ and if the contour C encloses that pole. One choice is

$$f(\beta,\psi) = \frac{1}{2\pi}\frac{e^{i\beta}}{e^{i\beta}-e^{-i\psi}}. \tag{26.4}$$

(We choose the pole to be at $\beta = -\psi$ rather than $\beta = \psi$ for reasons discussed later.) One valid choice for the contour is shown in fig. 26.2. This encloses the pole and vanishes as $|\mathrm{Im}\,\beta| \to \infty$ (as denoted by the shading). The sections D_1 and D_2 are congruent because they are displaced by 2π. However, they are traversed in an opposite sense and cancel, so our contour consists of just the sections C_1 and C_2. The motivation for expressing the solution in this complicated manner should become clear soon.

What have we done? We extended the space under consideration by a factor of two and then constructed a solution by assuming that there is also a source

in the unphysical space. We superimpose the solutions from the two sources and at the end only consider the solution in the physical space to be meaningful. Furthermore, we expressed the solution as a contour integral which reflects the 2π periodicity of the problem. The half line scattering problem follows by analogy.

Whereas for the full line the field is periodic in 2π, for the half line it is periodic in 4π. This can be seen by the fact that the field can be expanded in a series of the form $\{\sin(\phi/2),\sin(\phi),\sin(3\phi/2),\cdots\}$. As above, we extend the space by thinking of it as two sheeted. The physical sheet is as shown in fig. 26.1 and the unphysical sheet is congruent to it. The sheets are glued together along the half line so that a curve in the physical space which intersects the half line is continued in the unphysical space and vice-versa. The boundary conditions are that the total field is zero on both faces of the half line (which are physically distinct boundary conditions) and that as $r \to \infty$ the field is composed solely of plane waves and outgoing circular waves of the form $g(\phi)\exp(ikr)/\sqrt{kr}$. This last condition is a result of Huygens' principle.

We assume that the complete solution is also given by the method of images as

$$v_{\mathrm{tot}} = u(r,\phi-\alpha) - u(r,\phi+\alpha). \tag{26.5}$$

where $u(r,\psi)$ is a 4π-periodic function to be determined. The second term is interpreted as an incident field from the unphysical space and the negative sign guarantees that the solution vanishes on both faces of the half line. Sommerfeld then made the ansatz that u is as given in equation (26.3) with the same contour $C_1 + C_2$ but with the 4π periodicity accounted for by replacing equation (26.4) with

$$f(\beta,\psi) = \frac{1}{4\pi}\frac{e^{i\beta/2}}{e^{i\beta/2}-e^{-i\psi/2}}. \tag{26.6}$$

(We divide by 4π rather than 2π so that the residue is properly normalized.) The integral (26.3) can be thought of as a linear superposition of an infinity of plane waves each of which satisfies the Helmholtz equation $(\nabla^2+k^2)v = 0$, and so their combination also satisfies the Helmholtz equation. We will see that the diffracted field is an outgoing circular wave; this being a result of choosing the pole at $\beta = -\psi$ rather than $\beta = \psi$ in equation (26.4). Therefore, this ansatz is a solution of the equation and satisfies all boundary conditions and therefore constitutes a valid solution. By uniqueness this is the only solution.

In order to further understand this solution, it is useful to massage the contour. Depending on ϕ there may or may not be a pole between $\beta = -\pi$ and $\beta = \pi$. In region I, both functions $u(r,\phi\pm\alpha)$ have poles which correspond to the

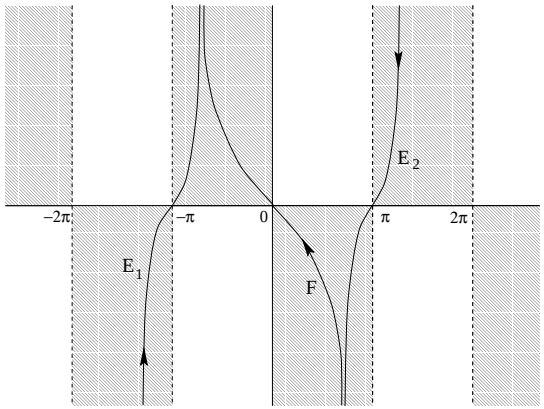

Figure 26.3: The contour used to evaluate the diffractive field after the contribution of possible poles has been explicitly evaluated. The curve F is traversed twice in opposite directions and has no net contribution.

incident and reflected waves. In region II, only $u(r, \phi - \alpha)$ has a pole corresponding to the incident wave. In region III there are no poles because of the shadow. Once we have accounted for the geometrical waves (i.e. the poles), we extract the diffracted waves by saddle point analysis at $\beta = \pm\pi$. We do this by deforming the contours C so that they go through the saddles as shown in fig. 26.2.

Contour C_1 becomes $E_2 + F$ while contour C_2 becomes $E_1 - F$ where the minus sign indicates that it is traversed in a negative sense. As a result, F has no net contribution and the contour consists of just E_1 and E_2.

As a result of these machinations, the curves E are simply the curves D of fig. 26.2 but with a reversed sense. Since the integrand is no longer 2π periodic, the contributions from these curves no longer cancel. We evaluate both stationary phase integrals to obtain

$$u(r, \psi) \approx -A \frac{e^{i\pi/4}}{\sqrt{8\pi}} \sec(\psi/2) \frac{e^{ikr}}{\sqrt{kr}} \tag{26.7}$$

so that the total diffracted field is

$$v_{\rm diff} = -A \frac{e^{i\pi/4}}{\sqrt{8\pi}} \left(\sec\left(\frac{\phi - \alpha}{2}\right) - \sec\left(\frac{\phi + \alpha}{2}\right) \right) \frac{e^{ikr}}{\sqrt{kr}}. \tag{26.8}$$

Note that this expression breaks down when $\phi \pm \alpha = \pi$. These angles correspond to the borders among the three regions of fig. 26.1 and must be handled more carefully - we can not do a stationary phase integral in the vicinity of a pole. However, the integral representation (26.3) and (26.6) is uniformly valid.

26.1 on p. 547

We now turn to the simple task of translating this result into the language of semiclassical Green's functions. Instead of an incident plane wave, we assume a source at point x' and then compute the resulting field at the receiver position x. If x is in region I, there is both a direct term, and a reflected term, if x is in region II there is only a direct term and if x is in region III there is neither. In any event these contributions to the semiclassical Green's function are known since the free space Green's function between two points x_2 and x_1 is

$$G_{\rm f}(x_2, x_1, k) = -\frac{i}{4} H_0^{(+)}(kd) \approx -\frac{1}{\sqrt{8\pi kd}} \exp\{i(kd + \pi/4)\}, \tag{26.9}$$

where d is the distance between the points. For a reflection, we need to multiply by -1 and the distance is the length of the path via the reflection point. Most interesting for us, there is also a diffractive contribution to the Green's function. In equation (26.8), we recognize that the coefficient A is simply the intensity at the origin if there were no scatterer. This is therefore replaced by the Green's function to go from the source to the vertex which we label x_V. Furthermore, we recognize that $\exp(ikr)/\sqrt{kr}$ is, within a proportionality constant, the semiclassical Green's function to go from the vertex to the receiver.

Collecting these facts, we say

$$G_{\rm diff}(x, x', k) = G_{\rm f}(x, x_V, k) d(\theta, \theta') G_{\rm f}(x_V, x', k), \tag{26.10}$$

where, by comparison with equations (26.8) and (26.9), we have

$$d(\theta, \theta') = \sec\left(\frac{\theta - \theta'}{2}\right) - \sec\left(\frac{\theta + \theta'}{2}\right). \tag{26.11}$$

Here θ' is the angle to the source as measured from the vertex and θ is the angle to the receiver. They were denoted as α and ϕ previously. Note that there is a symmetry between the source and receiver as we expect for a time-reversal invariant process. Also the diffraction coefficient d does not depend on which face of the half line we use to measure the angles. As we will see, a very important property of $G_{\rm diff}$ is that it is a simple multiplicative combination of other semiclassical Green's functions.

26.2 on p. 547

We now recover our classical perspective by realizing that we can still think of classical trajectories. In calculating the quantum Green's function, we sum over

the contributions of various paths. These include the classical trajectories which connect the points and also paths which connect the points via the vertex. These have different weights as given by equations (26.9) and (26.10) but the concept of summing over classical paths is preserved.

For completeness, we remark that there is an exact integral representation for the Green's function in the presence of a wedge of arbitrary opening angle [15]. It can be written as

$$G(x,x',k) = g(r,r',k,\theta'-\theta) - g(r,r',k,\theta'+\theta) \tag{26.12}$$

where (r,θ) and (r',θ') are the polar coordinates of the points x and x' as measured from the vertex and the angles are measured from either face of the wedge. The function g is given by

$$g(r,r',k,\psi) = \frac{i}{8\pi\nu}\int_{C_1+C_2} d\beta \frac{H_0^+(k\sqrt{r^2+r'^2-2rr'\cos\beta})}{1-\exp\left(i\frac{\beta+\psi}{\nu}\right)} \tag{26.13}$$

where $\nu = \gamma/\pi$ and γ is the opening angle of the wedge. (ie $\gamma = 2\pi$ in the case of the half plane). The contour $C_1 + C_2$ is the same as shown in fig. 26.2.

The poles of this integral give contributions which can be identified with the geometric paths connecting x and x'. The saddle points at $\beta = \pm\pi$ give contributions which can be identified with the diffractive path connecting x and x'. The saddle point analysis allows us to identify the diffraction constant as

$$d(\theta,\theta') = -\frac{4\sin\frac{\pi}{\nu}}{\nu}\frac{\sin\frac{\theta}{\nu}\sin\frac{\theta'}{\nu}}{\left(\cos\frac{\pi}{\nu}-\cos\frac{\theta+\theta'}{\nu}\right)\left(\cos\frac{\pi}{\nu}-\cos\frac{\theta-\theta'}{\nu}\right)}, \tag{26.14}$$

which reduces to (26.11) when $\nu = 2$. Note that the diffraction coefficient vanishes identically if $\nu = 1/n$ where n is any integer. This corresponds to wedge angles of $\gamma = \pi/n$ (eg. n=1 corresponds to a full line and n=2 corresponds to a right angle). This demonstration is limited by the fact that it came from a leading order asymptotic expansion but the result is quite general. For such wedge angles, we can use the method of images (we will require $2n-1$ images in addition to the actual source point) to obtain the Green's function and there is no diffractive contribution to any order. Classically this corresponds to the fact that for such angles, there is no discontinuity in the dynamics. Trajectories going into the vertex can be continued out of them unambiguously. This meshes with the discussion in the introduction where we argued that diffractive effects are intimately linked with classical discontinuities.

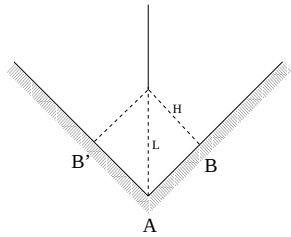

Figure 26.4: The billiard considered here. The dynamics consists of free motion followed by specular reflections off the faces. The top vertex induces diffraction while the bottom one is a right angle and induces two specular geometric reflections.

The integral representation is also useful because it allows us to consider geometries such that the angles are near the optical boundaries or the wedge angle is close to π/n. For these geometries the saddle point analysis leading to (26.14) is invalid due to the existence of a nearby pole. In that event, we require a more sophisticated asymptotic analysis of the full integral representation.

26.2 An application

Although we introduced diffraction as a correction to the purely classical effects; it is instructive to consider a system which can be quantized solely in terms of periodic diffractive orbits. Consider the geometry shown in fig. 26.4 The classical mechanics consists of free motion followed by specular reflections off faces. The upper vertex is a source of diffraction while the lower one is a right angle and induces no diffraction. This is an open system, there are no bound states - only scattering resonances. However, we can still test the effectiveness of the theory in predicting them. Formally, scattering resonances are the poles of the scattering S matrix and by an identity of Balian and Bloch are also poles of the quantum Green's function. We demonstrate this fact in appendix **??** for two dimensional scatterers. The poles have complex wave number k, as for the 3-disk problem.

Let us first consider how diffractive orbits arise in evaluating the trace of G which we call $g(k)$. Specifying the trace means that we must consider all paths which close on themselves in the configuration space while stationary phase arguments for large wavenumber k extract those which are periodic - just as for classical trajectories. In general, $g(k)$ is given by the sum over all diffractive and geometric orbits. The contribution of the simple diffractive orbit labeled γ shown in fig. 26.5 to $g(k)$ is determined as follows.

We consider a point P just a little off the path and determine the semiclassical Green's function to return to P via the vertex using (26.9) and (26.10). To leading order in y the lengths of the two geometric paths connecting P and V are $d_\pm = (L \pm x) + y^2/(L \pm x)^2/2$ so that the phase factor $ik(d_+ + d_-)$ equals $2ikL + iky^2/(L^2 - x^2)$. The trace integral involves integrating over all points P

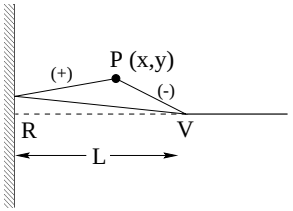

Figure 26.5: The dashed line shows a simple periodic diffractive orbit γ. Between the vertex V and a point P close to the orbit there are two geometric legs labeled $\pm$. The origin of the coordinate system is chosen to be at R.

and is

$$g_\gamma(k) \approx -2d_\gamma \frac{e^{i(2kL+\pi/2)}}{8\pi k}\int_0^L \frac{dx}{\sqrt{L^2-x^2}}\int_{-\infty}^{\infty} dy e^{\left(iky^2\frac{L}{L^2-x^2}\right)}. \tag{26.15}$$

We introduced an overall negative sign to account for the reflection at the hard wall and multiplied by 2 to account for the two traversal senses, $VRPV$ and $VPRV$. In the spirit of stationary phase integrals, we have neglected the y dependence everywhere except in the exponential. The diffraction constant d_γ is the one corresponding to the diffractive periodic orbit. To evaluate the y integral, we use the identity

$$\int_{-\infty}^{\infty} d\xi e^{ia\xi^2} = e^{i\pi/4}\sqrt{\frac{\pi}{a}}, \tag{26.16}$$

and thus obtain a factor which precisely cancels the x dependence in the x integral. This leads to the rather simple result

$$g_\gamma \approx -\frac{il_\gamma}{2k}\left\{\frac{d_\gamma}{\sqrt{8\pi k l_\gamma}}\right\} e^{i(kl_\gamma+\pi/4)} \tag{26.17}$$

where $l_\gamma = 2L$ is the length of the periodic diffractive orbit. A more sophisticated analysis of the trace integral has been done [6] using the integral representation (26.13). It is valid in the vicinity of an optical boundary and also for wedges with opening angles close to π/n.

Consider a periodic diffractive orbit with n_γ reflections off straight hard walls and μ_γ diffractions each with a diffraction constant $d_{\gamma,j}$. The total length of the orbit $L_\gamma = \sum l_{\gamma,j}$ is the sum of the various diffractive legs and l_γ is the length of the corresponding primitive orbit. For such an orbit, (26.17) generalizes to

$$g_\gamma(k) = -\frac{il_\gamma}{2k}\left\{\prod_{j=1}^{\mu_\gamma}\frac{d_{\gamma,j}}{\sqrt{8\pi k l_{\gamma,j}}}\right\}\exp\{i(kL_\gamma + n_\gamma\pi - 3\mu_\gamma\pi/4)\}. \tag{26.18}$$

26.3 on p. 547

Each diffraction introduces a factor of $1/\sqrt{k}$ and multi-diffractive orbits are thereby suppressed.

If the orbit γ is primitive then $L_\gamma = l_\gamma$. If γ is the r'th repeat of a primitive orbit β we have $L_\gamma = rl_\beta$, $n_\gamma = rp_\beta$ and $\mu_\gamma = r\sigma_\beta$, where l_β, p_β and σ_β all refer to the primitive orbit. We can then write

$$g_\gamma = g_{\beta,r} = -\frac{il_\beta}{2k}t_\beta^r \tag{26.19}$$

where

$$t_\beta = \left\{\prod_{j=1}^{\sigma_\beta}\frac{d_{\beta,j}}{\sqrt{8\pi k l_{\beta,j}}}\right\}\exp\{i(kl_\beta + p_\beta\pi - 3\sigma_\beta\pi/4)\}. \tag{26.20}$$

It then makes sense to organize the sum over diffractive orbits as a sum over the primitive diffractive orbits and a sum over the repetitions

$$g_{\rm diff}(k) = \sum_\beta\sum_{r=1}^{\infty} g_{\beta,r} = -\frac{i}{2k}\sum_\beta l_\beta\frac{t_\beta}{1-t_\beta}. \tag{26.21}$$

We cast this as a logarithmic derivative (12.7) by noting that $\frac{dt_\beta}{dk} = il_\beta t_\beta - \sigma_\beta t_\beta/2k$ and recognizing that the first term dominates in the semiclassical limit. It follows that

$$g_{\rm diff}(k) \approx \frac{1}{2k}\frac{d}{dk}\left\{\ln\prod_\beta(1-t_\beta)\right\}. \tag{26.22}$$

In the case that there are only diffractive periodic orbits - as in the geometry of fig. 26.4 - the poles of $g(k)$ are the zeros of a dynamical zeta function

$$1/\zeta(k) = \prod_\beta(1-t_\beta). \tag{26.23}$$

For geometric orbits, this function would be evaluated with a cycle expansion as discussed in chapter 15. However, here we can use the multiplicative nature of the weights t_β to find a closed form representation of the function using a Markov

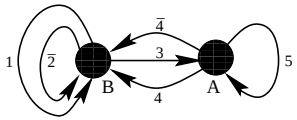

Figure 26.6: The two-node Markov graph with all the diffractive processes connecting the nodes.

graph, as in sect. 9.6.1. This multiplicative property of the weights follows from the fact that the diffractive Green's function (26.10) is multiplicative in segment semiclassical Green's functions, unlike the geometric case.

There is a reflection symmetry in the problem which means that all resonances can be classified as even or odd. Because of this, the dynamical zeta function factorizes as $1/\zeta = 1/\zeta_+\zeta_-$ (as explained in sects. 19.5 and 19.1.2) and we determine $1/\zeta_+$ and $1/\zeta_-$ separately using the ideas of symmetry decomposition of chapter 19.

In the Markov graph shown in fig. 26.6, we enumerate all processes. We start by identifying the fundamental domain as just the right half of fig. 26.4. There are two nodes which we call A and B. To get to another node from B, we can diffract (always via the vertex) in one of three directions. We can diffract back to B which we denote as process 1. We can diffract to B's image point B' and then follow this by a reflection. This process we denote as $\bar{2}$ where the bar indicates that it involves a reflection. Thirdly, we can diffract to node A. Starting at A we can also diffract to a node in three ways. We can diffract to B which we denote as 4. We can diffract to B' followed by a reflection which we denote as $\bar{4}$. Finally, we can diffract back to A which we denote as process 5. Each of these processes has its own weight which we can determine from the earlier discussion. First though, we construct the dynamical zeta functions.

The dynamical zeta functions are determined by enumerating all closed loops which do not intersect themselves in fig. 26.6. We do it first for $1/\zeta_+$ because that is simpler. In that case, the processes with bars are treated on an equal footing as the others. Appealing back to sect. 19.5 we find

$$\begin{aligned} 1/\zeta_+ &= 1 - t_1 - t_{\bar{2}} - t_5 - t_3t_4 - t_3t_{\bar{4}} + t_5t_1 + t_5t_{\bar{2}}\,, \\ &= 1 - (t_1 + t_{\bar{2}} + t_5) - 2t_3t_4 + t_5(t_1 + t_{\bar{2}}) \end{aligned} \tag{26.24}$$

where we have used the fact that $t_4 = t_{\bar{4}}$ by symmetry. The last term has a positive sign because it involves the product of shorter closed loops. To calculate $1/\zeta_-$, we note that the processes with bars have a relative negative sign due to the group theoretic weight. Furthermore, process 5 is a boundary orbit (see sect. 19.3.1) and only affects the even resonances - the terms involving t_5 are absent from $1/\zeta_-$. The result is

$$1/\zeta_- = 1 - t_1 + t_{\bar{2}} - t_3t_4 + t_3t_{\bar{4}}\,,$$

$$= 1 - (t_1 - t_{\bar{2}}). \tag{26.25}$$

26.4 on p. 547

Note that these expressions have a finite number of terms and are not in the form of a curvature expansion, as for the 3-disk problem.

It now just remains to fix the weights. We use equation (26.20) but note that each weight involves just one diffraction constant. It is then convenient to define the quantities

$$u_A^2 = \frac{\exp\{i(2kL + 2\pi)\}}{\sqrt{16\pi kL}} \qquad u_B^2 = \frac{\exp\{i(2kH + \pi)\}}{\sqrt{16\pi kH}}. \tag{26.26}$$

The lengths L and $H = L/\sqrt{2}$ are defined in fig. 26.4; we set $L = 1$ throughout. Bouncing inside the right angle at A corresponds to two specular reflections so that $p = 2$. We therefore explicitly include the factor $\exp(i2\pi)$ in (26.26) although it is trivially equal to one. Similarly, there is one specular reflection at point B giving $p = 1$ and therefore a factor of $\exp(i\pi)$. We have defined u_A and u_B because, together with some diffraction constants, they can be used to construct all of the weights. Altogether we define four diffraction coefficients: d_{AB} is the constant corresponding to diffracting from B to A and is found from (26.11) with $\theta' = 3\pi/4$ and $\theta = \pi$ and equals $2\sec(\pi/8) \approx 2.165$. With analogous notation, we have d_{AA} and $d_{BB} = d_{B'B}$ which equal 2 and $1 + \sqrt{2}$ respectively. $d_{ij} = d_{ji}$ due to the Green's function symmetry between source and receiver referred to earlier. Finally, there is the diffractive phase factor $s = \exp(-i3\pi/4)$ each time there is a diffraction. The weights are then as follows:

$$\begin{aligned} t_1 = sd_{BB}u_B^2 \quad t_{\bar{2}} &= sd_{B'B}u_B^2 \quad t_3 = t_4 = t_{\bar{4}} = sd_{AB}u_Au_B \\ t_5 &= sd_{AA}u_A^2. \end{aligned} \tag{26.27}$$

Each weight involves two u's and one d. The u's represent the contribution to the weight from the paths connecting the nodes to the vertex and the d gives the diffraction constant connecting the two paths.

The equality of d_{BB} and $d_{B'B}$ implies that $t_1 = t_{\bar{2}}$. From (26.25) this means that there are no odd resonances because 1 can never equal 0. For the even resonances equation (26.24) is an implicit equation for k which has zeros shown in fig. 26.7.

For comparison we also show the result from an exact quantum calculation. The agreement is very good right down to the ground state - as is so often the case with semiclassical calculations. In addition we can use our dynamical zeta function to find arbitrarily high resonances and the results actually improve in that limit. In the same limit, the exact numerical solution becomes more difficult

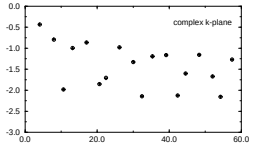

Figure 26.7: The even resonances of the wedge scatterer of fig. 26.4 plotted in the complex $k-$plane, with $L = 1$. The exact resonances are represented as circles and their semiclassical approximations as crosses.

to find so the dynamical zeta function approximation is particularly useful in that case.

26.5 on p. 547

In general a system will consist of both geometric and diffractive orbits. In that case, the full dynamical zeta function is the product of the geometric zeta function and the diffractive one. The diffractive weights are typically smaller by order $O(1/\sqrt{k})$ but for small k they can be numerically competitive so that there is a significant diffractive effect on the low-lying spectrum. It might be expected that higher in the spectrum, the effect of diffraction is weaker due to the decreasing weights. However, it should be pointed out that an analysis of the situation for creeping diffraction [7] concluded that the diffraction is actually *more* important higher in the spectrum due to the fact that an ever greater fraction of the orbits need to be corrected for diffractive effects. The equivalent analysis has not been done for edge diffraction but a similar conclusion can probably be expected.

To conclude this chapter, we return to the opening paragraph and discuss the possibility of doing such an analysis for helium. The important point which allowed us to successfully analyze the geometry of fig. 26.4 is that when a trajectory is near the vertex, we can extract its diffraction constant without reference to the other facets of the problem. We say, therefore, that this is a "local" analysis for the purposes of which we have "turned off" the other aspects of the problem, namely sides AB and AB'. By analogy, for helium, we would look for some simpler description of the problem which applies near the three body collision. However, there is nothing to "turn off". The local problem is just as difficult as the global one since they are precisely the same problem, just related by scaling. Therefore, it is not at all clear that such an analysis is possible for helium.

Commentary

Remark 26.1 Classical discontinuities. Various classes of discontinuities for billiard and potential problems discussed in the literature:

- a grazing condition such that some trajectories hit a smooth surface while others are unaffected, refs. [1, 2, 3, 7]
- a vertex such that trajectories to one side bounce differently from those to the other side, refs. [2, 4, 5, 8, 9].

- a point scatterer [10, 11] or a magnetic flux line [12, 13] such that we do not know how to continue classical mechanics through the discontinuities.

Remark 26.2 Geometrical theory of diffraction. In the above discussion we borrowed heavily from the ideas of Keller who was interested in extending the geometrical ray picture of optics to cases where there is a discontinuity. He maintained that we could hang onto that ray-tracing picture by allowing rays to strike the vertex and then leave at any angle with amplitude (26.8). Both he and Sommerfeld were thinking of optics and not quantum mechanics and they did not phrase the results in terms of semiclassical Green's functions but the essential idea is the same.

Remark 26.3 Generalizations Consider the effect of replacing our half line by a wedge of angle γ_1 and the right angle by an arbitrary angle γ_2. If $\gamma_2 > \gamma_1$ and $\gamma_2 \geq \pi/2$ this is an open problem whose solution is given by equations (26.24) and (26.25) (there will then be odd resonances) but with modified weights reflecting the changed geometry [8]. (For $\gamma_2 < \pi/2$, more diffractive periodic orbits appear and the dynamical zeta functions are more complicated but can be calculated with the same machinery.) When $\gamma_2 = \gamma_1$, the problem in fact has bound states [21, 22]. This last case has been of interest in studying electron transport in mesoscopic devices and in microwave waveguides. However we can not use our formalism as it stands because the diffractive periodic orbits for this geometry lie right on the border between illuminated and shadowed regions so that equation (26.7) is invalid. Even the more uniform derivation of [6] fails for that particular geometry, the problem being that the diffractive orbit actually lives on the edge of a family of geometric orbits and this makes the analysis still more difficult.

Remark 26.4 Diffractive Green's functions. The result (26.17) is proportional to the length of the orbit times the semiclassical Green's function (26.9) to go from the vertex back to itself along the classical path. The multi-diffractive formula (26.18) is proportional to the total length of the orbit times the product of the semiclassical Green's functions to go from one vertex to the next along classical paths. This result generalizes to any system — either a pinball or a potential — which contains point singularities such that we can define a diffraction constant as above. The contribution to the trace of the semiclassical Green's function coming from a diffractive orbit which hits the singularities is proportional to the total length (or period) of the orbit times the product of semiclassical Green's functions in going from one singularity to the next. This result first appeared in reference [2] and a derivation can be found in reference [9]. A similar structure also exists for creeping [2].

Remark 26.5 Diffractive orbits for hydrogenic atoms. An analysis in terms of diffractive orbits has been made in a different atomic physics system, the response of hydrogenic atoms to strong magnetic fields [23]. In these systems, a single electron is highly excited and takes long traversals far from the nucleus. Upon returning to a hydrogen nucleus, it is re-ejected with the reversed momentum as discussed in chapter 25. However, if the atom is not hydrogen but sodium or some other atom with one valence electron, the returning electron feels the charge distribution of the core electrons and not just the charge of the nucleus. This so-called quantum defect induces scattering in addition to the classical re-ejection present in the hydrogen atom. (In this case the local analysis consists of neglecting the magnetic field when the trajectory is near the nucleus.) This is formally similar to the vertex which causes both specular reflection and diffraction. There is then additional structure in the Fourier transform of the quantum spectrum corresponding to the induced diffractive orbits, and this has been observed experimentally [24].

Résumé

In this chapter we have discovered new types of periodic orbits contributing to the semiclassical traces and determinants. Unlike the periodic orbits we had seen so far, these are not true classical orbits. They are generated by singularities of the scattering potential. In these singular points the classical dynamics has no unique definition, and the classical orbits hitting the singularities can be continued in many different directions. While the classical mechanics does not know which way to go, quantum mechanics solves the dilemma by allowing us to continue in all possible directions. The likelihoods of different paths are given by the quantum mechanical weights called diffraction constants. The total contribution to a trace from such orbit is given by the product of transmission amplitudes between singularities and diffraction constants of singularities. The weights of diffractive periodic orbits are at least of order $1/\sqrt{k}$ weaker than the weights associated with classically realizable orbits, and their contribution at large energies is therefore negligible. Nevertheless, they can strongly influence the low lying resonances or energy levels. In some systems, such as the N disk scattering the diffraction effects do not only perturb semiclassical resonances, but can also create new low energy resonances. Therefore it is always important to include the contributions of diffractive periodic orbits when semiclassical methods are applied at low energies.

References

[26.1] A. Wirzba, CHAOS **2**, 77 (1992);

[26.2] G. Vattay, A. Wirzba and P. E. Rosenqvist, Phys. Rev. Lett. **73**, 2304 (1994); G. Vattay, A. Wirzba and P. E. Rosenqvist in *Proceedings of the International Conference on Dynamical Systems and Chaos: vol. 2*, edited by Y.Aizawa, S.Saito and K.Shiraiwa (World Scientific, Singapore, 1994).

[26.3] H. Primack, H. Schanz, U. Smilansky and I. Ussishkin, Phys. Rev. Lett. **76**, 1615 (1996).

[26.4] N. D. Whelan, Phys. Rev. E **51**, 3778 (1995).

[26.5] N. Pavloff and C. Schmit, Phys. Rev. Lett. **75**, 61 (1995).

[26.6] M. Sieber, N. Pavloff, C. Schmit, Phys. Rev. E **55**, 2279 (1997).

[26.7] H. Primack et. al., J. Phys. A **30**, 6693 (1997).

[26.8] N. D. Whelan, Phys. Rev. Lett. **76**, 2605 (1996).

[26.9] H. Bruus and N. D. Whelan, Nonlinearity, **9**, 1 (1996).

[26.10] P. Seba, Phys. Rev. Lett. **64**, 1855 (1990).

[26.11] P. E. Rosenqvist, N. D. Whelan and A. Wirzba, J. Phys. A **29**, 5441 (1996).

[26.12] M. Brack et. al., Chaos **5**, 317 (1995).

[26.13] S. M. Reimann et. al., Phys. Rev. A **53**, 39 (1996).

[26.14] A. Sommerfeld, Mathem. Ann. **47**, 317 (1896); *Optics* (Academic Press, New York 1954).

[26.15] H. S. Carslaw, Proc. London Math. Soc. (Ser. 1) **30**, 121 (1989); H. S. Carslaw, Proc. London Math. Soc. (Ser. 2) **18**, 291 (1920).

[26.16] J. B. Keller, J. Appl. Phys. **28**, 426 (1957).

[26.17] A. Voros, J. Phys. A **21**. 685 (1988).

[26.18] see for example, D. Ruelle, *Statistical Mechanics, Thermodynamic Formalism* (Addison-Wesley, Reading MA, 1978).

[26.19] see for example, P. Grassberger, Z. Naturforsch. **43a**, 671 (1988).

[26.20] P. Cvitanović and B. Eckhardt, Nonlinearity **6**, 277 (1993).

[26.21] P. Exner, P. Seba and P. Stovicek, Czech J. Phys **B39**, 1181 (1989).

[26.22] Hua Wu and D. W. L. Sprung, J. Appl. Phys. **72**, 151 (1992).

[26.23] P. A. Dando, T. S. Monteiro, D. Delande and K. T. Taylor, Phys. Rev. Lett. **74**, 1099 (1995). P. A. Dando, T. S. Monteiro and S. M. Owen, preprint (1997).

[26.24] D. Delande et. al., J. Phys. B **27**, 2771 (1994); G. Raithel et. al., J. Phys. B **27**, 2849 (1994); M. Courtney et. al., Phys. Rev. Lett., **73**, 1340 (1994).

Exercises

(N. Whelan)

Exercise 26.1 Stationary phase integral. *Evaluate the two stationary phase integrals corresponding to contours E_1 and E_2 of fig. 26.3 and thereby verify (26.7).*

Exercise 26.2 Scattering from a small disk *Imagine that instead of a wedge, we have a disk whose radius a is much smaller than the typical wavelengths we are considering. In that limit, solve the quantum scattering problem - find the scattered wave which result from an incident plane wave. You can do this by the method of partial waves - the analogous three dimensional problem is discussed in most quantum textbooks. You should find that only the $m = 0$ partial wave contributes for small a. Following the discussion above, show that the diffraction constant is*

$$d = \frac{2\pi}{\log\left(\frac{2}{ka}\right) - \gamma_e + i\frac{\pi}{2}} \tag{26.28}$$

where $\gamma_e = 0.577\cdots$ is Euler's constant. Note that in this limit d depends weakly on k but not on the scattering angle.

Exercise 26.3 Several diffractive legs. *Derive equation (26.18). The calculation involves considering slight variations of the diffractive orbit as in the simple case discussed above. Here it is more complicated because there are more diffractive arcs - however you should convince yourself that a slight variation of the diffractive orbit only affects one leg at a time.*

Exercise 26.4 Unsymmetrized dynamical zeta function. *Assume you know nothing about symmetry decomposition. Construct the three node Markov diagram for fig. 26.1 by considering A, B and B' to be physically distinct. Write down the corresponding dynamical zeta function and check explicitly that for $B = B'$ it factorizes into the product of the the even and odd dynamical zeta functions. Why is there no term $t_{\bar{2}}$ in the full dynamical zeta function?*

Exercise 26.5 Three point scatterers. *Consider the limiting case of the three disk game of pinball of fig. 1.1 where the disks are very much smaller than their spacing R. Use the results of exercise 26.2 to construct the desymmetrized dynamical zeta functions, as in sect. 19.6. You should find $1/\zeta_{A_1} = 1 - 2t$ where $t = de^{i(kR-3\pi/4)}/\sqrt{8\pi kR}$. Compare this formula with that from chapter ??. By assuming that the real part of k is much greater than the imaginary part show that the positions of the resonances are $k_nR = \alpha_n - i\beta_n$ where $\alpha_n = 2\pi n + 3\pi/4$, $\beta_n = \log\left(\sqrt{2\pi\alpha_n}/d\right)$ and n is a non-negative integer. (See also reference [11].)*

Epilogue

> Nowadays, whatever the truth of the matter may be (and we will probably never know), the simplest solution is no longer emotionally satisfying. Everything we know about the world militates against it. The concepts of indeterminacy and chaos have filtered down to us from the higher sciences to confirm our nagging suspicions.
>
> L. Sante, "Review of 'American Tabloid' by James Ellroy", *New York Review of Books* (May 11, 1995)

A motion on a strange attractor can be approximated by shadowing long orbits by sequences of nearby shorter periodic orbits. This notion has here been made precise by approximating orbits by prime cycles, and evaluating associated curvatures. A curvature measures the deviation of a long cycle from its approximation by shorter cycles; the smoothness of the dynamical system implies exponential fall-off for (almost) all curvatures. We propose that the theoretical and experimental non–wandering sets be expressed in terms of the symbol sequences of short cycles (a topological characterization of the spatial layout of the non–wandering set) and their eigenvalues (metric structure)

Cycles as the skeleton of chaos

> Étant données des équations ... et une solution particuliére quelconque de ces équations, on peut toujours trouver une solution périodique (dont la période peut, il est vrai, étre trés longue), telle que la différence entre les deux solutions soit aussi petite qu'on le veut, pendant un temps aussi long qu'on le veut. D'ailleurs, ce qui nous rend ces solutions périodiques si précieuses, c'est qu'elles sont, pour ansi dire, la seule bréche par où nous puissions esseyer de pénétrer dans une place jusqu'ici réputée inabordable.
>
> H. Poincaré, *Les méthodes nouvelles de la méchanique céleste*

We wind down this chatty chapter by asking: why cycle?

We tend to think of a dynamical system as a smooth system whose evolution can be followed by integrating a set of differential equations. Traditionally one used integrable motions as zeroth-order approximations to physical systems, and accounted for weak nonlinearities perturbatively. However, when the evolution is actually followed through to asymptotic times, one discovers that the strongly nonlinear systems show an amazingly rich structure which is not at all apparent in their formulation in terms of differential equations. In particular, the periodic orbits are important because they form the *skeleton* onto which all trajectories trapped for long times cling. This was already appreciated century ago by H. Poincaré, who, describing in *Les méthodes nouvelles de la méchanique céleste* his discovery of homoclinic tangles, mused that "the complexity of this figure will be striking, and I shall not even try to draw it". Today such drawings are cheap and plentiful; but Poincaré went a step further and, noting that hidden in this apparent chaos is a rigid skeleton, a tree of *cycles* (periodic orbits) of increasing lengths and self-similar structure, suggested that the cycles should be the key to chaotic dynamics.

The zeroth-order approximations to harshly chaotic dynamics are very different from those for the nearly integrable systems: a good starting approximation here is the stretching and kneading of a baker's map, rather than the winding of a harmonic oscillator.

For low dimensional deterministic dynamical systems description in terms of cycles has many virtues:

1. cycle symbol sequences are *topological* invariants: they give the spatial layout of a non–wandering set
2. cycle eigenvalues are *metric* invariants: they give the scale of each piece of a non–wandering set
3. cycles are *dense* on the asymptotic non–wandering set
4. cycles are ordered *hierarchically*: short cycles give good approximations to a non–wandering set, longer cycles only refinements. Errors due to neglecting long cycles can be bounded, and typically fall off exponentially or superexponentially with the cutoff cycle length
5. cycles are *structurally robust*: for smooth flows eigenvalues of short cycles vary slowly with smooth parameter changes
6. asymptotic averages (such as correlations, escape rates, quantum mechanical eigenstates and other "thermodynamic" averages) can be efficiently computed from short cycles by means of *cycle expansions*

Points 1, 2: That the cycle topology and eigenvalues are invariant properties of dynamical systems follows from elementary considerations. If the same dynam-

ics is given by a map f in one set of coordinates, and a map g in the next, then f and g (or any other good representation) are related by a reparametrization and a coordinate transformation $f = h^{-1} \circ g \circ h$. As both f and g are arbitrary representations of the dynamical system, the explicit form of the conjugacy h is of no interest, only the properties invariant under any transformation h are of general import. The most obvious invariant properties are topological; a fixed point must be a fixed point in any representation, a trajectory which exactly returns to the initial point (a cycle) must do so in any representation. Furthermore, a good representation should not mutilate the data; h must be a smooth transformation which maps nearby cycle points of f into nearby cycle points of g. This smoothness guarantees that the cycles are not only topological invariants, but that their linearized neighborhoods are also metrically invariant. In particular, the cycle eigenvalues (eigenvalues of the Jacobian matrixs $df^n(x)/dx$ of periodic orbits $f^n(x) = x$) are invariant.

Point 5: An important virtue of cycles is their *structural robustness*. Many quantities customarily associated with dynamical systems depend on the notion of "structural stability", that is robustness of non–wandering set to small parameter variations.

Still, the sufficiently short unstable cycles are structurally robust in the sense that they are only slightly distorted by such parameter changes, and averages computed using them as a skeleton are insensitive to small deformations of the non–wandering set. In contrast, lack of structural stability wreaks havoc with long time averages such as Lyapunov exponents (see sect. **??**), for which there is no guarantee that they converge to the correct asymptotic value in any finite time numerical computation.

?? on p. ??

The main recent theoretical advance is **point 4:** we now know how to control the errors due to neglecting longer cycles. As we seen above, even though the number of invariants is infinite (unlike, for example, the number of Casimir invariants for a compact Lie group) the dynamics can be well approximated to any finite accuracy by a small finite set of invariants. The origin of this convergence is geometrical, as we shall see in chapter J.1.2, and for smooth flows the convergence of cycle expansions can even be super-exponential.

The cycle expansions such as (15.5) outperform the pedestrian methods such as extrapolations from the finite cover sums (16.2) for a number of reasons. The cycle expansion is a better averaging procedure than the naive box counting algorithms because the strange attractor is here pieced together in a topologically invariant way from neighborhoods ("space average") rather than explored by a long ergodic trajectory ("time average"). The cycle expansion is co-ordinate and reparametrization invariant - a finite nth level sum (16.2) is not. Cycles are of finite period but infinite duration, so the cycle eigenvalues are already evaluated in the $n \to \infty$ limit, but for the sum (16.2) the limit has to be estimated by numerical extrapolations. And, crucially, the higher terms in the cycle expansion

(15.5) are deviations of longer prime cycles from their approximations by shorter cycles. Such combinations vanish exactly in piecewise linear approximations and fall off exponentially for smooth dynamical flows.

In the above we have reviewed the general properties of the cycle expansions; those have been applied to a series of examples of low-dimensional chaos: 1-d strange attractors, the period-doubling repeller, the Hénon-type maps and the mode locking intervals for circle maps. The cycle expansions have also been applied to the irrational windings set of critical circle maps, to the Hamiltonian period-doubling repeller, to a Hamiltonian three-disk game of pinball, to the three-disk quantum scattering resonances and to the extraction of correlation exponents, Feasibility of analysis of experimental non–wandering set in terms of cycles is discussed in ref. [**?**].

Homework assignment

> "Lo! thy dread empire Chaos is restor'd, Light dies before thy uncreating word; Thy hand, great Anarch, lets the curtain fall, And universal darkness buries all."
> Alexander Pope, *The Dunciad*

We conclude cautiously with a homework assignment posed May 22, 1990 (the original due date was May 22, 2000, but alas...):

1. **Topology** Develop optimal sequences ("continued fraction approximants") of finite subshift approximations to generic dynamical systems. Apply to (a) the Hénon map, (b) the Lorenz flow and (c) the Hamiltonian standard map.

2. **Non-hyperbolicity** Incorporate power–law (marginal stability orbits,"intermittency") corrections into cycle expansions. Apply to long-time tails in the Hamiltonian diffusion problem.

3. **Phenomenology** Carry through a convincing analysis of a genuine experimentally extracted data set in terms of periodic orbits.

4. **Invariants** Prove that the scaling functions, or the cycles, or the spectrum of a transfer operator are the maximal set of invariants of an (physically interesting) dynamically generated non–wandering set.

5. **Field theory** Develop a periodic orbit theory of systems with many unstable degrees of freedom. Apply to (a) coupled lattices, (b) cellular automata, (c) neural networks.

6. **Tunneling** Add complex time orbits to quantum mechanical cycle expansions (WKB theory for chaotic systems).

7. **Unitarity** Evaluate corrections to the Gutzwiller semiclassical periodic orbit sums. (a) Show that the zeros (energy eigenvalues) of the appropriate Selberg products are real. (b) Find physically realistic systems for which the "semiclassical" periodic orbit expansions yield the exact quantization.

8. **Atomic spectra** Compute the helium spectrum from periodic orbit expansions (already accomplished by Wintgen and Tanner!).

9. **Symmetries** Include fermions, gauge fields into the periodic orbit theory.

10. **Quantum field theory** Develop quantum theory of systems with infinitely many classically unstable degrees of freedom. Apply to (a) quark confinement (b) early universe (c) the brain.

Conclusion

> Good-bye. I am leaving because I am bored.
> George Saunders' dying words

> Nadie puede escribir un libro. Para Que un libro sea verdaderamente, Se requieren la aurora y el poniente Siglos, armas y el mar que une y separa.
> Jorge Luis Borges El Hacedor, *Ariosto y los arabes*

The buttler did it.

Index

, 68
Schrödinger, E, 595

abscissa
  absolute conv., 286
  conditional conv., 286
accelerator mode, 381
action, 465, 476
  helium, 506
  relation to period, 515
admissible
  periodic points, 158
  trajectories, number of, 155
Airy function, 485
  at a bifurcation, 485
alphabet, 138
analyticity
  domain, 195
anomalous diffusion, 390
antiharmonic extension, 608
area
  preserving map, 652
Artin-Mazur zeta function, 164
attractor, 36
  basin, 36
  Hénon, 61
  strange, 36, 40, 128
autonomous flow, 39, 247
average
  space, 107
  time, 107
averages
  chaotic, 336
averaging, 28
  space, 122
  time, 120
Axiom A
  systems, 228

baker's map, 89
Balmer spectrum, 456
basin of attraction, 36
Bernoulli
  polynomials, 222
  shift, 221, 346
bifurcation
  Airy function approximation, 485
  bizarre, 607
  generic, 89
  Hopf, 401
  saddle-node, 59
billiard
  map, 85
  stadium, 84
billiards, 84, 89
  stability, 86
binary
  symbolic dynamics
    collinear helium, 511
Birkhoff
  coordinates, 11
  ergodic theorem, 108
Bohr
  – de Broglie picture, 456
  -Sommerfeld quantization, 456, 495, 581
  helium, 503, 517
  Uetli Schwur, 580
Bohr, N., 679
Boltzmann, 23
  equation, 397
boredom, 313, 553
Borges, J.L., 553
boundary orbits, 364

bounded operators, 667
Bowen, 25
brain, rat, 3, 26
branch cut, 330
  singularity, 331
Bunimovich
  billiard, *see* stadium
Burnett coefficient, 387

C_{3v} symmetry, 369
canonical
  transformation, 83
canonical transformations, 588
Cartwright M.L., 576
Cauchy criterion, 665
caustic, 468
ceiling function, 51, 192, 235
center, 68
center manifold, 45
chain rule, 74
  matrix, 663
change
  of coordinates, 93
chaos, 5–7
  caveats, 8
  diagnostics, 46
  skeleton of, 10, 12
  successes, 8
character
  orthonormalitity, 644
  representation, 640
characteristic
  function, 102
  polynomial, 161
chicken
  heart palpitations, 6
circle map
  critical, 404
coarse graining, 154
coarse-graining, 102
coding, *see* symbolic dynamics
collinear helium
  symbolic dynamics, 511
combinatorics
  teaching, 149
complete
  N-ary dynamics, 139
complexity
  algorithmic, 174
confession
  C.N. Yang, 107
  Kepler, 572
  St. Augustine, 101
conjugacy, 93, 95
  invariant, 97
  smooth, 93, 97, 99, 685
  topological, 151
conservation
  equation, 593
  phase space volume, 83
  phase-space volume, 110, 594
continuity
  equation, 112
continuity equation, 109, 466, 594
contour integral, 200
contracting
  flow, 36, 40, 73
  map, 80
  stability eigenvalues, 76, 185
convergence
  abscissa of, 286
  mediocre, 658
  radius, 195
  super-exponential, 217, 256
convexity, 134
coordinate
  change, 93, 95
  longitudinal, 477
  transformations, 99
Copenhagen School, xi, 581
correlation
  decay
    power law, 324
  function, 232
  spectrum, 233
  time, 300
cost function, 251
critical
  point, 148
  value, 148, 384

critical point, 75
cumulant
  expansion, 160, 163, 274
    Plemelj-Smithies, 672
curvature
  correction, 271
  expansion, 27, 271
cycle, 10
  expansion, 18, 271
    3-disk, 290
    finite subshift, 281
    stability ordered, 282
  expon, 494
  fundamental, 161, 271
  limit, 128
  prime, 177, 186, 241
    3-disk, 260
    Hénon map, 254
  pruning, 168
  stability, 74, 260
  stable, 75
  superstable, 75
  unstable, 12
  weigth, 198
cycle expansion
  Lyapunov exponent, 280
cycles
  fundamental, 656
cyclic
  invariance, 241
  symmetry, 158

D'Alambert's wave equation, 583
de Broglie wavelength, 460
decay
  rate, 206
degree of freedom, 8
delta function
  Dirac, 104, 459
density, 102, 593
  evolution, 23
density of states
  Green's function, 459
  quantum, 459
  semiclassical, 491
desymmetrization
  3-disk, 375
determinant
  Fredholm, 675
  graph, 173
  Hadamard, 196
  spectral, 22, 160, 196
    for flows, 197
  trace relation, 160
  trace-class operator, 668
deterministic
  dynamics, 34
deterministic dynamics, 5
deterministic flow, 109
differential equations
  ordinary
    almost, 48
diffraction
  Green's function, 536
  Keller, 544
  Sommerfeld, 544
diffusion
  partial differential equations, 584
  anomalous, 390
  constant, 124
dimension
  box counting, 316
  fractal, 315
  generalized, 3
  Hénon attractor, 261
  information, 316
  intrisic, 8
Dirac delta function, 104
Dirichlet series, 285
dissipative
  map, 80
distribution, 585
divergence rate
  local, 131
doubling map, 226
Duffing oscillator, 38
Duffing system, 45
dynamical
  system, 33, 34
    deterministic, 34

gradient, 48
smooth, 34
systems
equivalent, 95
transitivity, 157
zeta function, 17, 199
Euler product rep., 199
dynamical system
infinite, 50
smooth, 18, 19, 27, 171, 442, 445, 447, 576
dynamics
deterministic, 5
hyperbolic, 141
irreversible, 37
reversible, 37
stochastic, 6
symbolic, 9, 138, 303
symmetry, 643
topological, 138

eigendirections, 64
eigenfunction
energy, 457
eigenfunctions
Perron-Frobenius, 216
eigenstate, *see* eigenfunction
eigenvalue
exponential spacing, 197
spectral determinant, 217
zero, 475
eigenvalues, 206
elliptic
partial differential equations, 584
stability, 83
enemy
thy, 325
ensemble
microcanonical, 134
entropy
barrier, 287
topological, 7, 156, 169, 173
equation
of variations, 64
equilibrium
measure, *see* natural measure
point, 38, 70, 106
equivalence
of dynamical systems, 95
ergodic
average, 108
theorem
multiplicative, 134
theory, 108
escape
intermittency, 334
rate, 13, 297
3-disk, 279, 291
escape rate, 105
3-disk, 295
essential
spectral radius, 222
essential spectral radius, 218
Euler
formula, 217, 691
limit, 71
product, 202
product rep.
dynamical zeta function, 199
totient function, 406
Euler-MacLaurin
formula, 233
evolution
group, 48, 683
kernel
probabilistic, 109
operator, 20, 127
quantum, 458
semigroup, 127
expanding
stability eigenvalues, 76, 185
expectation value, 123, 136
exponent
stability, 77
exponential
convergence, 195, 217
of a matrix, 66
exponential proliferation, 20, 174
extremal point, 474

false zeros, 202
Farey
map, 323, 347
mediant, 407
series, 406
tree, 407
Feynman path integral, 473
Feynman, R.P., 679
finite subshift
cycle expansion, 281
first return function, 51
first return time, 344
fixed point, 241
maps, 62
marginally stable, 323
Floquet multipliers, 185
flow, 34, 37
autonomous, 39, 247
contracting, 36, 40, 73
deterministic, 109
generator of, 110, 596
Hamiltonian, 81, 652
hyperbolic, 83, 206
incompressible, 73, 110, 594
infinite-dimensional, 41, 54, 583
inverse hyperbolic, 83
linear, 65
linearized, 64
spectral determinant, 197
stability, 70
stationary, 39
stochastic, 109
stretch&fold, 148
Fourier
mode, 584
spatial, 43
truncation, 44
fractal, 314
aggregates, 3, 303
dimension, 315
geometry of nature, 3
probabilistic, 3
science, 2
Fredholm
determinant, 675
integral equations, 220
integral operator, 219
Fredholm theory, 219
frequency analysis, 46
Fresnel integral, 474, 484
function
space
piecewise constant, 187
functional, 584
Lyapunov, 36
functions
L^2 square integrable, 218
analytic, 218
fundamental
cycle, 161
cycles, 656
domain, 143
collinear helium, 510
fundamental matrix, 73, *see* Jacobian matrix

Galerkin truncation, 43
Gatto Nero
professor, 680
Gauss shift, 407
gaussian
integral, d-dimensional, 470
generator
of flow, 110, 596
golden mean
pruning, 162
gradient algorithm, 252
grandmother
of fractals, 318
Green's function
analogue of, 600
density of states, 459
diffraction, 536
energy dependent, 459
regularized, 492
semiclassical, 481, 485
short distance, 479
trace, 459
long orbits, 478
short distance, 479

group, 639
dynamical, 37
evolution, 48, 683
finite, 639
integration, 643
matrix, 640
order of, 639
representation, 640
semi-, 109, 595
Gutzwiller
trace formula, 490

Hadamard determinant, 196
Hadamard product, 493
Hamilton
-Jacobi equation, 461
equations, 462
principal function, 464
Hamiltonian, 457, 463
flow, 652
spectral determinant, 204
stability, 590
flows, stability, 82, 587
repeller, periodic orbits, 267
Hankel function, 479
Hausdorff dimension
Hénon attractor, 261
Heaviside function, 460
Heisenberg, 581
picture, 665
Heisenberg, W, 595
Helfand moments, 386
helium, 503, 581
collinear, 49, 61, 81, 529
cycles, 267, 529
eigenenergies, 530
fundamental domain, 510
Poincar/'e section, 529
stabilities, 530
stability, 266
Hénon
-Heiles
symbolic dynamics, 373
attractor, 61, 108
Hausdorff dimension, 261
Lyapunov exponent, 261
topological entropy, 261
map, 57, 59, 252, 267
fixed points, 61
prime cycles, 254, 267
stability, 74
symmetries, 652
Hénon, M., 59
heroes
unsung, xiv
Hessian matrix, 83
Hilbert
-Schmidt condition, 220
-Schmidt operators, 667
space, 457
Hopf bifurcation, 401
hydrodynamical
interpretation of QM, 480
hyperbolic
partial differential equations, 584
flow, 206
flows, 83
non-, 24
hyperbolicity assumption, 15, 185

in/out nodes, 68
incompressible flow, 73
indecomposability, 157
metric, 138
index
Maslov, *see* topological index
induced map, 339
inertial manifold, 43, 45, 584
infinite-dimensional flows, 41, 54, 583
inflection point, 402
information
dimension, 316
initial
conditions
sensitivity to, 6
point x_0, 14, 35, 64
state x_0, 14, 35
integrated observable, 120
integration
group, 643

Runge-Kutta, 49
intermittency, 89, 322
escape rate, 334
piecewise linear model, 325
resummation, 341
stability ordering, 284
invariance
cyclic, 241
of flows, 78
symplectic, 82, 587
invariant
measure, 106
metric, 75, 97
topological, 74
inverse
hyperbolic flows, 83
inverse iteration, 242
Hamiltonian repeller, 267
inward/outward spirals, 68
irreducible
segment, 354
irreversibility, 23, 154
irreversible
dynamics, 37
iteration, 34
inverse, 242
Hamiltonian repeller, 267
itinerary, 9, 12, 138
bi-infinite, 140
future, 149

Jacobian, 72, 103
matrix, 14, 15, 64, 599
mapping, 73
Jonquière function, 327, 390, 396
Jordan form, 67

KAM
tori, 322
Keller
diffraction, 544
Keplerian orbit, 456
kernel
resolving, 221
Koopman operator, 304, 595, 600
Kramers, 581
KS, *see* Kustaanheimo-Stiefel
Kuramoto, Y., 45
Kuramoto-Sivashinsky system, 42, 70, 583
kurtosis, 136, 386
Kustaanheimo-Stiefel transformation, 506

L^2 function space, 218
Lagrangian, 464
manifold, 466
laminar states, 322
Laplace
transform, 22, 111, 164, 189, 194, 459, 481, 596
transform, discrete, 159, 186, 346
Laplacian, 583
Lautrup, 679
Legendre transform, 465
Leibniz, 5
libration orbit, 513, *see* self–retracing
lifetime, 13
limit
cycle, 128
linear
flows, 65
stability, 63
linearized flow, 64
Liouville
equation, 112
operator, 113
theorem, 83, 110, 594
Littlewood J.E., 576
local
divergence rate, 131
stability, 63
logistic map, *see* unimodal
longitudinal
coordinate, 477
loop
intersecting, 161
Lorentz gas, 322
Lorentz system, 347
Lorenz, E.N., 59
loxodromic, 83

loxodromic eigenvalues, 590
Lozi map, 57, 59
Lyapunov
  exponent, 6, 73, 128
    natural measure, 131
    numerically, 130
  functional, 36
  time, 6, 8, 37
Lyapunov exponent
  cycle expansion, 280
  Hénon attractor, 261
  numerical, 134

Mandelbrot set, 303
manifold
  stable, 146
map, 35
  area preserving, 652
  contracting, 80
  dissipative, 80
  expanding, 139
  Hénon, 57, 252, 652
    prime cycles, 254
  logistic, *see* unimodal
  Lozi, 57, 59
  order preserving, 151
  orientation preserving, 652
  orientation reversing, 652
  quadratic, 58, 148
  return, 11, 15, 51
  sawtooth, 355
  stability, 73
  tent, 148
  Ulam, 290
  unimodal, 148
maps
  fixed point, 62
marginal
  stability, 15, 323
    fixed point, 323
  stability eigenvalues, 76, 185
Markov
  graph
    infinite, 163
  partition, 387
    finite, 139, 141
    not unique, 142
Maslov index, *see* topological index
material invariant, 593
matrix
  exponential, 66
  exponential of, 597
  group, 640
  normal, 67
  of variations, 64
measure, 102
  cylinder, 303
  equipartition, 303
  invariant, 106
  natural, 107, 122
  smooth, 121
mechanics
  quantum, 456
  statistical, 23
mediocre
  convergence, 658
memory
  finite, 152
metric
  indecomposability, 138, 660
  invariant, 75, 97
  transitivity, 660
microcanonical ensemble, 134
Mira, C., 59
Misiurewicz, M., 59
mixing, 6, 7, 15, 108
mode
  Fourier, 43
Moebius inversion, 166
monodromy matrix, 589
monodromy matrix, 184
Morse index, *see* topological index
mother
  of fractals, 318
multifractals, 318, 438
multiplicative ergodic theorem, 134
multipoint shooting method, 244

natural measure, 107, 122, 131
nature

  geometry of, 3
Navier-Stokes equation, 41
Nero
  Gatto, professor, 680
neutral, *see* marginal
Newton's method, 243
  convergence, 245
  flows, 247
  optimal surface of section, 250
non-hyperbolicity, 78
non-wandering set, 36
nonequilibrium, 377
norm, 666
normal
  matrix, 67

obscure
  foundations, 581
  jargon, 138
  topology, 45, 54
observable, 107, 120
ODE, *see* ordinary differential equations
open system, 13
open systems, 125
operator
  evolution, 127
  Hilbert-Schmidt, 667
  Koopman, 595, 600
  Liouville, 113
  norm, 665
  Perron-Frobenius, 104, 134
  positive, 667
  regularization, 674
  resolvent, 111, 597
  semigroup
    bounded, 111, 596
  trace-class, 666
orbit, 35
  Keplerian, 456
  periodic, 488, 490
  returning, 488
order preserving map, 151
ordinary differential equations
  almost, 48
orientation
  preserving map, 652
  reversing map, 652
Oseledec multiplicative ergodic theorem, 134

palpitations
  chicken hearts, 6
parabolic
  partial differential equations, 584
paradise
  this side of, 295
partial differential equations, 41, 583
partition, 138
  infinite, 169, 173
  Markov, 139
  phase space, 102
partition function, 134
PDE, *see* partial differential equations
period
  doubling
    repeller, 303
  relation to action, 515
periodic
  orbit, 488, 490
  orbit condition, 241
  orbit extraction, 241–260
    Hamiltonian repeller, 267
    inverse iteration, 242
    multipoint shooting, 244
    Newton's method, 243–245
    relaxation algorithm, 252
  point, 10, 20
    admissible, 158
    count, 165
    unstable, 12
Perron-Frobenius
  matrix, 157
  operator, 104, 134, 216
  theorem, 231, 235, 441
phase
  space
    partition, 102
phase space, 34
  3-disk, 660

Piecewise
linear maps, 347
piecewise
constant functions, 187
piecewise linear model
intermittency, 325
piecewise-linear
repeller, 105
pinball, 4, *see* 3-disk
Plemelj-Smithies cumulants, 672
Poincaré
-Cartan theorem, 466
return map, 51
polynomial, 57
section, 11, 51, 85
3-disk, 85
Hénon trick, 59
point
non-wandering, 36
periodic, 10
wandering, 35
point scatterers, 547
Poisson
bracket, 112
resummation, 22
summation, 342
Pollicott, M., 134, 345
polylogarithm, 327
polynomial
characteristic, 161
topological, 164
Pomeau, Y., 59
positive operators, 667
potential
partial differential equations, 584
power law
correlation decay, 324
pressure, 134
thermodynamic, 134
prime cycle, 177, 186, 241
3-disk, 140, 177, 260
count, 166
Hénon map, 254
primitive cycle, *see* prime cycle
probabilistic approximation, 345
propagator, 458
semiclassical, 469
short time, 470, 479
Van Vleck, 472
pruning, 10, 323
golden mean, 162
individual cycles, 168
rules, 141
pseudocycles, 270

quadratic map, 58
quantization
Bohr-Sommerfeld, 456
semiclassical, 487
quantum
evolution, 458
interference, 460
mechanics, 456
potential, 480
propagator, 458
theory, old, 581

radius
of convergence, 195
recoding, 142
rectification
flows, 95
recurrence, 36, 138
time, *see* return time
regularization, 493, 506
Green's function, 492
operator, 674
relaxation algorithm, 252
renormalization, 89
repeller, 13, 36, 125
piecewise-linear, 105
single fixed point, 216
representation
character, 640
equivalent, 641
faithful, 641
matrix, 640
regular, 641
representative point, 34
residue
stability, 83

resolvent operator, 111, 597
resolving kernel, 221
resonance
Ruelle-Pollicott, 134, 345
resummation
intermittency, 341
return map, 11, 15
return time, 345
distribution, 345
returning orbit, 488
reversible
dynamics, 37
Riemann zeta function, 285
Riemann zetafunction, 347
Rössler system, 39, 148
Ruelle, 25
-Pollicott resonances, 134, 345
zeta function, *see* dynamical zeta function
Runge-Kutta integration, 49
running orbits
Lorentz gas, 381
Rutherford, 503
Rydberg series, 517

S gradient
system, 48
saddle point, *see* stationary phase
saddle-node
bifurcation, 59
sawtooth map, 355
SBR measure, *see* natural measure
scatterer
point, 547
scattering
3-dimensional spheres, 90
Schrödinger
equation, 456
picture, 665
Schwartz, 585
section
Poincaré, 11, 51, 85
Selberg
product
eigenvalue index, 217
self-retracing cycle, 513
self-similar, 21
semiclassical
spectral determinant
collinear helium, 520
approximation, 461
density of states, 491
Green's function, 481, 485
propagator, 469
quantization, 487
wave function, 467
semiclassical zeta function, 494
semigroup, 109, 595
dynamical, 37
evolution, 127
operator, 111, 596
sensitivity to initial conditions, 6, 128
shadowing, 18, 171
3-disk, 279
shift
Bernoulli, 221, 346
map, 402
Sinai, 25
Sinai-Bowen-Ruelle measure, *see* natural measure
single fixed point
repeller, 216
spectral determinant, 216
singularity
branch cut, 331
Sivashinsky, G.I., 45
skeleton of chaos, 10, 12
Smale, 9, 25, 208
wild idea, 197, 207
Smale S., 173, 576
smooth
conjugacy, 93, 97, 99, 685
dynamical system, 50
dynamics, 18, 19, 27, 34, 171, 442, 445, 447, 576
approximated, 655
Spectral determinant, 235
interaction, 448
measure, 121
potential, 89

Sommerfeld
diffraction, 544
space
analytic functions, 218
average, 107
averaging, 122
density functions, 187
spectral
determinant, 22, 160, 196
1-d maps, 203
2-d hyperbolic Hamiltonian flow, 204
entire, 197, 217
for flows, 197
infinite product rep., 198
single fixed point, 216
weighted, 204
spectral determinant
1-dimensional, 495
2-dimensional, 496
radius, 222
essential, 218
staircase, 460
spectral stability, 390
spectrum
Balmer, 456
specular reflection, 84
SRB measure, 59
St. Augustine, 101
stability
billiards, 86
cycle, 260
eigenvalues, 76, 185
exponents, 77
flow, 70
Hamiltonian flow, 590
Hamiltonian flows, 82, 587
linear, 63
maps, 73
neutral, *see* marginal
ordering
cycle expansions, 282
intermittent flows, 284
residue, 83
spectral, 390
structural, 172, 389
window, 75
stable
cycle, 75
manifold, 15, 146
flow, 146
map, 146
stadium billiard, 84
stagnation point, 38, *see* equilibrium point
staircase
mean eigenvalue density, 520
spectral, 460
standard map, 322
standing orbit
Lorentz gas, 381
state, 138
set, 138
state space, 34, *see* phase space
stationary
flow, 39
phase approximation, 472, 474, 484, 485, 489, 535, 547, 704
point, 38, *see* equilibrium point
state, 106
statistical mechanics, 23
Sterling formula, 485
stochastic dynamics, 6
stochastic flow, 109
Stokes theorem, 466
stosszahlansatz, 23, 397
strange
attractor, 36, 40
strange attractor, 128
stretch & fold dynamics, 58
stretch&fold flow, 148
strobe method, 51
structural stability, 172, 389
subshift
finite type, 141
super-exponential
convergence, 256
super-stable fixed point, 256
superstable cycle, 75
surface of section

optimal, 250
survival probability, 13, *see* escape rate
symbolic
dynamics, 303
at a bifurcation, 89
complete N-ary, 139
symbolic dynamics, 9, 138
3-disk, 31, 140
binary
collinear helium, 511
coding
Markov graph, 281
complete, 148
Hénon-Heiles, 373
recoding, 142
unimodal, 148
symmetry
C_{3v}, 369
3-disk, 143, 354, 369, 375
cyclic, 158
discrete, 142
dynamical system, 643
Hénon map, 652
symplectic
form, 82
group $Sp(2D)$, 588
integrator, 599
invariance, 82, 587
transformation, 83, 112
systems
open, 125

tangent
bundle, 38
tangent space, 64
Tauberian theorem, 347
teaching
combinatorics, 149
tessalation
smooth dynamics, 655
thermodynamical
pressure, 134
3-body problem, 487, 503, 571, 582
3-dimensional sphere
scattering, 90
3-disk
boundary orbits, 364
convergence, 224, 655
cycle
analytically, 92
count, 373, 619
expansion, 290
escape rate, 214, 279, 291, 295
fractal dimension, 314
geometry, 85
hyperbolicity, 185
phase space, 12, 314, 660
pinball, 4, 86, 89
point scatterer, 547
prime cycles, 16, 140, 177, 260
shadowing, 279
simulator, 91, 92
symbolic dynamics, 10, 31, 140
symmetry, 143, 354, 369, 375
transition matrix, 139
time
arrow of, 23
as parametrization, 94
average, 107, 129
averaging, 120
ceiling function, *see* ceiling function
ordered integration, 70
topological
conjugacy, 151
dynamics, 138
entropy, 7, 156, 169
Hénon attractor, 261
equivalence, 68
future coordinate, 150
index, 468
invariant, 74
polynomial, 164
trace formula, 159
transitivity, 157
zeta function, 164
topological index, 491, 582
totient function, 406
t_p

cycle weigth, 198
trace
formula
classical, 22
flows, 190
Gutzwiller, 490
maps, 186
topological, 159, 164
local, 158
trace-class operator, 666
determinant, 668
trajectory, 35, 65
transfer
matrix, 105
transfer operator, 207
spectrum, 196
transformation
coordinate, 99
transient, 36, 138, 264
transition matrix, 139, 156, 158
3-disk, 139
transverse
stability, 478
Trotter product formula, 665
truncation
Galerkin, 43
truncations
Fourier, 44
turbulence
problem of, 41

Ulam map, 266, 290
unimodal map, 148
symbolic dynamics, 148
unstable
cycle, 12, 75
manifold, 15, 146
map, 146
manifold, flow, 146
periodic point, 12
unsung
heroes, xiv

Van Vleck
propagator, 472
vector field, 38
vector fields
singularities, 95
visitation sequence, *see* itinerary
Viswanath, 679
volume preservation, 88
von Neumann
ergodicity, 600

wandering point, 35
wave
partial differential equations, 584
wave function
semiclassical, 467
WKB, 468
weight
multiplicative, 28
Wentzel-Kramers-Brillouin, 461, *see* WKB
winding number, 402, 404
WKB, 461, 585
wave function, 468

Yang, C.N., 107
Young, L.-S., 59

zero eigenvalue, 475
zeros
false, 202
zeta function
Artin-Mazur, 164
dynamical, 17, 199
Ruelle, *see* dynamical
topological, 164